UNICA

UNIVERSITÀ
DEGLI STUDI
DI CAGLIARI

Ph.D. DEGREE IN
NEUROSCIENCE

Cycle XXXVII

Phenotyping Behavioral Disorders in REM Sleep: Study of Digital Biomarkers of Neurodegeneration

Scientific Disciplinary Sector(s)

IBIO-01/A

Ph.D. Student:	Parisa Sattar
Supervisor	Monica Maria Francesca Puligheddu
Co-Supervisor	Danilo Pani

Final exam. Academic Year 2023/2024
Thesis defence session: April 2025

"Knowledge is better than wealth. Knowledge guards you, while you guard wealth."

Ali ibn Abi Talib

Declaration

I hereby declare that, except where specific reference is made to the work of others, the content of this dissertation is the result of my own independent research. It has not been submitted, either in full or in part, for consideration towards any other degree or qualification at this or any other university.

This dissertation reflects my individual effort and contributions, with no collaborative work included unless explicitly stated in the text or Acknowledgements section. Any references to the work of others, whether published or unpublished, have been duly acknowledged in accordance with academic and ethical standards.

The dissertation comprises fewer than 34,000 words, which includes appendices, bibliography, footnotes, tables, and equations, and features fewer than 30 figures. I take full responsibility for the content of this work and its presentation.

January 2025
Parisa Sattar

Acknowledgements

I gratefully acknowledge the Ministry of University and Research (MUR) for supporting my PhD research work under National Operational Program for Research and Innovation 2014–2020

I would like to express my deepest gratitude to my scientific supervisor Danilo Pani, whose scientific guidance, constant encouragement, and invaluable support made this research possible. His mentorship has been a source of inspiration and has provided me with the tools to navigate the challenges of this work.

I am also profoundly thankful to my supervisor Monica Puligheddu, for her expert supervision as a neurologist providing insightful suggestions, and critical feedback, which greatly contributed to the development of this research.

My sincere thanks go to Pablo Laguna and Raquel Bailón from Biomedical Signal Interpretation & Computational Simulation (BSICoS) Group, Universidad de Zaragoza, and to Nicola Rizzo and Raffaele Orsato from Micromed Solutions, for their clinical and technical support, as well as their collaborative spirit, which enriched this study. I would also like to thank Giulia Baldazzi for her thoughtful comments and efforts on part of this thesis work that helped in enhancing the quality of this thesis.

I am immensely grateful to my research group and colleagues, who provided a stimulating and supportive environment throughout this journey. Special thanks to Prof. Danilo Pani, whose encouragement and teamwork made the process both productive and enjoyable.

Finally, I want to acknowledge the contribution of the my Undergraduate/Master's students or other group members, including Nicla Mandas, Elisa Facshini, Damiano Virdis, and Daniel Secci for their dedication and assistance. Their efforts added valuable insights and supported the progress of this dissertation.

Dedication

This thesis is dedicated to my parents, who may never have fully understood the complexities of my studies but supported me with love—and the occasional “Are you done yet?” To my sibling(s), who teased me relentlessly yet secretly bragged about me to their friends—don’t think I didn’t notice.

To all my amazing friends, and most notably to my dearest friend, Hira Shahid, who kept me sane (or at least tried) with endless rants, terrible jokes, and an abundance of emotional support. Your distractions were at once my greatest annoyance and my greatest joy.

And above all, to Allah, who gave me the strength to overcome every obstacle. Without His mercy and guidance, this thesis would still be nothing more than a blank page.

Abstract

Neurodegenerative disorders remain a significant challenge in modern medicine, with early diagnosis and intervention being critical for improving patient outcomes. This thesis focuses on advancing the understanding and detection of REM Sleep Behavior Disorder (RBD), a recognized prodromal symptom of alpha-synucleinopathies, among which Parkinson's Disease (PD). By integrating computational approaches with physiological insights, this research presents novel tools and methods for identifying early-stage biomarkers and understanding autonomic dysfunction in RBD. Heart Rate Variability (HRV) and QT Variability (QTV), studied across different sleep stages, were investigated as potential digital biomarkers of neurodegeneration. Apart from traditional HRV analysis, this thesis also considered the influence of respiration on spectral HRV analysis.

A major outcome of HRV studies carried out in this thesis is that patients with idiopathic RBD (iRBD) exhibit distinct HRV profiles during sleep, specifically during N2 and REM phase, characterized by reduced autonomic modulation and decreased complexity compared to healthy controls and PD patients, with or without RBD. iRBD patients showed early sympathetic dominance, likely due to initial neurodegenerative changes in parasympathetic control centers such as the dorsal motor nucleus of the vagus nerve (DMNV), while PD patients exhibited a more balanced autonomic activity due to broader neurodegeneration. These findings highlight the potentialities of HRV analysis during sleep as an early biomarker for neurodegenerative progression in alpha-synucleinopathies. Moreover, respiration guided HRV analysis also revealed the disruption in automatic regulation also in N3 phase which is typically not observed in conventional spectral analysis. The QTV studies also showed that both iRBD and PD patients with RBD exhibited adaptive physiological changes after sleep, potentially reflecting compensatory mechanisms for poor sleep quality. PD-RBD patients demonstrated more pronounced alterations in autonomic regulation, likely due to broader neurodegenerative changes, which were distinct from those seen in iRBD patients. Furthermore, physiological analysis during the REM sleep phase provided insights into autonomic dysfunction in PD and its subtypes, suggesting progressive disruption in regulatory processes.

In order to ease the HRV analysis in sleep studies, during my Ph.D. I also developed and released (open-source) the UNICA-HRV tool, a customizable, user-friendly MATLAB user interface designed to analyze HRV metrics across different sleep phases, by exploiting the hypnogram information. Moreover, during my research period in the industry (Micromed), I contributed to the development of signal processing methods for real-time denoising of EEG signals from polysomnographic data. A novel algorithm, the Adaptive Sigmoid Normalized Least Mean Square (AS-NLMS), was developed to address the challenges of artifact removal in dynamic and non-linear environments.

The findings presented in this thesis underscore the transformative potential of interdisciplinary research, where engineering and medicine converge to solve complex problems. By introducing new tools, refining analytical methods, and proposing novel approaches to digital phenotyping, this work contributes to the broader effort of early detection and personalized treatment of neurodegenerative diseases.

Table of Contents

Title Page 1

Declaration 4

Acknowledgements 5

Dedication 6

Abstract 7

List of Publications 16

Acronyms and Abbreviations 18

Introduction 21

i. Thesis Structure 23

Chapter 1: Background and Related Work 27

1.1.1. Sleep Architecture 27
1.1.2. Sleep Stages and Structure: 28
1.1.3. Sleep Characteristics 31
1.1.4. Physiological Changes During Sleep 32
1.2. REM Sleep Behavior Disorder (RBD) 34
1.2.1. Types of RBD 34
1.2.2. Prevalence of RBD 35
1.2.3. Phenoconversion in RBD 35
1.3. Neurodegenerative Biomarkers in RBD 36
1.4. Autonomic Nervous System (ANS) 38
1.5. Basic anatomy and physiology of heart 41
1.5.1. Electrical Activity of Heart 42
1.5.2. Electrocardiogram (ECG) Signal 43
1.5.3. Waves and complexes of the ECG Signal 44
1.6. Heart Rate Variability (HRV) 45
1.6.1. Significance of HRV 45

1.7. QT Variability (QTV) 46
1.7.1. Significance of QTV 47
1.8. Confounding factors of HRV and QTV 47

Chapter 2: Dataset 49

2.1. Polysomnography (PSG) 49
2.2. PSG Data Acquisition 50
2.3. Demographic, Clinical and PSG Features 52
2.4. Sleep Scoring Criteria 52
2.5. Diagnosis of the relevant conditions 53
2.6. Study Population 54
2.7. Inclusion Criteria: 55
2.8. Exclusion Criteria: 55
2.9. Ethical Approval: 56
2.10. Challenges in ECG Data: Signal Quality and Sleep Stage Duration: 57
2.11. Data Preprocessing: 57

Chapter 3: Development of Customized Tool for HRV Analysis during sleep 60

3.1. Introduction 60
3.2. Development of Sleep Heart Rate Variability Analysis tool 62
3.2.1. Overview of Front End 62
i. Single-subject assessment 64
ii. Multiple subjects' assessment (batch analysis) 68
3.2.2. Overview of Back End 69
i. ECG data pre-processing 69
ii. QRS detection 69
iii. Featured Heart Rate Variability Metrics 70
3.3. Assessment of the developed Sleep Heart Rate Variability Analysis software 76
i. Polysomnography Database 77
ii. Comparative analysis with currently established toolboxes 77
3.4. Exemplary analysis performed by UNICA-HRV 79
3.5. Conclusion 82

Chapter 4: Autonomic Regulation in REM sleep behavior disorder and Parkinson's Disease During Sleep 84

4.1. Introduction 84
4.2. Methodology 87
4.2.1. Study population 87
4.2.2. Signal processing 87
4.2.3. Heart Rate Variability Analysis 88
4.3. Results 88
4.3.1. Demographic and Polysomnographic Parameters 88
4.3.2. HRV parameter comparisons across the groups 89
4.4. Discussion 93
4.5. Conclusions 97

Chapter 5: Impact of Respiration on Autonomic Regulation in REM sleep behavior disorder 98

5.1. Introduction 98
5.2. Methodology 100
5.2.1. Study Population 100
5.2.2. Respiration-Guided HRV Analysis 101
5.2.3. Statistical Analysis 104
5.3. Results & Discussion 104
5.4. Conclusion 107
5.5. Limitation and future work 108

Chapter 6: Ventricular repolarization variability in REM sleep behavior disorder 109

6.1. Introduction 110
6.2. Methodology 112
6.2.1. Study population 112
6.2.2. Signal processing 113
6.3. Results and Discussion 114

6.4. Conclusion 118

Chapter 7: Adaptive Sigmoid NLMS Filter for Cardiac and Ocular Noise Removal in Polysomnographic EEG 119

7.1. Introduction 119
7.2. Methodology: 121
7.2.1. Dataset 121
7.2.2. Adaptive Sigmoid NLMS 121
7.3. Results and Discussion 124
7.4. Conclusion 129

Chapter 8: Conclusion and Future Directions 131

8.1. Future Directions 132

Reference: 134

List of Figures

Figure 1. 2: Example of an Hypnogram.....30

Figure 1. 3: Autonomic Nervous System.....39

Figure 1. 4: (a) Blood Circulation System in the (b) The Heart Anatomy.....41

Figure 1. 5: Electrical Conduction Pathway of Heart.....43

Figure 1. 6: Typical ECG wave with Components.....45

Figure 1. 7: Example of RR Intervals.....46

Figure 1. 8: Example of QT Intervals.....47

Figure 2. 2: Example Polysomnographic Exam.....50

Figure 2. 3: (a) Gender Distribution Across Groups (b) Age Distribution Gender wise Across the Groups.....55

Figure 2. 4 Insights into the data.....58

Figure 3. 1: Layout of UNICA Sleep HRV Analysis tool.....63

Figure 3. 2: Hypnogram labels mapping.....64

Figure 3. 3: Heart Rate Variability Analysis Panels.....66

Figure 3. 4: HRV Analysis Setting Window.....67

Figure 3. 5: Comparative analysis of HRV metrics across different HRV analysis tools, namely UNICA-HRV, Kubios, PhysioZoo, HRVAS, and gHRV.....78

Figure 3. 6: (a) ECG segmentation of SN012 subject based on three methods i.e., Method AAE, Method AEWO and Method FEO, where (- - -) is for visual clarity. (b) Hypnogram of a complete sleep cycle representing time taking by each phase wake, N1, N2, N2 and REM sleep phase of SN012 subject.....81

Figure 4. 1: Results for HRV time-domian indexes for the four distinct populations (Control Group (CG), idiopathic REM Sleep Behavior Disorder (iRBD), Parkinson's Disease (PD), and PD with RBD (PD-RBD)) during three sleep phases (N2, N3 and REM). 90

Figure 4. 2: Results for HRV frequency-domian indexes for the four distinct populations (Control Group (CG), idiopathic REM Sleep Behavior Disorder (iRBD), Parkinson's Disease (PD), and PD with RBD (PD-RBD)) during three sleep phases (N2, N3 and REM). 91

Figure 4. 3: Results for HRV non-linear indexes for the four distinct populations (Control Group(CG), idiopathic REM Sleep Behavior Disorder (iRBD), Parkinson's Disease (PD), and PD with RBD (PD-RBD)) during three sleep phases (N2, N3 and REM). 93

Figure 5. 1: Respiratory frequency content (a) and respiratory rate (b) for CG (in white) and iRBD (in grey) in different sleep phases. Statistical significances for CG vs. iRBD analysis is represented as * ($p < 0.05$) or ** ($p < 0.01$).....105

Figure 5. 2: Respiration-guided HRV indexes for CG (in white) and iRBD (in grey) in different sleep phases. The statistically significant results across (CG vs. iRBD) are represented as * ($p < 0.05$) or ** ($p < 0.01$). 106

Figure 5. 3: Respiration-guided HRV indexes for CG (in white) and iRBD (in grey) in different sleep phases. The stastically significant results across (CG vs. iRBD) are represented as * ($p < 0.05$) or ** ($p < 0.01$). 107

Figure 6. 1: Time domain indexes, Frequency domain indexes and QTV related and unrelated to RRV indexes during wakefulness before (WBS, white) and after (WAS, grey) sleep. Significant differences are marked by *.....115
Figure 6. 2: Time and frequency domain QTV indexes during REM. The statistically significant results are marked by *.....117

Figure 7. 1: Mean Square Error (MSE) comparison of the Adaptive LMS filter, Adaptive NLMS filter, Adaptive RLS filter, and Adaptive AS-NLMS filter across filter orders 32, 64, and 128. 124
Figure 7. 2: Comparison of Adaptive Filtering Algorithms for EEG Signal Noise Suppression, Highlighting Overfitting Behavior in the LMS Filter. 126
Figure 7. 3: Peak signal to noise ratio (pSNR) comparison of the Adaptive LMS filter, Adaptive NLMS filter, Adaptive RLS filter, and Adaptive AS-NLMS filter across filter orders 32, 64, and 128. 127
Figure 7. 4: Comparison of mean execution times for different adaptive filters (LMS, NLMS, RLS, and AS-NLMS) across filter orders of 32, 64, and 128 (a). A zoomed-in view of the execution times for LMS, NLMS, and AS-NLMS filters (b) 128
Figure 7. 5: Raw EEG signal, filtered EEG signals using Adaptive LMS, NLMS, RLS, and AS-NLMS filters, and the reference ECG signal (a). The power spectrum comparison of these signals is shown in (b),. A zoomed-in view of the power spectrum comparison in the 0–15 Hz range is presented in (c) for detailed analysis. 129

List of Tables

Table 2. 1: Distribution of the original sampling frequencies of the signals included in the study: 59

Table 3. 1: HRV time-domain metrics [70].....71

Table 3. 2: HRV frequency-domain metrics [70].....72

Table 3. 3: HRV metrics with customizable parameters 76

Table 3. 4: Feature comparison for the HRV analysis tools used for the UNICA-HRV comparative assessment 79

Table 3. 5: Results (mean ± standard deviation) of HRV time-domain analysis during all phases by three different segment selection methods (AAE, AEWO, and FEO) using UNICA-HRV. (N.A.: not available). 82

Table 4.1: Comparisons across the iRBD, PD-RBD, PD and control groups for demographic and polysomnographic parameters. The * marks those parameters exhibiting statistically different differences. 90

Table 5. 1: Comparisons across idiopathic REM sleep behaviour disorder (iRBD) and control group (CG) for demographics and polysomnographic (PSG) parameters.....105

List of Publications

Sattar, P*., Baldazzi, G., Puligheddu, M. and Pani, D., 2025. **The UNICA sleep HRV analysis tool: an integrated open-source tool for heart rate variability analysis during sleep.** Physiological Measurement, 13(1), p.015008.

Hasan MA., **Sattar P.,** Qazi SA., Fraser M., Vuckovic A. **Brain Networks with Modified Connectivity in Patients with Neuropathic Pain, and Spinal Cord Injury**. Clin EEG Neurosci. 2021 Oct 29:15500594211051485. doi: 10.1177/15500594211051485. Epub ahead of print. PMID: 34714181.

N. Mandas, M. Mollura, G. Baldazzi, **P. Sattar,** M. Mura, E. Casaglia, M. Figorilli, L. Giorgetti, P. Mattioli, F. Calizzano, F. Famà, D. Arnaldi, M. Puligheddu, D. Pani, and R. Barbieri, **Characterization of Sleep Structure and Autonomic Dysfunction in REM Sleep Behavior Disorder**, *IEEE Open Journal of Engineering in Medicine and Biology, Special Issue, 2024*

Sattar, P*., Baldazzi, G., Mandas, N., Casaglia, E., Figorilli, M., Giorgetti, L., Mattioli, P., Calizzano, F., Fama, F., Arnaldi, D., Puligheddu, M., Pani, D., Laguna, P., & Bailon, R. (2024). **Assessment of QT variability in Parkinson's Disease and REM Sleep Behaviour Disorder during REM phase.** (*2024) International conference of the European Study Group on Cardiovascular Oscillations, 2024*.

Sattar, P*., Baldazzi, G., Mandas, N., Casaglia, E., Figorilli, M., Giorgetti, L., Mattioli, P., Calizzano, F., Fama, F., Arnaldi, D., Pani, D., Laguna, P., & Bailon, R. (2024). **Assessment of ventricular repolarization variability in wake states in REM Sleep Behaviour disorder and Parkinson's Diseases.** (*2024) Computing in Cardiology (CinC). IEEE, 2024*.

Sattar, P*., Mandas, N., Baldazzi, G., Facchini, E., Casaglia, E., Figorilli, M., Giorgetti, L., Mattioli, P., Calizzano, F., Fama, F., Arnaldi, D., Puligheddu, M., Pani, D., Laguna, P., & Bailon, R. (2024). **Autonomic Dysfunction in REM Sleep Disorder: The Role of Respiration in HRV Analysis.** *Annual International Conference of the IEEE Engineering in Medicine and Biology. IEEE, 2024*

Sattar, P*., Elisa, F., Baldazzi, G., Mandas, N., Casaglia, E., Figorilli, M., Puligheddu, M. Mattioli, P., Arnaldi, D., Puligheddu, M., and Pani, D**. Heart Rate Variability during Sleep-Related Wake Phases in REM sleep Behavior Disorder**. *(2023) Computing in Cardiology (CinC). IEEE, 2023*

Sattar, P*., Baldazzi, G., Mandas, N., Casaglia, E., Figorilli, M., Puligheddu, M. and Pani, D. Parkinson and **REM Sleep Behavior Disorder: HRV Difference During Polysomnography**. In Proceedings of the 16th International Joint Conference on Biomedical Engineering Systems and Technologies (BIOSTEC 2023) - Volume 4: BIOSIGNALS, pages 366-370 ISBN: 978-989-758-631-6; ISSN: 2184-4305

Shahid H., Ejaz O., **Sattar P*.,** Khan MM., Zubair F., Mukhtar M., Farooq U., Nehal M, Sheikh H, Lodhi H., Hasan, MA. 2021. Transcranial Direct Current Stimulation (tDCS): **A Promising Therapy for Attentional Enhancement.** In: *1st International Conference on Applied Physics and Engineering 2021*.

Ejaz O., Shahid H., **Sattar P*.,** Farooq U., Nehal M., Sheik H., Khan MM., Zubair F., Mukhtar M., Lodhi H., Hasan MA. 2021.Transcranial Direct Current Stimulation (tDCS): **An Effective & Non-Medicated Treatment for Psychological Disorders**. In: *1st International Conference on Applied Physics and Engineering 2021*.

Acronyms and Abbreviations

AAE: All Available Epochs

AASM: American Academy of Sleep Medicine

AD: Alzheimer's Disease

AE: Approximate Entropy

AEWO: all ECG epochs greater or equal to five minutes with 50% overlap

AHI: Apnea-Hypopnea Index

ANS: Autonomic Nervous System

ApEn: Approximate Entropy

AS-NLMS: Adaptive Sigmoid Normalized Least Mean Square

AV: Atrioventricular

CG: Control Group

CSF: Cerebrospinal Fluid

DFA: Detrended Fluctuation Analysis

DLB: Dementia with Lewy Bodies

ECG: Electrocardiogram

EDR: ECG-derived respiratory signals

EEG: Electroencephalogram

EMG: Electromyogram

EOG: Electrooculogram

FDS: Flexor Digitorum Superficialis

FEO: First Epoch Only

HF: High Frequency

HMM: Hidden Markov Model

HRV: Heart Rate Variability

iRBD: Idiopathic REM Sleep Behavior Disorder

LF: Low Frequency

LMS: Least Mean Square

MCI: Mild Cognitive Impairment

MSA: Multiple System Atrophy

NfL: NeuroFilament Light chain,

NLMS: Normalized Least Mean Square

NREM: Non-Rapid Eye Movement

ODI: Oxygen Desaturation Index

OSA: Obstructive Sleep Apnea

PD: Parkinson's Disease

PD-RBD: Parkinson's Disease with REM Sleep Behavior Disorder

PLMI: Periodic Limb Movement Index

PSG: Polysomnography

PNS: Parasympathetic Nervous System

QRS: A Component of ECG Representing Ventricular Depolarization

QTV: QT Variability

RBD: REM Sleep Behavior Disorder

REM: Rapid Eye Movement

RLS: Recursive Least Squares

RSA: Respiratory Sinus Arrhythmia

RWA: REM Sleep without Atonia

R&K: Rechtschaffen and Kales

SA: Sinoatrial

SE: Sleep Efficiency

SNS: Sympathetic Nervous System

TBT: Total Bed Time

TIB: Total Time in Bed

TST: Total Sleep Time

VLF: Very Low Frequency

VPSG: video-polysomnographic

WASO: Wake After Sleep Onset

W.H.O: World Health Organization

Introduction

The prevalence of neurodegenerative disease is about 50 million globally, according to the report of world health organization (W.H.O) and this burden is expected to double by the next two decades. Early detection of neurodegenerative diseases, particularly Parkinson's disease (PD) and dementia with Lewy bodies (DLB), remains a critical challenge in modern medicine. By the time these conditions are clinically diagnosed, irreversible damage to the nervous system has already occurred, limiting the effectiveness of interventions.

Rapid Eye Movement (REM) sleep behavior disorder (RBD) has emerged as one of the strongest prodromal symptoms of these diseases, thus instilling the idea that it could represent a predictor of phenoconversion, i.e. neurodegeneration to the manifest disease. However, not all RBD patients experience neurodegeneration, and the precise mechanisms that links RBD to these diseases is still unclear.

As autonomic nervous system dysfunction is a known early sign of neurodegeneration, a promising digital biomarker for early neurodegeneration is heart rate variability (HRV). Previous studies indicated HRV as one of the stronger biomarkers for various neurodegenerative disorders such as PD, DLB, Alzheimer's Disease (AD), Multiple System Atrophy (MSA), and also Mild Cognitive Impairment (MCI). Moreover, some studies postulated that HRV has the potential to enable the identification of those RBD patients most at risk of developing neurodegenerative diseases. As HRV is influenced by various physiological factors, its interpretation is complex and requires advanced analytical techniques. Moreover, to date there is a lack of studies reporting a comprehensive analysis of HRV with the aim of characterizing RBD in patients where this is an isolated symptom (idiopathic RBD) and in those that photoconverted to the manifest neurodegenerative disease, compared to the affected people without the RBD symptoms. Therefore, the identification specific pattern of

HRV and other cardiac biomarkers for the early diagnosis of neurodegeneration in RBD patients represents an innovative and promising approach, motivating this research.

Accordingly, this thesis aims at exploring HRV and QT variability (QTV) as digital biomarkers to characterize these population, paving the way to their future use also in longitudinal studies to aid diagnosis and phenoconversion prediction. In particular, the thesis studies the specific HRV or QTV patterns that are indicative of autonomic dysfunction in RBD patients and tries to infer a possible trajectory of HRV or QTV patterns as patient progress form RBD to PD, with the limitations of a dataset mainly enabling a transversal study.

Along with the intrinsic complexity of this research, from the clinical perspective, several challenges must be considered, which will determine limitations of the analysis:

- Variability and noise: HRV signals can be affected by many factors such as age, cardiovascular health, and external influences. Extracting meaningful features from this variable and noisy data to detect early neurodegeneration is a major challenge.
- Complexity of HRV analysis: HRV consists of various time-domain, frequency-domain, and non-linear measures, each reflecting different aspects of autonomic function. Determining which features are most relevant for early neurodegenerative detection requires careful exploration.
- Generalizability: ensuring that the results obtained on specific datasets can be generalized well to other populations with different characteristics is essential for clinical application.

i. Thesis Structure

The thesis has been structured into eight chapters, which show the specific work conducted during the course of my Ph.D.

Chapter 1: Background and Related Work

This chapter provides a comprehensive overview of RBD disease and the associated neurodegenerative biological and digital biomarkers. It explains RBD, detailing its clinical features and prevalence as a prodromal sign of some neurodegenerative diseases. The progression from RBD to conditions like Parkinson's disease is discussed, further emphasizing the need for early diagnosis. The chapter highlights neurodegenerative biomarkers, specifically on HRV and its physiological basis while considering potential confounding factors. Lastly, introducing how machine learning can be a powerful tool for analyzing complex HRV and clinical datasets to identify predictive digital biomarkers.

Chapter 2: Dataset

This chapter provides a detailed description of the dataset used in this study, highlighting its relevance to the research objectives. It begins with an introduction to polysomnography (PSG), outlining its role in sleep studies and its significance. The process of PSG data acquisition is then explained, followed by a presentation of the demographic, clinical, and PSG features of the study population. The chapter further details the sleep scoring criteria and the diagnostic approach for relevant diseases. Moreover, the study population, inclusion and exclusion criteria, and ethical approval are discussed to ensure methodological transparency. This chapter also provides insights into the challenges associated with ECG signal quality recorded during PSG and the variability in sleep stage durations, which made it difficult to extract consistent,

noise-free, sleep-stage-specific ECG segments. Lastly, the data preprocessing steps are described, focusing on the procedures used to prepare the dataset for subsequent analysis.

Chapter 3: Development of Customized Tool for Heart Rate Variability Analysis During Sleep

This chapter discusses the development of a MATLAB software tool for analyzing HRV during sleep. It begins by introducing the software purpose and features, which support both single-subject and multiple-subject assessments for flexible HRV analysis. A technical overview of the back-end includes steps for preprocessing ECG data, detecting QRS complexes with a wavelet-based ECG delineator, and conducting HRV analysis. The software's performance is evaluated through comparative analysis with existing toolboxes. The chapter concludes with an exemplary analysis, showcasing the software features in HRV analysis for sleep studies.

Chapter 4: Autonomic Regulation in REM sleep behavior disorder and Parkinson's Disease During Sleep

This chapter focuses on identifying the trend of autonomic dysfunction in different types of RBD patients and in patients with PD. It details participant selection, data acquisition, and signal processing for HRV analysis. The chapter explores the potential of various classical and advanced HRV metrics to assess autonomic function associated with RBD and PD.

Chapter 5: Impact of Respiration on Autonomic Regulation in REM Sleep Behavior Disorder

The chapter explores the impact of respiration on autonomic regulation in RBD patients. The chapter uses two different approaches of handling the influence of respiration on HRV analysis

i.e., centering low-frequency and high-frequency bands around the respiratory rate, and orthogonal space projection.

Chapter 6: Ventricular Repolarization Variability in REM Sleep Behavior Disorder

This chapter delves into ventricular repolarization variability in RBD patients, a rarely explored marker of cardiovascular dysfunction. The chapter performed QT variability to assess the risk of cardiac mortality in RBD and PD.

Chapter 7: Adaptive Sigmoid Normalized Least Mean Square (AS-NLMS) algorithm for EEG Denoising in PSG Data

This chapter presents an enhanced version of the Normalized Least Mean Squares (NLMS) filter, integrating sigmoid based activation and variable step based on error signal, improving adaptability, stability, and robustness, particularly for non-linear and dynamic artifact removal scenarios in EEG signals, particularly in PSG data. This is important for the correct sleep staging and for the detection of anomalies in the EEG, even in real-time. The developed algorithm is compared against the standard LMS, NLMS and RLS methods to demonstrate its performance.

Chapter 8: Conclusions and Future Directions

This chapter provides a comprehensive summary of the thesis, presenting the key findings and their implications in the context of RBD, neurodegeneration biomarkers, and advanced signal processing methodologies, highlighting the contributions to HRV and EEG analysis and the

development of innovative algorithms, while proposing future directions such as exploring other features and exploring additional biomarkers.

Chapter 1: Background and Related Work

Sleep is a fundamental biological process essential for the maintenance of physical, cognitive, and emotional well-being [1]. It is a dynamic state characterized by altered consciousness, reduced sensory activity, and decreased voluntary muscle activity [2]. Sleep is critical for memory consolidation, emotional regulation, immune system function, and metabolic homeostasis [1]. Insufficient or poor-quality sleep has been linked to various health issues, including cardiovascular disease, metabolic disorders, and mental health problems [3]. Understanding the nature and structure of sleep is pivotal for comprehending its role in health and disease.

Additionally, sleep facilitates energy restoration, tissue repair, and the removal of metabolic waste from the brain via the glymphatic system. The circadian rhythm, regulated by the suprachiasmatic nucleus in the hypothalamus, plays a crucial role in determining sleep timing and duration [4].

1.1.1. Sleep Architecture

Sleep is organized into distinct cycles that recur throughout the night. Each cycle typically lasts about 90 to 110 minutes and consists of two main phases: Non-Rapid Eye Movement (NREM) sleep and REM sleep. On an average night, adults experience four to six sleep cycles, with the proportion of REM sleep increasing in later cycles. The typical structure of sleep involves progression from shallow stages to deeper stages of NREM sleep, followed by a period of REM sleep [5].

These cycles are regulated by homeostatic sleep pressure and circadian rhythms, which work in synchrony to promote sleep-wake transitions. Sleep cycles vary with age, with infants having shorter cycles and elderly individuals having more fragmented sleep [5].

1.1.2. Sleep Stages and Structure:

Sleep staging also known as sleep scoring, involves classifying sleep into different stages based on physiological signals recorded during PSG. Both the Rechtschaffen and Kales (R&K) and American Academy of Sleep Medicine (AASM) criteria are methods for scoring stages staging, but they differ in their approach, detail, and updates over time. The R&K criteria, developed in 1968, were the first standardized method for scoring sleep stages. They divided sleep into five stages: Stage 1 (light sleep), Stage 2 (stable sleep with sleep spindles and K-complexes), Stages 3 and 4 (deep slow-wave sleep), and REM sleep. This system was widely used for decades but had limitations, such as the separation of Stages 3 and 4, which had overlapping characteristics.

To address these limitations and incorporate advances in sleep science, the AASM introduced updated scoring criteria in 2007, which have since become the global standard. The AASM criteria simplify sleep stages into four categories: N1 (light sleep), N2 (stable sleep), N3 (deep slow-wave sleep), and REM sleep, combining R&K's Stages 3 and 4 into a single N3 stage.

The AASM scoring system defines sleep stages based on specific patterns of EEG, EOG, and EMG. Sleep is categorized into the following stages [6]:

i. Non-Rapid Eye Movement (NREM) Sleep Stages

   NREM sleep is divided into three distinct stages:

   Stage N1. This is the transition from wakefulness to sleep. It is a light sleep stage that lasts for a few minutes and is characterized by slow eye movements, reduced muscle activity, and theta brain waves (4-7 Hz). It represents the initial stage into sleep and

accounts for approximately 5-10% of total sleep time. During this stage, external stimuli can still awaken an individual, and hypnic jerks[1] may occur [5].

Stage N2. This stage represents deeper sleep than N1 and accounts for about 50% of total sleep time. It is marked by sleep spindles (sudden bursts of brain activity) and K-complexes (high-amplitude waveforms), which play roles in memory processing and sensory isolation. Muscle activity decreases, and eye movements stop at this stage. This stage is essential for blocking sensory input to the brain, promoting sleep stability [5].

Stage N3. Also known as slow-wave sleep or deep sleep, Stage N3 is dominated by delta waves (0.5-4 Hz). This stage is associated with restorative processes, immune function, and growth hormone release. It is often referred to as the most "restorative" sleep phase. It accounts for 15-20% of total sleep time in young adults but tends to decrease with age. Stage N3 is critical for cellular repair, immune system function, and synaptic shortening [5].

ii. Rapid Eye Movement (REM) Sleep

REM sleep is characterized by rapid movements of the eyes, vivid dreams, and temporary muscle atonia (muscle paralysis). Unlike NREM sleep, brain activity during REM resembles wakefulness, with mixed-frequency, low-amplitude waves. REM sleep is essential for memory consolidation, emotional processing, and brain development. Loss of muscle atonia during REM sleep is a hallmark of RBD. REM sleep accounts for about 20-25% of total sleep time, with its duration increasing in successive sleep cycles [5].

[1] Hypnic jerks, also known as sleep starts, are sudden, involuntary muscle contractions or sensations of falling that typically occur during the transition from wakefulness to sleep. They are considered normal physiological phenomena

REM sleep is also associated with the processing of emotional experiences and the integration of memories. This phase plays a role in emotional resilience and creative problem-solving, as the brain synthesizes and organizes information from waking experiences [5].

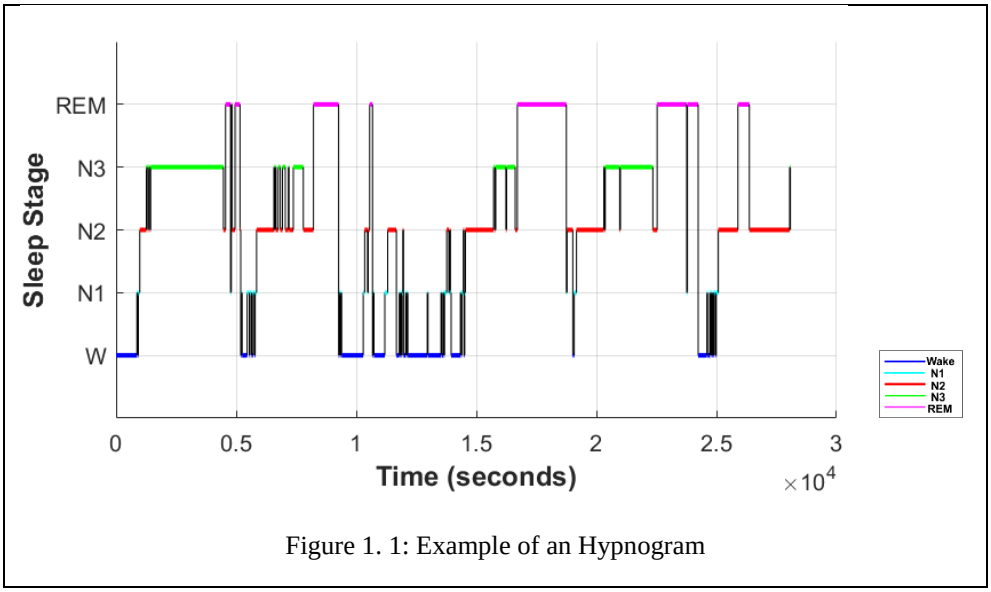


Figure 1. 1: Example of an Hypnogram

The duration of each sleep phase varies across the sleep cycles and changes throughout the night. A typical sleep cycle lasts about 90 to 120 minutes and repeats 4 to 6 times during a full-night sleep. NREM sleep consists of three stages: N1, which lasts 1-7 minutes and serves as the transition from wakefulness to sleep; N2, the most prevalent stage, lasting 10-25 minutes in the first cycle and increasing in subsequent cycles; and N3 (deep sleep or slow-wave sleep), lasting 20-40 minutes, but it becomes shorter as the night progresses. REM sleep, characterized by rapid eye movement and vivid dreaming, initially lasts 10 minutes but can extend to 60 minutes in later cycles. Early in the night, NREM sleep (especially N3) is more dominant, while REM sleep increases in duration toward the morning. This distribution of sleep phases reflects the body's need for both restorative slow-wave sleep and cognitive processing during REM [7–9].

To represent the progression of sleep stages over time, generally a hypnogram Figure 1. 1 is used [10]. It visually illustrates the transitions between wake, NREM (N1, N2, N3), and REM sleep throughout the sleep period. The x-axis represents time, while the y-axis indicates the different sleep stages. This graphical depiction provides a clear overview of sleep architecture, highlighting the timing, duration, and sequence of sleep stages, which is essential for assessing sleep quality and continuity in both research and clinical settings.

1.1.3. Sleep Characteristics

Several key metrics are used to evaluate sleep quality and structure [11].

Sleep Latency. The duration of the transition from wakefulness to sleep (usually to Stage N1 sleep). A typical sleep latency for healthy adults is around 10-20 minutes. Delays in sleep latency are often observed in individuals with insomnia or anxiety disorders [11].

Sleep Efficiency. The ratio of total sleep time (TST) to the total time in bed (TIB), expressed as a percentage. Normal sleep efficiency is considered to be 85% or higher. Low sleep efficiency indicates fragmented sleep or prolonged wakefulness during the night [11].

Total Sleep Time (TST). The actual duration of sleep, excluding periods of wakefulness. It varies depending on age, but adults typically require 7-9 hours of total sleep time. Sleep debt, caused by chronic sleep deprivation, can accumulate and affect cognitive function and physical health [11].

Total Time in Bed (TIB). The total time spent lying in bed, regardless of whether the person is asleep or awake. TIB is often higher than TST, especially in individuals with sleep disturbances [11].

Wake After Sleep Onset (WASO). The cumulative time spent awake after initially falling asleep. High WASO values are associated with sleep fragmentation and are often seen in insomnia or other sleep disorders. High WASO is commonly observed in individuals with sleep apnea or nocturnal awakenings caused by environmental disturbances [11].

Sleep Fragmentation. The frequency of brief arousals[2] during sleep, which can reduce sleep quality. Fragmentation is measured by the number of arousals per hour and is often linked to health conditions such as sleep apnea. Fragmented sleep is associated with cognitive impairments, mood disturbances, and metabolic dysregulation [11].

These characteristics are used in clinical and research settings to evaluate sleep disturbances and diagnose sleep disorders.

1.1.4. Physiological Changes During Sleep

Sleep is a period of dynamic physiological change that affects multiple bodily systems. Key physiological changes include [12]:

Cardiovascular System. Heart rate, blood pressure, and heart rate variability (HRV) change across sleep phases. Parasympathetic activity dominates during NREM sleep, leading to reductions in heart rate and blood pressure. In REM sleep, sympathetic activity increases, leading to greater fluctuations in HRV. These changes help reducing cardiovascular strain and support cardiac recovery. Sleep-related dips in blood pressure are associated with cardiovascular health benefits.

Autonomic Nervous System (ANS) Modulation. The ANS shifts from sympathetic dominance during wakefulness to parasympathetic dominance during NREM sleep, while REM sleep exhibits heightened sympathetic activity. This shift plays a crucial role in sleep-

[2] 2. Arousals refer to brief awakenings or shifts to a lighter sleep stage triggered by external stimuli (e.g., noise, movement) or internal factors (e.g., breathing irregularities). They are usually transient and may or may not be perceived by the individual.

dependent autonomic control. Disruptions in ANS balance are linked to sleep disorders like obstructive sleep apnea (OSA) and cardiovascular diseases.

Respiratory System. Breathing becomes slower and more regular during NREM sleep, while REM sleep is associated with irregular breathing patterns. The decrease in respiratory drive during REM sleep can exacerbate conditions such as obstructive sleep apnea (OSA). Breathing irregularities are more frequent during REM sleep due to changes in autonomic control.

Brain Activity. During NREM sleep, brain activity slows down with increased delta wave activity, which is linked to restorative processes such as synaptic homeostasis. In contrast, REM sleep is associated with fast, low-amplitude brain waves, similar to those seen during wakefulness.

Endocrine System. Hormonal activity shifts significantly during sleep. Growth hormone release peaks during slow-wave sleep (Stage N3), while cortisol follows a circadian rhythm, peaking shortly after awaking. Melatonin production increases prior to sleep onset, promoting sleep initiation. The secretion of other hormones, such as leptin and ghrelin, also depends on sleep-wake cycles and regulates appetite.

Muscular System. Muscle tone decreases during NREM sleep and is completely absent during REM sleep due to atonia, which prevents movement. This atonia serves a protective role, preventing individuals from physically acting out their dreams.

Thermoregulation. Body temperature drops during sleep, especially during NREM sleep. Thermoregulation is less effective during REM sleep, which explains why temperature fluctuations can disturb REM sleep.

1.2. REM Sleep Behavior Disorder (RBD)

RBD is a sleep disorder characterized by the abnormal behavior of physically acting out dreams during the REM sleep stage. Normally, during REM sleep, the body experiences muscle atonia, a temporary paralysis that prevents individuals from moving during sleep. However, in RBD, this paralysis is absent or incomplete, allowing individuals to engage in vigorous movements and vocalizations that can be violent or aggressive, often mirroring the content of their dreams. RBD can occur as an isolated condition (idiopathic) or as a symptom associated with neurodegenerative diseases [13, 14].

1.2.1. Types of RBD

RBD can be classified into two primary types: idiopathic RBD and symptomatic RBD [15–17].

Idiopathic RBD occurs spontaneously without any underlying neurological condition. This form is often seen in middle-aged to elderly individuals and is characterized by the enactment of vivid dreams, which may include violent or aggressive behaviors. Many patients with idiopathic RBD eventually develop neurodegenerative disorders, particularly those associated with alpha-synucleinopathies, such as PD and dementia with Lewy bodies [15]. Alpha-synucleinopathy refers to a group of neurodegenerative disorders characterized by the abnormal accumulation of alpha-synuclein protein in the brain and, in some cases, other parts of the body. Alpha-synuclein is a normal protein predominantly found in the nervous system, but when it misfolds and aggregates, it can form pathological structures, such as Lewy bodies or glial cytoplasmic inclusions, which are associated with neuronal dysfunction and death.

Symptomatic RBD (or secondary RBD) arises as a consequence of other medical conditions or factors. This includes neurodegenerative diseases, psychiatric disorders, or withdrawal from

substances such as alcohol or medications. In younger individuals, symptomatic RBD may also be linked to conditions like narcolepsy or the use of certain antidepressants. Additionally, there is a subtype known as pseudo-RBD, which mimics RBD symptoms but is primarily caused by obstructive sleep apnea [16, 17].

Both types of RBD share common features, yet their underlying causes can differ significantly. Among these shared characteristics, autonomic dysfunction stands out as a prominent symptom, indicating impairments in the autonomic nervous system that may precede or coincide with neurodegenerative processes. Recognizing these distinctions and their implications is essential for accurate diagnosis and effective disease management, particularly given the role of autonomic dysfunction as a potential early biomarker for neurodegenerative conditions [15–17].

1.2.2. Prevalence of RBD

The prevalence of RBD in the general population is relatively low, estimated at less than 1%. However, its occurrence significantly increases among individuals with neurodegenerative disorders. Research suggests that approximately 15% to 75% of patients with Parkinson's disease exhibit symptoms of RBD, particularly in older population over the age of 50. The disorder is also prevalent in patients with other synucleinopathies, such as multiple system atrophy and dementia with Lewy bodies [18–20].

1.2.3. Phenoconversion in RBD

The concept of phenoconversion in iRBD refers to the transition or evolution of idiopathic RBD into a more serious neurodegenerative condition. It is one of the most concerning phenomena in neurology. Studies have shown that individuals diagnosed with iRBD eventually

develop α-synucleinopathies such as PD, DLB, or MSA. Out of which 90% of the cases often converts to either PD or DLB. This progression is not immediate but typically unfolds over years or even decades with reported 6% annually and 73.5% conversion rate converting over a 12-year period [1–3].

1.3. Neurodegenerative Biomarkers in RBD

"Neurodegenerative" refers to the progressive loss of structure or function of neurons, often leading to their death. This degeneration occurs in the brain and nervous system, impacting essential functions such as movement, cognition, and memory. A "biomarker" is a measurable biological molecule or indicator that reflects a specific physiological or pathological state within the body. Biomarkers can be derived from various biological sources, such as blood, cerebrospinal fluid (CSF), urine, or tissue samples. With technological advancements, biomarkers can also be "digital", using data recorded from sensors, wearable devices, imaging technologies, or other digital platforms able to collect physiological information. They will progressively play a more important role in diagnosing diseases, predicting outcomes, and monitoring disease progression or treatment response. Thus, neurodegeneration biomarkers, both biological or digital, are indicators that reflect changes associated with neurodegenerative diseases, offering insights into the diagnosis, progression, and potential treatment responses of these conditions [21–23].

The most common biological biomarkers for RBD, particularly associated to its role as a prodromal indicator of phenoconversion to PD and DLB, include alpha-synuclein, neurofilament light chain (NfL), and tau proteins. Alpha-synuclein is a protein that plays a central role in synucleinopathies like PD and DLB, both of which are common in patients with RBD. Misfolded alpha-synuclein aggregates into Lewy bodies and Lewy neurites, which are hallmark pathological features of these conditions. Alpha-synuclein can be detected in CSF,

and its abnormal accumulation in RBD patients suggests a high risk of neurodegenerative progression, making it a key biomarker for identifying prodromal stages of PD and DLB. NfL is a marker for axonal damage and neurodegeneration, detectable in both CSF and blood. High NfL levels are linked to neuronal injury in several neurodegenerative diseases, including PD, DLB, and MSA. In RBD patients, increased NfL levels suggest ongoing neurodegeneration, which can signal the likely conversion of RBD into a more advanced neurodegenerative disorder. Both total tau and phosphorylated tau are relevant biomarkers for neurodegeneration, primarily in AD but also in RBD-related neurodegenerative conditions. Elevated tau levels in the CSF are associated with neuronal damage and disease progression. In the context of RBD, tau protein abnormalities can indicate a heightened risk of developing DLB, as tau pathology often overlaps with alpha-synuclein pathology [21, 22].

Among digital biomarkers, HRV and gait analysis are the two most commonly used indicators for neurodegenerative diseases. While out-of-the-lab gait analysis can be approximately performed through wearable inertial sensors, providing insights into changes in gait patterns like stride length or walking speed as early indicators of motor dysfunction in conditions such as Parkinson’s disease and Huntington’s disease, HRV can be exactly detected in clinical and ambulatory condition, either from the ECG or, more approximately, from a photoplethysmography (and then included in smart wearables like fitness trackers or smart watches). Apart from HRV, a QTV has gained significance as a marker of the measurement of ventricular repolarization [24–26]. However, this last digital biomarker requires an accurate detection of the ECG signal.

1.4. Autonomic Nervous System (ANS)

The ANS is a critical component of the peripheral nervous system responsible for regulating involuntary physiological functions, including heart rate, blood pressure, respiration, digestion, and glandular activity. It functions involuntarily and plays a central role in maintaining homeostasis (the body's stable internal environment) by responding to internal and external stimuli. The ANS is divided into two primary branches: the sympathetic nervous system (SNS) and the parasympathetic nervous system (PNS), which influence various organs and tissues in distinct but complementary ways as depicted in Figure 1. 2.

The SNS is often referred to as the "fight or flight" system because it prepares the body for stressful or emergency situations. The dominance of SNS increases heart rate, elevates blood pressure, dilates airways, and manages blood flow in response to physical needs. This response is aimed at enhancing physical performance and enable the body to respond quickly to perceived threats or challenges [27].

In contrast, the PNS is often referred to as the "rest and digest" system, as it promotes restorative processes and conserves energy. The PNS is responsible for slowing down the heart rate, promoting digestion, and facilitating recovery after periods of stress or exertion. By slowing heart rate, reducing blood pressure, and enhancing gastrointestinal activity, the PNS enables the body to return to a state of balance after the stress response has subsided [27].

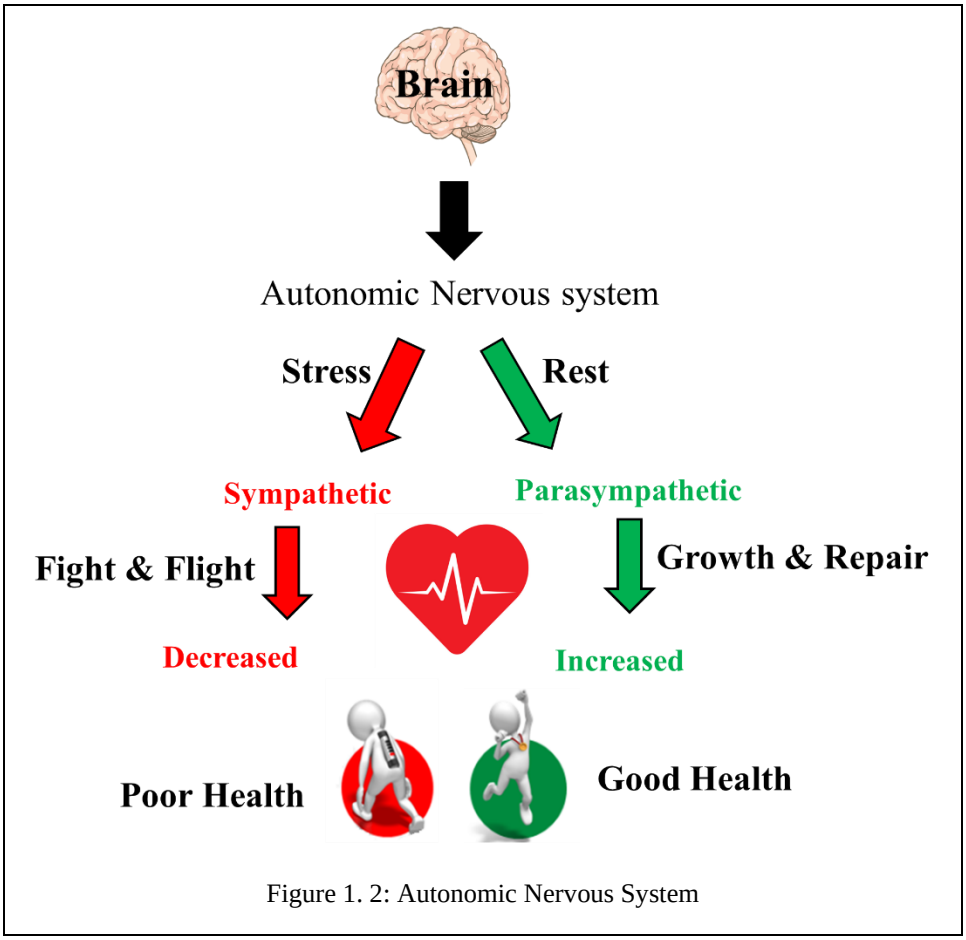


Figure 1. 2: Autonomic Nervous System

The balance between the SNS and PNS also play a central role in regulating heart function. Their interaction governs crucial aspects of cardiac activity, including heart rate, strength of contraction, electrical responsiveness, and the speed of electrical signal transmission [28].

Heart Rate Regulation (Chronotropic Effects)

The SNS increases heart rate by stimulating receptors in the heart's natural pacemaker, the sinoatrial (SA) node. This triggers faster electrical impulses and shortens the time between beats. On the other hand, the PNS slows the heart rate by activating vagal pathways that reduce electrical signalling within the SA node, increasing the interval between heartbeats.

Contractile Strength (Inotropic Effects)

The SNS enhances the force of heart contractions by increasing calcium entry into heart cells, that enables the stronger interactions between muscle fibres, making the heart pump more forcefully to deliver blood efficiently during activities that require more energy. In contrast, the PNS has a minimal effect on contraction strength in the heart's ventricles, though it can slightly reduce the contractility of the atria.

Electrical Responsiveness (Batmotropic Effects)

The heart's responsiveness to electrical signals is modulated by the SNS and PNS. The SNS lowers the threshold for activation, making heart cells more likely to generate action potentials in response to stimuli. The PNS, however, increases this threshold, making it harder for cells to activate and results in overall reduced electrical activity.

Signal Transmission Speed (Dromotropic Effects)

The speed at which electrical signals travel through the heart, especially through the atrioventricular (AV) node, is another critical factor. SNS activity accelerates this transmission, ensuring efficient coordination between the heart’s upper and lower chambers. The PNS slows the process, which can create a longer delay in signal propagation.

The balance between the SNS and PNS is crucial for maintaining ideal health. The dynamic interplay between activation and relaxation is reflected in physiological parameters such as HRV or QTV, which serve as markers of autonomic function. A healthy individual typically demonstrates a balance between the two systems, with neither the SNS nor the PNS being chronically dominant [29–31].

1.5. Basic anatomy and physiology of heart

The human heart is a vital muscular organ located in the mediastinum, slightly left of the midline within the thoracic cavity, encased by the lungs. It is approximately the size of a fist, weighing between 250 and 350 grams in an average adult. Its primary role is to maintain a continuous flow of blood throughout the body, facilitating the delivery of oxygen and essential nutrients while removing carbon dioxide and metabolic waste products. Anatomically Figure 1. 3(b), the heart is divided into four chambers: the right and left atria, which act as receiving chambers, and the right and left ventricles, which serve as pumping chambers. The right atrium collects deoxygenated blood from the body via the superior and inferior vena cava, passing it into the right ventricle, which pumps it to the lungs through the pulmonary artery for oxygenation. Oxygenated blood from the lungs enters the left atrium via the pulmonary veins and is subsequently pumped by the left ventricle into the systemic circulation through the aorta, the body's largest artery [32]. This process is graphically represented in Figure 1. 3(a).

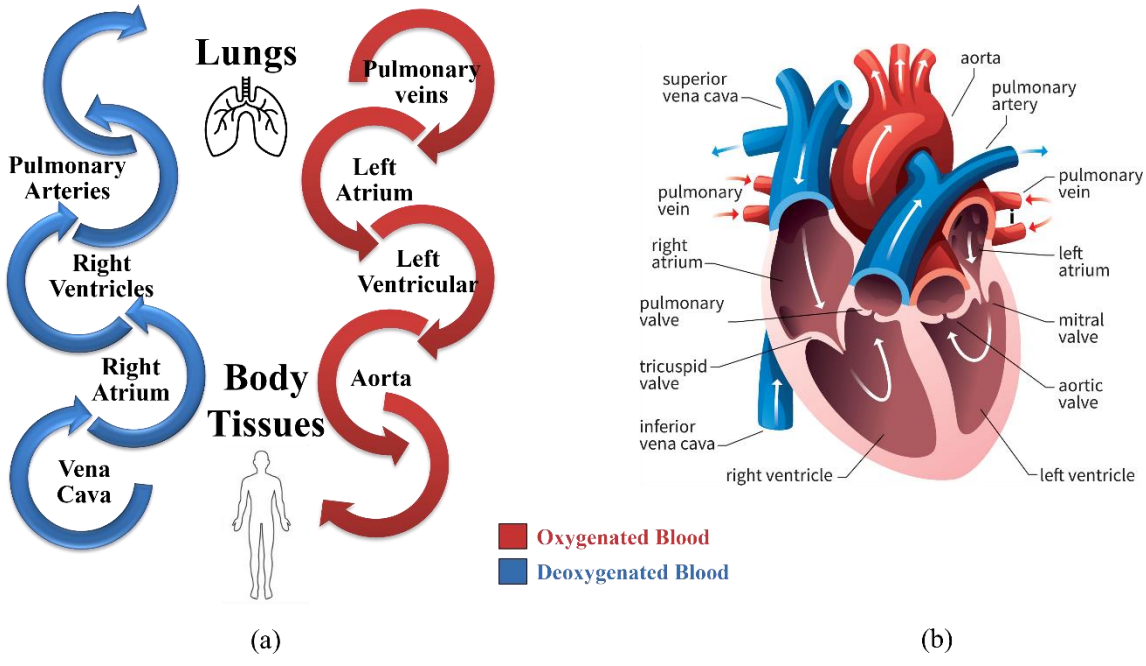


Figure 1. 3: (a) Blood Circulation System in the (b) The Heart Anatomy
(b) is taken from www.cardofmich.com

The structural and functional efficiency of the heart are maintained by specialized components, including the septum, which separates the left and right sides to prevent the mixing of oxygenated and deoxygenated blood, and the heart valves, which ensure unidirectional blood flow. The AV valves, comprising the tricuspid valve on the right and the mitral (bicuspid) valve on the left, regulate blood flow between the atria and ventricles. The semilunar valves, including the pulmonary valve and the aortic valve, control the outflow from the ventricles to the pulmonary and systemic circulations, respectively. The pericardium surrounds the heart; it is a double-layered membranous sac that provides mechanical protection, lubricates the cardiac surface to minimize friction during contractions, and helps anchoring the heart in its anatomical position [32].

The walls of the heart are composed of three layers: the epicardium, the myocardium, and the endocardium. The outer epicardium is a thin, protective layer that forms part of the pericardium. The myocardium, the thick middle layer, is composed of cardiac muscle cells and is primarily responsible for the contractile force required to pump blood. The innermost endocardium lines the heart's interior, covering the chambers and valves, and plays a critical role in maintaining a smooth surface to reduce turbulence and clot formation [32].

1.5.1. Electrical Activity of Heart

The physiology of the heart is underpinned by its intrinsic electrical conduction system presented in Figure 1. 4, which coordinates the rhythmic contractions necessary for effective pumping. The SA node, located in the right atrium, acts as the natural pacemaker, generating electrical impulses that initiate the cardiac cycle. These impulses spread through the atrial walls, causing atrial contraction, before reaching the AV node. The signal is then transmitted via the bundle of His and Purkinje fibres to the ventricles, stimulating synchronized ventricular

contraction. This sequence of electrical and mechanical events constitutes the cardiac cycle, which comprises systole (contraction phase) and diastole (relaxation phase) [32].

The heart's activity is dynamically regulated by the autonomic nervous system and endocrine factors. The sympathetic nervous system and hormones like adrenaline increase heart rate and contractile force during stress or physical exertion while the parasympathetic system mediates resting heart rate and promotes recovery. These adaptive mechanisms ensure the heart meets the varying metabolic demands of the body. Overall, the heart's anatomical and physiological characteristics emphasize its critical role in maintaining systemic homeostasis, a theme of significant relevance in understanding cardiovascular health and disease [32].

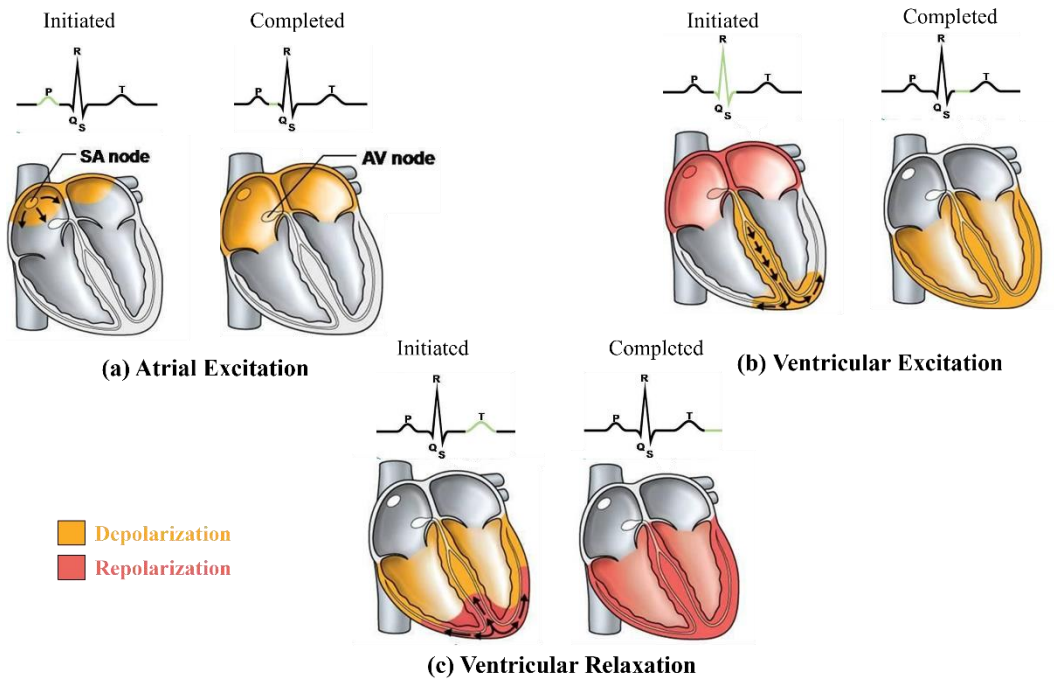


Figure 1. 4: Electrical Conduction Pathway of Heart

Part of the picture is taken from https://ptreviewer.com/

1.5.2. Electrocardiogram (ECG) Signal

An ECG is a diagnostic tool used to measure the electrical activity of the heart. It records the voltage changes produced on the body surface by the heart's electrical activity and displays them graphically as shown in Figure 1. 4. The ECG is essential in diagnosing various heart

diseases and serves as a foundation for investigating HRV, QT variability, and other autonomic markers relevant to neurodegenerative diseases like RBD [33].

1.5.3. Waves and complexes of the ECG Signal

Figure 1. 5: Typical ECG wave with Components represent a typical ECG signal which is composed of several waves and complexes that represent different phases of the heart's electrical activity, named by Willem Einthoven. The P wave is associated to the depolarization of the atria, lasting about 80-100 milliseconds. Following this is the QRS complex, which represents ventricular depolarization. It includes three distinct parts: the Q wave, a small downward deflection, the R wave, a sharp upward peak, and the S wave, another downward deflection. This complex lasts between 80 and 120 milliseconds and is the most prominent part of the ECG signal. After ventricular depolarization, the T wave appears, reflecting ventricular repolarization as the heart prepares for the next cycle. Occasionally, a U wave may follow the T wave, though its origin is not entirely clear, and it is thought to represent after-potentials in the ventricles or delayed repolarization of the Purkinje fibres. The PR interval, measured from the start of the P wave to the beginning of the QRS complex, indicates the time it takes for electrical impulses to travel from the atria to the ventricles, typically ranging from 120 to 200 milliseconds. Another important component is the QT interval, spanning from the start of the Q wave to the end of the T wave, which reflects the total time for ventricular depolarization and repolarization. Lastly, the RR interval, the time between two consecutive R waves, is reflects the balance between the sympathetic and parasympathetic nervous systems [33].

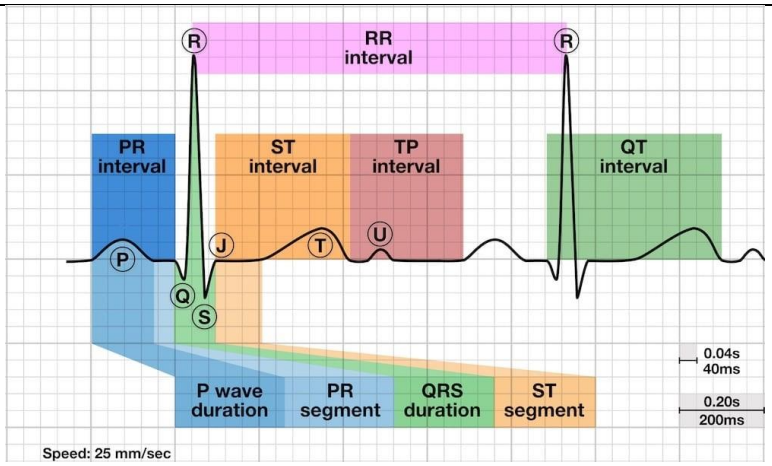


Figure 1. 5: Typical ECG wave with Components

1.6. Heart Rate Variability (HRV)

HRV refers to the physiological phenomenon of variation in the time interval between heartbeats, measured through the variability in beat-to-beat intervals as seen in Figure 1. 6. This variability is a crucial indicator of ANS function, reflecting the balance between SNS and PNS activity. The measurement of HRV is performed by detecting R-peaks from ECG signal, which are considered the gold standard due to their accuracy in capturing the electrical rhythm of the heart [29, 31].

1.6.1. Significance of HRV

HRV is significant as it serves as a non-invasive marker of ANS function and overall cardiovascular health. High HRV is generally associated with good health, resilience to stress, and effective recovery from exertion, while low HRV can indicate stress, fatigue, or underlying health issues such as cardiovascular disease. Studies have shown that individuals with higher HRV tend to have better outcomes in various health contexts, including lower mortality rates following myocardial infarction and improved recovery. Studying HRV particularly in context of RBD is significantly important as it is a key biomarker for assessing autonomic dysfunction

that can provide early insights into the risk of disease progression [29, 31]. Another important contributor to physiological HRV is respiratory sinus arrhythmia (RSA), a natural variation in heart rate that occurs with the breathing cycle. RSA reflects the parasympathetic regulation of the heart, with heart rate increasing during inhalation and decreasing during exhalation. This physiological component of HRV indicates healthy autonomic function and cardiovascular adaptability.

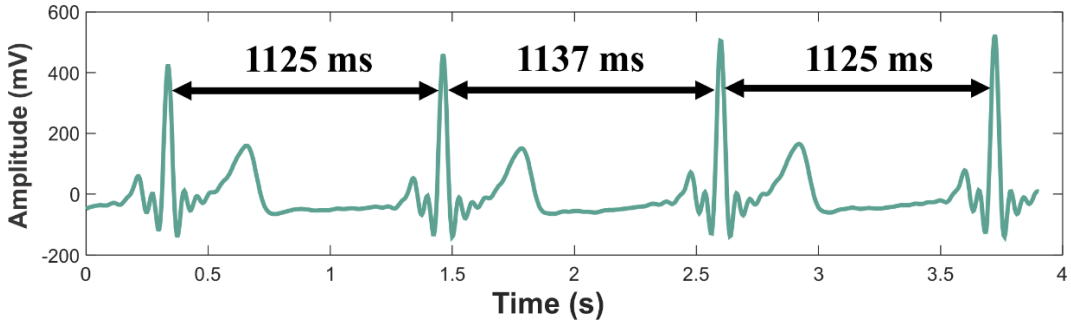


Figure 1. 6: Example of RR Intervals

1.7. QT Variability (QTV)

QTV refers to the physiological phenomenon of variation in the time interval between the onset of the Q-wave and the end of the T-wave in the cardiac cycle as seen in Figure 1. 7. This variability reflects fluctuations in ventricular depolarization and repolarization times, offering insight into myocardial electrophysiological stability. The measurement of QTV is performed by detecting Q-onsets and T-ends from the ECG signal, with the QT interval serving as a key biomarker for assessing ventricular function. Accurate detection of Q and T points is essential for capturing fluctuations in cardiac electrical repolarization. QTV is particularly an important biomarker for detecting autonomic dysfunction, especially when the dysfunction affects ventricular repolarization, which may not always be captured by HRV alone [30, 31].

1.7.1. Significance of QTV

QTV is significant as it serves as a non-invasive marker of ventricular repolarization variability and overall cardiac electrophysiological health. Increased QTV has been associated with an increased risk of arrhythmias, sudden cardiac death, and proarrhythmic drug effects. While reduced QTV, may indicate improved myocardial stability. The clinical relevance of QTV is important to study the relation between increased QTV and cardiac dysfunction, ischemia, and mortality, particularly in patients with heart failure or post-myocardial infarction. Monitoring QTV provides critical insights into autonomic control, cardiac stress, and potential drug-induced proarrhythmic effects. Thus, QTV holds significant importance for studying the RBD population [30, 31].

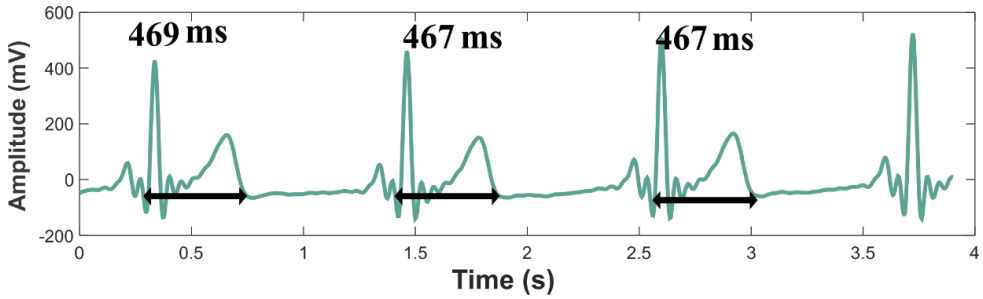


Figure 1. 7: Example of QT Intervals

1.8. Confounding factors of HRV and QTV

Several confounding factors can influence both HRV and QTV measurements, complicating their interpretation. Factors such as age, gender, physical fitness levels, and lifestyle habits (including diet and sleep quality) play a role in modulating these cardiac biomarkers. Respiratory rate is a key confounder for HRV, as breathing patterns directly influence parasympathetic activity, while for QTV, it can indirectly affect repolarization variability through changes in autonomic balance. Acute stressors, such as illness, emotional distress, or physical pain, can reduce HRV and increase QTV due to shifts in sympathetic and parasympathetic activity. Environmental conditions, such as temperature and altitude, also

impact autonomic regulation, thereby affecting both HRV and QTV. Since HRV reflects autonomic control of heart rate and QTV reflects variability in ventricular repolarization, understanding these confounding factors is essential for accurately interpreting these biomarkers in relation to cardiac health, autonomic dysfunction, and neurodegenerative disease prognosis [34, 35].

Chapter 2: Dataset

2.1. Polysomnography (PSG)

PSG is a comprehensive diagnostic examination used to assess and monitor various physiological parameters during sleep. The typical setup of PSG exam is displayed in Figure 2. 1. It is considered the gold standard for diagnosing a range of sleep disorders, including obstructive sleep apnea (OSA), restless legs syndrome, narcolepsy, insomnia, and parasomnias such as sleepwalking or RBD. The test is typically conducted overnight in a sleep laboratory or, in some cases, at home with portable equipment, depending on the clinical need [36].

During a polysomnography exam, multiple physiological signals are recorded simultaneously to provide a detailed understanding of sleep architecture and any underlying abnormalities. These signals include brain activity, measured through an electroencephalogram (EEG), which helps identifying different stages of sleep and their transitions. Eye movements are tracked using the electrooculogram (EOG), providing information about REM sleep. Muscle activity, particularly in the chin and legs, is recorded via an electromyogram (EMG) to detect issues such as periodic limb movements or muscle atonia during REM sleep. Breathing patterns are closely monitored, including airflow through the nose and mouth, as well as chest and abdominal movements, to identify disruptions such as apneas or hypopneas. Blood oxygen levels are measured using pulse oximetry to assess oxygen desaturation during sleep. Additionally, heart activity is recorded using an ECG, and body position is tracked to correlate posture with breathing disturbances [36].

For parasomnias like RBD, video recording in the sleep laboratory is also performed as it is a critical component of PSG. Video monitoring allows for direct observation and documentation of abnormal movements or behaviors during sleep, which is essential for differentiating RBD from other disorders and assessing the severity of the condition. This visual data, when

combined with the physiological recordings, provides a more comprehensive understanding of the patient's sleep and allows reaching an accurate diagnosis.

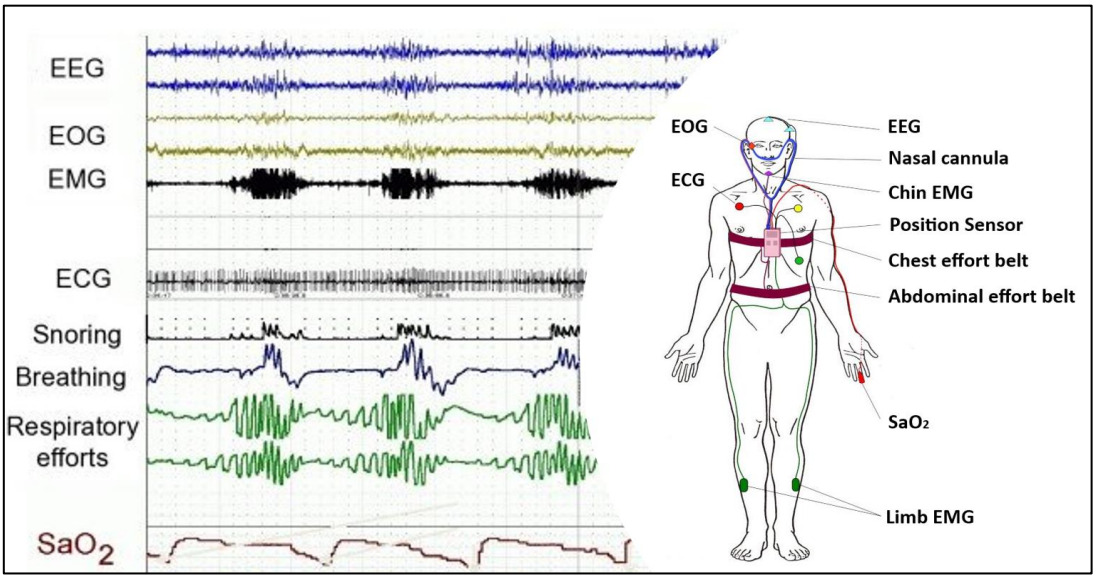


Figure 2. 1: Example Polysomnographic Exam

The data collected during PSG offers a comprehensive overview of an individual's sleep, not uncovering only its structure and quality but also identifying disruptions caused by breathing irregularities, abnormal movements, autonomic dysfunction, and other contributing factors. This diagnostic tool is invaluable for understanding the intricate connections between sleep and overall health, playing a critical role in enhancing patient outcomes through accurate diagnosis and targeted treatment strategies

2.2. PSG Data Acquisition

The PSG data acquisition for this study utilized advanced equipment to ensure high-quality recordings, reflecting the reliability and precision required for sleep research. At the Interdepartmental Centre for Sleep Medicine of the University of Cagliari, data collection was conducted using the Morpheus EEGv-PSG Holter system (Micromed S.p.A., Treviso, Italy).

This system is widely recognized for its ability to record high-quality sleep data, making it a preferred choice for use in sleep laboratories. For this study, all data collected at this institute were based exclusively on laboratory settings, ensuring a controlled environment for comprehensive polysomnographic evaluations.

Conversely, at the Sleep and Epilepsy Centre of the IRCCS San Martino Hospital of the University of Genova, data were acquired using the BE Plus LTM with MizAR 40 system (EBN Euro S.p.A., Firenze, Italy). This system is similarly esteemed for its capability to deliver high-quality multimodal data. Unlike the Cagliari site, the Genova center extended data acquisition to include some home-based recording, allowing for a more naturalistic assessment of sleep patterns in addition to traditional laboratory settings. This dual approach enhanced the ecological validity of the data while maintaining high standards of accuracy.

Both institutes performed full-night video-polysomnographic (VPSG) exams, incorporating multimodal data acquisition. The standardized montages included six EEG leads (F3-A2, F4-A1, C3-A2, C4-A1, O1-A2, O2-A1), left and right EOG channels for tracking eye movements, and bilateral surface EMG channels to monitor the submentalis muscle, flexor digitorum superficialis (FDS) on the upper limbs, and tibialis anterior on the lower limbs. Additional physiological parameters recorded included ECG for cardiac activity, respiratory signals captured using thermistors and nasal pressure sensors, oxygen saturation (SpO2) measured by a cutaneous finger pulse oximeter, and audio data recorded via a microphone to detect snoring or other sleep-related sounds.

The integration of high-quality data from both controlled laboratory environments and home-based recordings offers a comprehensive and versatile dataset. This approach ensures precise evaluation of sleep architecture, autonomic function, respiratory dynamics, and movement-related abnormalities, contributing significantly to advancing research in sleep medicine.

2.3. Demographic, Clinical and PSG Features

Apart from the PSG biosignals, additional demographic, clinical, and PSG-derived features are available for the study population. These variables provide comprehensive context and facilitate more robust analysis. The demographic information includes gender (male/female) and age, which are essential for understanding population characteristics and potential confounding factors. Clinical sleep-related measures derived from PSG include TBT in minutes, TST in minute), and SE in %, which collectively offer insight into sleep continuity and efficiency. Other sleep architecture-related metrics include SL in minutes, number of awakenings, and WASO in minutes, which quantify disruptions during sleep. Additionally, sleep stage distribution is captured through the percentage of time spent in N1, N2, N3, and REM sleep. Moreover, the data set also includes sleep-disordered breathing and movement indexes i.e., the periodic limb movement index (PLMI), apnea-hypopnea index (AHI), and oxygen desaturation index (ODI), provide critical information on respiratory and motor abnormalities during sleep. Collectively, these variables along the PSG biosignals, offering a multidimensional perspective on sleep physiology and in comprehensive analysis of the study population.

2.4. Sleep Scoring Criteria

The Interdepartmental Centre for Sleep Medicine of the University of Cagliari and the Sleep and Epilepsy Centre of the IRCCS San Martino Hospital of the University of Genova, both followed a standardized protocol for sleep stage scoring to ensure consistency and reliability across datasets. Sleep staging was manually performed by trained technicians or clinicians, in accordance with the criteria established by AASM, 2013[6] By adhering to these standardized criteria, both centers ensured accurate, reproducible, and comparable data analysis across all

participants. The uniform scoring methodology not only facilitates inter-center collaboration but also strengthens the validity and generalizability of the study findings.

2.5. Diagnosis of the relevant conditions

The diagnosis of Idiopathic REM Sleep Behavior Disorder (iRBD), Parkinson's Disease (PD), and Parkinson's Disease with RBD (PD-RBD) was conducted using standardized and international guidelines widely accepted criteria. [37–39]:

Participants with iRBD were diagnosed in accordance with the criteria outlined in the International Classification of Sleep Disorders, Third Edition (ICSD-3). This diagnostic criterion defines iRBD as a parasomnia characterized by the absence of muscle atonia during REM sleep, often accompanied by complex motor behaviors or vocalizations that align with dream content. Diagnosis requires confirmation via PSG, which detects REM sleep without atonia (RWA) and excludes other potential causes of similar symptoms, such as neurodegenerative conditions or medication effects [37, 38].

Participants with PD were diagnosed using the Movement Disorder Society (MDS) Clinical Diagnostic Criteria for Parkinson's Disease. This includes the presence of cardinal motor features (bradykinesia, rigidity, tremor) and the exclusion of secondary causes of parkinsonism. Additional support for the diagnosis is often provided by non-motor symptoms such as hyposmia, constipation, and sleep disturbances, which are common in PD patients [39].

For participants diagnosed with PD-RBD, the ICSD-3 criteria for RBD were applied alongside the MDS Clinical Diagnostic Criteria for Parkinson's Disease. These criteria require the presence of motor symptoms characteristic of PD, such as bradykinesia, rigidity, or resting tremors, combined with evidence of RBD on PSG. The co-occurrence of RBD and PD has been linked to specific phenotypic and pathophysiological features, providing valuable insights into disease progression [37–39].

2.6. Study Population

The study population comprised a total of 135 participants, distributed into four well-defined groups based on their diagnosis. The distribution of age and gender is visually presented in Figure 2. 2. These groups were carefully selected to provide a robust dataset for analyzing HRV and other physiological parameters in relation to neurodegenerative diseases and sleep disorders. The participants were grouped as follows:

Control group (CG): The control group consisted of 35 unaffected participants with no history of neurological or sleep disorders. This group served as the baseline reference for comparisons. The mean age of the control participants was 59 ± 10 years. Approximately one half (46%) of the participants in this group were male. These participants were screened to ensure the absence of confounding conditions such as arrhythmias, sleep apnea, or other sleep-related breathing disorders.

The iRBD group, comprising 98 participants, included individuals with confirmed idiopathic RBD but without any diagnosed neurodegenerative disease at the time of the study. The mean age in this group was 67 ± 8 years. The majority of the participants in this group (73%) were male, which is consistent with the known male predominance in RBD prevalence. The inclusion of this group was essential for exploring HRV and autonomic dysfunction as potential early biomarkers for neurodegenerative diseases, given the known progression of iRBD to conditions like PD or dementia.

The PD group included 31 participants diagnosed with the mean age of this group was 67 ± 10 years, indicating a population largely reflective of the typical age range for PD diagnosis. Gender distribution in this group was balanced, with 50% male participants.

PD-RBD Group consisted of 60 participants diagnosed with both PD and RBD, representing a critical intersection of neurodegenerative and parasomnia conditions. The mean age of the PD-

RBD group was 71 ± 10 years, making it the oldest cohort in the study. Male participants made up 66% of this group, again consistent with the higher prevalence of RBD in males. The presence of RBD in these patients increases the complexity to the clinical characteristics, making them an important subgroup for understanding the interplay between PD, sleep disturbances, and autonomic dysfunction.

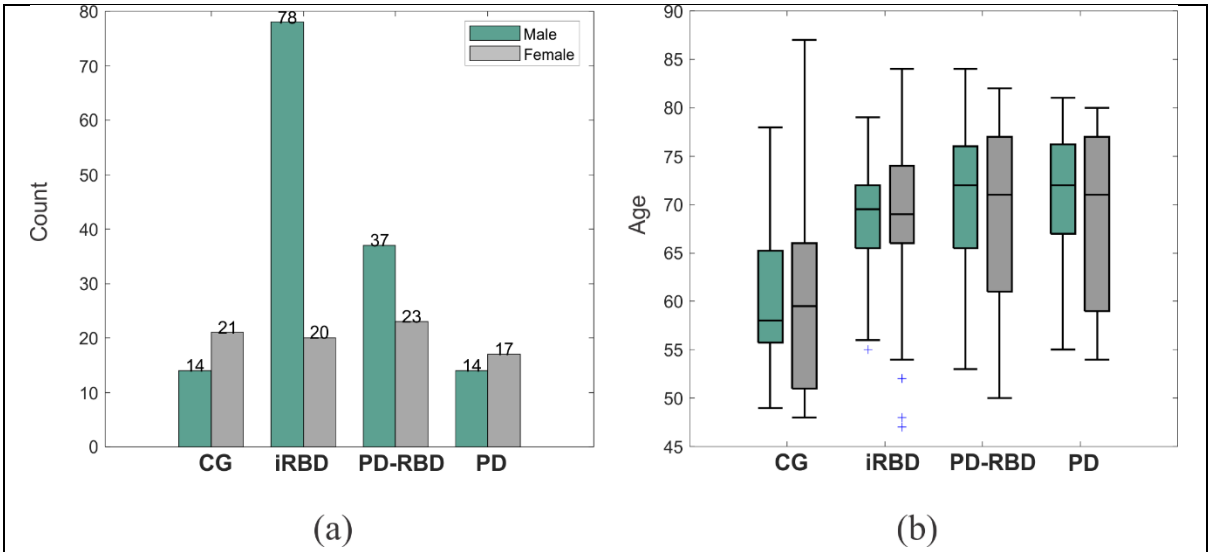


Figure 2. 2: (a) Gender Distribution Across Groups (b) Age Distribution Gender wise Across the Groups

2.7. Inclusion Criteria:

The inclusion criteria for this study include participants who underwent a full-night vPSG examination, ensuring comprehensive physiological data collection. Additionally, individuals diagnosed as iRBD, PD, or PD-RBD were included in the study. The diagnoses were established based on the criteria mentioned above.

2.8. Exclusion Criteria:

To maintain the integrity and homogeneity of the dataset, exclusion criteria were uniformly applied across all study groups. Participants with arrhythmias or cardiac pacing devices were excluded, as these conditions could significantly alter heart rate dynamics and confound the

analysis of HRV Similarly, individuals diagnosed with sleep apnea or other sleep-related breathing disorders, as defined by the ICSD-3, were excluded to avoid physiological interference from these conditions. Participants taking pharmacological treatments that influence heart rate or HRV were also excluded, ensuring that the autonomic function measured during the study reflected the natural state without medication-induced variability.

For the affected groups, including individuals with iRBD, PD-RBD, and PD, additional exclusions were implemented. Patients with any neurological or sleep disorders beyond RBD and PD were excluded, as these could introduce variability unrelated to the primary conditions of interest. For the control group, the exclusion criteria were even more stringent, i.e., people with no history of neurological or sleep-related diseases were considered.

A specific exclusion criteria was applied to PD and PD-RBD groups regarding dopaminergic therapy. Patients under treatment with such medications were excluded due to the known effects of dopaminergic drugs on EEG synchronization, sleep quality, and HRV. These medications can cause significant fluctuations in autonomic and regulatory processes, especially during ON and OFF states, as seen in Parkinson's patients with motor symptoms such as freezing of gait. By excluding participants on dopaminergic therapy, the study ensured that the observed physiological changes were intrinsic to the conditions under investigation rather than influenced by pharmacological interventions. This rigorous application of exclusion criteria was essential for isolating the relevant autonomic and physiological features, allowing for reliable and meaningful analysis.

2.9. Ethical Approval:

The research was conducted in compliance with the highest ethical standards and received approval from relevant institutional review boards. Ethical clearance was granted by the Institutional Review Committee of the University Hospital of Cagliari (Approval Reference:

PG/2018/11699) and the Neurology Clinics at Policlinico San Martino in Genoa (IRB Approval Number: 105/2023 – Database ID: 13027). The study adhered to the principles outlined in the Declaration of Helsinki, ensuring the protection of participants' rights, safety, and well-being throughout the research process. Prior to participation, all patients provided written informed consent, acknowledging their voluntary involvement and the confidentiality of their data. This ethical framework ensured the study was conducted responsibly and transparently.

2.10. Challenges in ECG Data: Signal Quality and Sleep Stage Duration:

The quality of ECG signals was a critical factor in this study, directly influencing the reliability of HRV analysis across different sleep stages. Ensuring artifact-free signal segments posed significant challenges, particularly during specific phases of sleep, due to both physiological activity and technical limitations. Among all the sleep stages, the REM phase was most affected by signal quality issues as represented in Figure 2. 3 (b). The more intense physiological activity during REM sleep—including rapid eye movements, muscle twitches, and irregular breathing patterns—causes substantial noise and artifacts, complicating the detection of clean ECG data. This limitation reduced the availability of continuous, long REM-phase ECG segments, as depicted in Figure 2. 3 (a).

In contrast, the N1 sleep stage offered the shortest data segments for the analysis. Typically, N1 exhibit a short duration within the sleep cycle. As shown in Figure 2. 3 (a) the durations of all identified N1 phases were generally brief, with the longest segment of approximately 200 seconds. This limited the analysis of HRV parameters during the N1 stage

2.11. Data Preprocessing:

To ensure accurate HRV analysis, a systematic process was employed to preprocess and extract ECG signals from distinct sleep phases (N1, N2, N3, REM, and wakefulness). Initially, a

hypnogram was generated to segment the ECG signals according to these phases. Each segment was then visually inspected for artifacts, and significantly noisy segments were rejected.

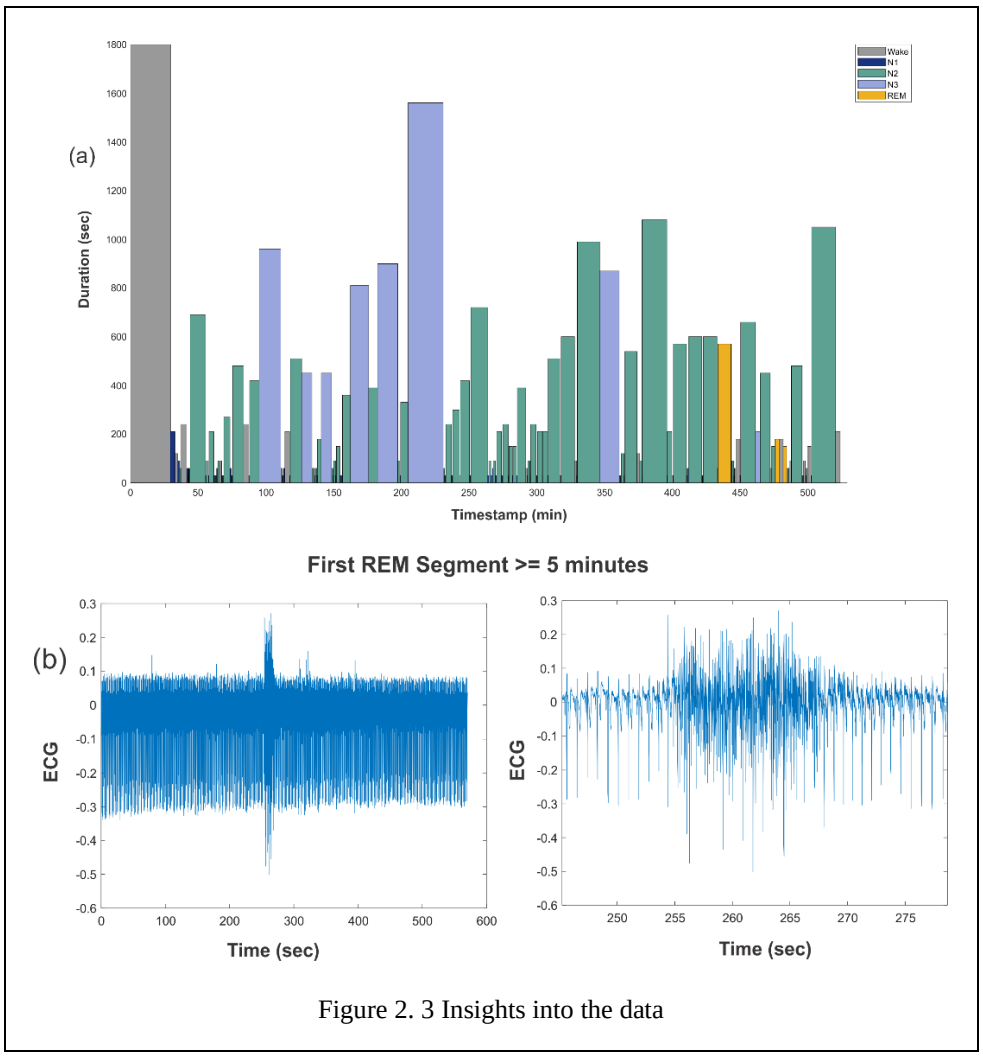


Figure 2. 3 Insights into the data

A wavelet-based ECG delineator was employed for the automatic R-peak annotation [40]. Since this algorithm has been conceived for signals sampled at 250 Hz, during R-peak detection all ECG signals have been down-sampled to 256 Hz. However, the original sampling frequencies varied across subjects, as detailed in Table 2. 1. To address this inconsistency and standardize the data for subsequent analysis, all ECG signals were up-sampled to 512 Hz after R-peak annotations, the position of the R-peak refined at the highest sampling rate to improve the precision of HRV computations.

Table 2. 1: Distribution of the original sampling frequencies of the signals included in the study:

Groups	**128 Hz**	**256 Hz**	**512 Hz**
CG	3	12	20
iRBD	16	29	53
PD-RBD	3	47	10
PD	0	31	0

R-peak refinement was performed by considering a window of 0.02 s around the detected peak to avoid any bias in RR intervals estimation. Moreover, we also automatically examined the tachograms for any false positive or negative R-peak detection, by comparing all the estimated RR intervals with the median RR interval. The false positive R-peaks, where RR interval was less than 70% of the median RR interval, were removed. Conversely, the false negative R-peaks, where RR interval(s) exceeded 15% of the median RR interval, were corrected by partitioning the distance between the two correctly detected R-peaks according to the median RR-interval. This procedure was then followed by R-peak refinement. Epochs with more than 3 missing R-peaks were excluded.

Chapter 3: Development of Customized Tool for HRV Analysis during sleep[3]

HRV analysis during sleep plays a key role for understanding autonomic nervous system function and assessing cardiovascular health. The UNICA Sleep HRV analysis (UNICA-HRV) tool is a novel, open-source MATLAB tool designed to fill the gap in current HRV analysis tools. In particular, the integration of ECG and HRV data with hypnogram information, which illustrates the progression through the different sleep stages, ease the computation of HRV metrics in polysomnographic recordings. This integration is crucial for accurate phase-specific analysis, as autonomic regulation changes markedly across different sleep stages. The tool supports single- and multiple-subject analyses and is tailored to enhance usability and accessibility for researchers and clinicians without requiring extensive technical expertise. It implements and supports a variety of data inputs and configurations, allowing for flexible, detailed HRV analyses across sleep stages, employing classical and advanced metrics, such as time-domain, frequency-domain, non-linear, complexity, and Poincaré plot indexes. Validation of the tool against established tools like Kubios and PhysioZoo indicates its robustness and precision in generating reliable HRV metrics, that are essential not only for sleep research, but also for clinical diagnostics. The introduction of UNICA-HRV represents a significant simplification for sleep studies, and its open-source nature (licensed under a Creative Commons Attribution 4.0 International License) allows to easily extend the functionality to other needs.

3.1. Introduction

HRV provides hints on the ANS status. HRV analysis dates back to the early 1960s, when it was initially used to study fetal distress during labor [41]. The technique gained more attention in the 1970s, when Akselrod [42] demonstrated its value in understanding autonomic regulation through spectral analysis. Then, HRV analysis has become an important tool for evaluating cardiac health and detecting autonomic dysfunction [43, 44]. It serves as a valuable indicator of physiological resilience and adaptability [45]. HRV has diverse applications across various

[3] Note: This chapter/part of the chapter is the reprint of article submitted in the physiological measurements journal

fields, including medical diagnosis [46], sports science [47], and mental health [48]. Clinical studies have proved its utility for the diagnosis of myocardial infarction [49], the detection of atrial fibrillation [46], the scoring of sepsis severity [50], the diagnosis of obstructive sleep apnea [51], and the measurement of mental stress levels [52], just to cite a few application areas.

HRV analysis is highly sensitive to accurate R-peak detection [53–55]. However, detecting R-peaks accurately can be challenging due to noise, ectopic beats [56], and the intrinsic variability of ECG waveforms. Noise can stem from various sources, such as muscle contractions, electrode movement, respiration, or external electrical interference, hampering the correct R-peak annotation [57]. Ectopic beats complicate the detection process by introducing anomalous waveforms, compared to normal heart cycles, that do not follow the other cycles' timing. Additionally, the morphology of ECG signals exhibits not only a strong inter-individual variability, but also an intra-individual variability due to different physiological and pathological conditions, further complicating the R-peak detection process [58]. Therefore, the availability of graphical user interfaces (GUI) that facilitate accurate visualization/correction of R-peak annotations by automatic software routines is of paramount importance. Moreover, significant advancements in HRV research have been fostered by the development and release of tools for the automatic computation of the different indexes. HRV analysis software such as Kubios [59], PhysioZoo [60], HRVAS [61], gHRV [62] and HRnV-Calc [63], although well-established and reliable, suffer some limitations when used on polysomnographic data analysis. In fact, none of them can allow the full-night HRV analysis on a sleep-stage-basis, i.e., by performing the analysis in the different sleep stages. This is because currently available tools do not incorporate hypnogram data, so the automatic segmentation of the traces according to this signal is not supported. However, the analysis of HRV evolution during the different sleep

stages is fundamental to understand possible ANS dysregulations impacting the overall sleep structure [64].

Based on the significant use of HRV analysis in sleep research, and considered the limits of current solutions, we present an open-source tool for sleep-related HRV analysis based on a MATLAB GUI not requiring any programming skill. This tool simplifies HRV analysis in sleep studies by integrating hypnogram data in order to enable the analysis separately in the different sleep stages, including several presets for automatic analysis. Developed with a strong interaction with the neurologists specialized in sleep studies, it was expressly conceived to support both clinical and non-clinical researchers, regardless of their technical or programming expertise on the use of similar tools, by putting in a single GUI all the controls and analysis results they need. UNICA-HRV, version 1.0, is licensed under a Creative Commons Attribution 4.0 International License and can be downloaded from Zenodo website.

3.2. Development of Sleep Heart Rate Variability Analysis tool

This section presents an in-depth exploration of the UNICA Sleep HRV Analysis tool (UNICA-HRV), detailing both the front-end user interface, which allows for intuitive interaction and data visualization, as well as the back-end framework, which manages data processing and algorithmic computations for HRV analysis.

3.2.1. Overview of Front End

Figure 3. 1: Layout of UNICA Sleep HRV Analysis tool displays the front-end layout of the UNICA-HRV. Different panels group the features required for the analysis to facilitate their use. On the top left side, the Data Input & Configuration area allows users to import single or multiple-subject ECG signals from ECG/PSG files for (batch) analyses. This area also enables users to specify the sampling rate of the data and supports resampling and plot features.

Moreover, users can select the specific sleep phases and relative segments, as well as the time window to be displayed, expressed in different units. Just below it, the ECG Display Panel shows the imported ECG trace with R-peak annotations marked by the automatic QRS-detection algorithm featured by the back-end of the tool, enabling manual correction of misplaced peaks. Next to the Data Input & Configuration area, the Analysis Configuration area enables users to specify various analysis methods and perform the QRS detection. The HRV Analysis Panel allows starting the computation of the HRV metrics; it also shows, in different tabs, the results of the performed analysis in a simple and interactive way. On the top right, the Output File Generation area allows users to save obtained HRV metrics, the ECG signal and the associated R-peak annotations. All these panels are better detailed in the following sections.

Hereafter, the settings and features supporting single individual and batch analyses of multiple subjects are presented, whereas the detail of the signal processing methods adopted to achieve them is reported in the next section.

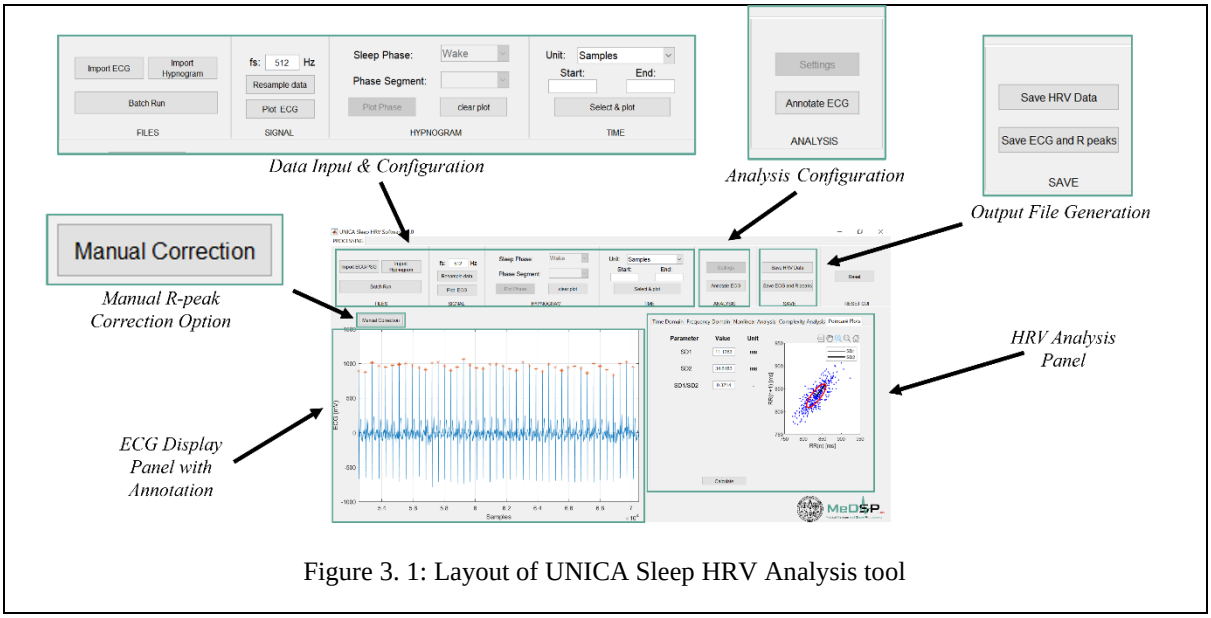


Figure 3. 1: Layout of UNICA Sleep HRV Analysis tool

i. Single-subject assessment

A. Data Input and Configuration section

In this section, both ECG and hypnogram files are managed. ECG signals acquired from either polysomnography (PSG) data or just ECG recordings can be uploaded in the software using the "Import ECG/PSG" button, which opens the operating system window for the file selection. The current implementation of the software computes everything from the raw ECG signal, so it is not designed to accept tachograms (i.e., the time series of the RR intervals). The accepted file formats for raw ECG signals, both single- and multi-channel, are: .mat, .edf, and .txt. As the software is conceived to analyze a single ECG lead, in case of multi-channel ECG data, the GUI requires the indication of the lead to be used for HRV analysis. Similarly, if PSG data is provided in input, provided that PSG is multichannel by nature, the software asks the user to specify the channel number containing the ECG signal.

After that, if an HRV analysis during sleep is pursued, users can select the "import hypnogram" button to load a file containing the hypnogram in .xlsx, .csv, or .txt formats. Remarkably, this step is not mandatory, as the UNICA-HRV enables HRV analysis also independently from sleep phases. If hypnogram data has been imported, the GUI presents a guided procedure to enable reading of hypnograms described in different formats, assuming that the information is stored column-wise. To this aim, users are prompted to select the criteria used to mark the sleep phases (i.e., duration, end time, or 30-second epochs). Then, the user needs to select the unit of measure and specify the column numbers for the relevant data, such as the start time column, end time/duration column, and phase label column. Then, a label-mapping interface (Figure 3.2) is prompted to associate the names adopted for the different

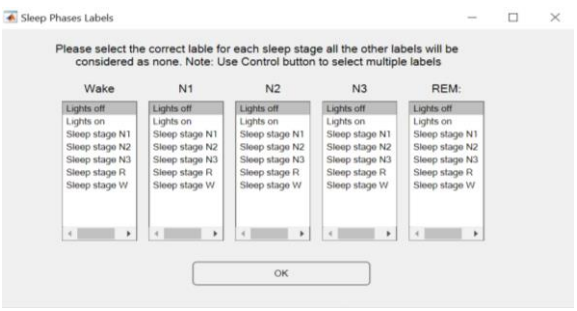


Figure 3. 2: Hypnogram labels mapping

sleep phases in the file with the unique ones used by the tool. At the moment, the software is designed to use the sleep stages described by the American Academy of sleep medicine (AASM) in their scoring criteria.

After successful data loading, the user must specify, in the “Signal” subsection, the sampling rate of the ECG to proceed in the analysis. In order to increase time resolution or reduce the number of samples of a long signal, the user can resample the ECG by pressing “Resample data” and entering the desired sampling rate.

In the “Hypnogram” subsection, users can select the specific sleep phase to be analyzed, and the specific segment of that phase, by selecting its number (segments are phase-wise progressively numbered, from the first to the last one). Once a segment of a given phase has been selected, users can choose to plot it by pressing the “Plot Phase” button. For improved visual inspection, the “Time” subsection allows users to extract a portion of the selected phase and segment, by specifying the start and end points, before pressing the “Select & plot” button.

In the same panel, the “Batch run” button allows for the multiple subjects’ assessment, as described in Section 3.2.1 (ii)

B. Analysis Configuration

This section encloses the settings and the modality for HRV analysis during sleep.

To perform the HRV analysis only on the selected phase and segment (either on the entire segment or on the specified timeframe of that segment), the user must click the “Annotate ECG” button. Then, the back-end performs the QRS detection at first, and the R-peak locations are marked with red mark on the display panel of the GUI. Once the annotation is over, the “Calculate” buttons are enabled, allowing users to compute a large number of HRV metrics,

including time domain, frequency domain, nonlinear, complexity-based, and Poincaré plot-based. An exemplary visual output of this computation is reported in Figure 3. 3.

Alternatively, HRV analysis can be automatically performed on the entire ECG, for all or specific sleep phases, via the "Settings" button in the "Analysis" subsection. Upon clicking the "Settings" button, a pop-up window with several options for analysis appears, as shown in Figure 3. 4. In this window, the desired sleep phase(s) for analysis can be chosen; for each of them, three options for the segments are proposed:

- all available ECG epochs of sleep phase/s regardless of their duration (Method AAE) are considered;
- all ECG epochs of sleep phase/s greater or equal to five minutes with 50% overlap (Method AEWO) are considered;
- the first five-minute ECG epoch of sleep phase/s only (Method FEO) is/are considered;

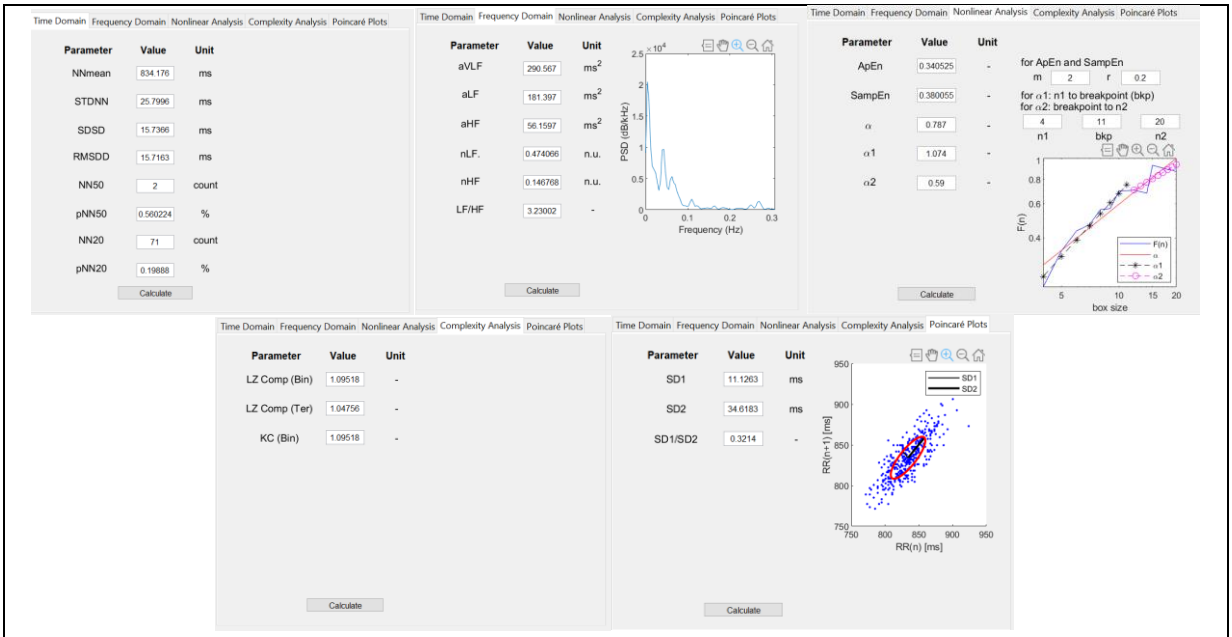


Figure 3. 3: Heart Rate Variability Analysis Panels

These options are offered because different HRV metrics are influenced by the duration of the analyzed segment. Notably, complex HRV metrics such as Detrended Fluctuation Analysis (DFA) require longer segments to accurately assess long-range correlations and chaotic behaviors. The three segment settings provided by the tool can be extended according to the researchers' needs. Once the users selected the appropriate method and sleep phase(s) for the analysis, they simply need to click the "Analyze" button to start the analysis. The software will then begin the analysis, displaying the current sleep phase and segment being analyzed along with the progress towards the end. Upon completion, the GUI will automatically generate a .mat file and an .xlsx file for each analyzed sleep phase. More details on the generated output files are provided in the following section.

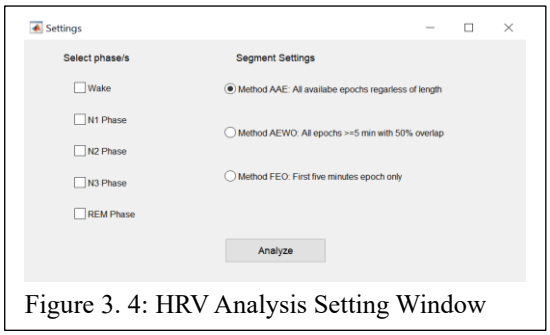


Figure 3. 4: HRV Analysis Setting Window

C. Output File Generation section

The GUI generates two distinct output files: a .mat file and an .xlsx file for the selected sleep phase(s). The former consists of a two-column table variable: the first column contains the segmented ECG signals of a given phase, according to the user settings, while the second column contains the locations of the R peaks within that ECG segment. This file enables the creation of a dataset for further comparative analyses, review, or can be employed for further HRV metrics and feature extraction.

The second output is an .xlsx file structured to facilitate statistical analyses. It begins with two columns indicating the start and end times of the ECG segments, respectively, followed by the segment number/information, and 25 additional columns, each one representing a different HRV metric. These include time domain, frequency domain, nonlinear, complexity-based, and Poincaré plot-based indexes. The .xlsx file also includes a report on issues encountered during the analysis, which includes data quality concerns or annotation errors. Examples:

- If the analysis was targeting ECG segment in N1 phase of 5 minutes or longer, and no segment with such characteristics can be extracted, the Excel file will report that no N1 phase of the required length is available in the ‘segment information’ column.
- If the data is corrupted by noise, it will be reported that QRS detection could not be trustable due to poor signal quality. In this case, users can manually review the specific segment in the .mat file using the provided start and end time information.

ii. Multiple subjects’ assessment (batch analysis)

Multiple subjects’ analyses are allowed by the “Batch Run” button in the “Files” subsection.

In case of HRV analysis during sleep, to run a multiple subjects’ analysis, the user must provide the software with the hypnogram files and their corresponding ECG data files with identical names (regardless of the file extension). This naming consistency is crucial for the back-end to analyze matched files, considering that the procedure is completely automatized. In case ECG and hypnograms are both in .txt format, the naming consistency requires them to be stored in different folders, as the simultaneous existence of the files with the same name and extension is impossible. Upon all hypnogram data files loaded, the GUI asks if the hypnograms have a uniform file structure among them or not. If not, the GUI will present the guided procedure to enable reading of hypnograms described in different formats, including the phase-labelling mapping (Figure 3. 2) for each file, otherwise only once.

From this point on, the procedure is similar to that described in the single-subject case when uploading PSG or ECG files: the back-end checks whether all ECG files are uniformly structured and share the same sampling frequency. If so, the GUI prompts the PSG or ECG data setup window only once, otherwise the GUI will provide the handling and configuration options separately for each file, requiring the selection of a uniform sampling rate for all the recordings.

This approach ensures the correct handling and analysis of both homogeneous and heterogeneous datasets, avoiding uncoherent parameterizations and preventing errors. Once the hypnogram and ECG data files have been correctly loaded, the GUI will prompt the HRV Analysis Setting Window (Figure 3. 4), as in the single-subject case, to proceed with the same analysis approach on the whole dataset. During the analysis, the GUI provides real-time updates on the processing, indicating the specific subject, sleep phase, and segment currently being processed. Upon completion, the GUI will display a notification indicating the directory where the generated files have been saved, following the format previously described. These output files retain the names of the originally uploaded files but include a prefix corresponding to the selected sleep phase (e.g., N2-SN0012).

3.2.2. Overview of Back End

i. ECG data pre-processing

The ECG pre-processing consists in a single zero-phase bandpass filtering between 0.67 Hz [65] and 100 Hz [66], like in other HRV analysis tools [67], to attenuate baseline wander, respiration artifacts and high-frequency noise. According to the chosen QRS detection algorithm downstream, there is no need for a more aggressive filtering, thus preserving the possibility to analyze and correct the R-peak annotations on a signal with adequate morphology. This is obtained by using a 4th-order Butterworth infinite impulse response (IIR) filter applied bidirectionally to obtain a zero-phase response without delays and phase distortions [68, 69].

ii. QRS detection

A renowned wavelet-based QRS detector [40] was selected to accurately identify the R peaks. As the optimal performance of this delineator is achieved at a sampling frequency of about

250 Hz, the back-end resamples all the input signals to match this sampling frequency, resampling back to the selected sampling frequencies after the detection has been accomplished. To ensure an accurate marking of the R-peak locations, a refinement process is implemented on the output of the QRS detector: a window with a number of samples equal to the maximum between ±10 samples and ±20 ms around the identified R peaks is used to detect the exact maxima/minima location corresponding to the R-peaks after resampling. This refined information is used to create the tachograms, which are automatically inspected by the back-end to identify and correct potential false positives or negatives in R-peak detection by comparing all estimated RR intervals against the median RR interval: RR intervals that are less than 70% of the median RR interval are assumed to be the effect of a false positive, whereas false negatives are associated to RR intervals larger than 130% of the median RR interval. In the former case, the second R peak contributing to the suspicious RR interval is deleted; in the latter, missing beat annotations are added. The location of the missing annotations is determined as follows: the distance between two detected R peaks is measured and compared to the median RR interval; if it is twice larger, a single R peak is added. Similarly, up to three R-peak may be added, depending on the RR distance. This procedure is then followed by subsequent R-peak refinement. Remarkably, epochs with more than three missing R peaks are discarded as noise-corrupted by the back-end, ensuring signal integrity and reliability in the analysis.

iii. Featured Heart Rate Variability Metrics

The back-end implements different HRV analysis metrics including time-domain, frequency-domain, non-linear, complexity-based, and Poincaré plot based.

Time Domain Analysis: The following time-domain parameters are computed by the back-end (see Table 3. 1 for the mathematical definition):

1. the mean normal-to-normal (NN) RR interval (NNmean), where "normal" is referred to a physiological beat,
2. standard deviation of all NN intervals (STDNN),
3. standard deviation of differences between adjacent NN intervals (SDSD),
4. square root of the mean of the sum of the squares of differences between adjacent NN intervals (RMSDD),
5. number of adjacent NN interval pairs with differences greater than 50 ms (NN50),
6. NN50 divided by total number of NN intervals (pNN50),
7. number of adjacent NN interval pairs with differences of greater than 20 ms (NN20),
8. NN20 divided by total number of NN intervals (pNN20).

Table 3. 1: HRV time-domain metrics [70]

Metrics	Unit	Formula
NNmean	ms	$\overline{NN} = \frac{1}{N}\sum_{i=1}^{N} NN_i$
STDNN	ms	$\text{STDNN} = \sqrt{\frac{1}{N-1}\sum_{i=1}^{N}\left(NN_i - \overline{NN}\right)^2}$
SDSD	ms	$\text{SDSD} = \sqrt{\frac{1}{N-1}\sum_{i=1}^{N-1}\left((NN_{i+1} - NN_i) - \overline{(NN_{i+1} - NN_i)}\right)^2}$
RMSSD	ms	$RMSSD = \sqrt{\frac{1}{N-1}\sum_{i=1}^{N-1}(NN_{i+1} - NN_i)^2}$
NN50	count	$NN50 = \#\{NN : \lvert NN_{i+1} - NN_i\rvert > 50ms\}$
pNN50	%	$pNN50 = \frac{NN50}{N} \times 100$
NN20	count	$NN20 = \#\{NN : \lvert NN_{i+1} - NN_i\rvert > 20ms\}$
pNN20	%	$pNN20 = \frac{NN20}{\#NN} \times 100$

Frequency Domain Analysis: The following frequency-domain parameters are computed by the back-end (see Table 3. 2 for the mathematical definition):

1. spectral power in the very-low frequency band (aVLF), i.e., in [0.0033 0.04] Hz range,
2. spectral power in the low frequency band (aLF), i.e., in [0.046 0.158] Hz range,
3. spectral power in the high frequency band (aHF), i.e., in [0.158 0.400] Hz range.

These metrics were computed in ms^2 using the Welch's method for the power spectral density estimation, performed on the interpolated tachograms (at 4 Hz) by cubic spline method. Furthermore, the following frequency indexes are also featured by the GUI:

1. normalized aLF (nLF),
2. normalized aHF (nHF),
3. ratio between the aLF and aHF, namely LF/HF [70]

Table 3. 2: HRV frequency-domain metrics [70]

Metrics	Unit	Formula
aVLF	ms^2	$aVLF = \int_{0}^{0.04} PSD(f)df$
aLF	ms^2	$aLF = \int_{0.04}^{0.15} PSD(f)df$
aHF	ms^2	$aHF = \int_{0.15}^{0.4} PSD(f)df$
nLF	n.u.	$nLF = \frac{aLF}{aLF + aHF}$
nHF	n.u.	$nHF = \frac{aHF}{aLF + aHF}$
LF/HF	a.u.	$\frac{LF}{HF} = \frac{aLF}{aHF}$

Non-linear HRV Analysis metrics: For non-linear HRV analysis, the back-end implements approximate entropy (ApEn) [71], sample entropy (SampEn) [71]and detrended fluctuation analysis (DFA) [72].

ApEn is used to quantify the amount of regularity and the unpredictability of fluctuations over time-series data. Mathematically, it is defined as:

$$ApEn(m,r,N) \approx -\frac{1}{N-m}\sum_{i=1}^{N-m} log\left[\frac{\sum_{j=1}^{N-m}(number\ of\ times\ that\ d[x_{m+1}(i),x_{m+1}(j)]\leq r)}{\sum_{j=1}^{N-m}(number\ of\ times\ that\ d[x_m(i),x_m(j)]\leq r)}\right] \quad (2.2)$$

where N is the number of NN intervals, m is the embedding dimension, i.e. the number of the compared runs, r is a filtering parameter, and d represents a distance function. The data of length *m* is examined for recurring pattern and to estimate the probability that other sequence of length *m* will be comparable, within a tolerance of *r*. As m and r should be fixed to compute ApEn, the back-end uses default values of m =2 and r = 0.2 fraction of standard deviation of NN interval. It is important to recall that ApEn is sensitive to the data size [71].

Conversely, SampEn is independent from the length of the data, and it is also a measure of time-series complexity. Basically, SampEn is an adaptation of ApEn that decreases the recalled bias by excluding self-matches. Similarly to ApEn, SampEn uses the parameters m and r [71]:

$$SampEn(m,r,N) = -log\left[\frac{\sum_{i=1}^{N-m}\sum_{j=1,j\neq 1}^{N-m}(number\ of\ times\ that\ d[x_{m+1}(i),x_{m+1}(j)]\leq r)}{\sum_{i=1}^{N-m}\sum_{j=1,j\neq 1}^{N-m}(number\ of\ times\ that\ d[x_m(i),x_m(j)]\leq r)}\right] \quad (2.2)$$

DFA is a powerful statistical method used to assess the fractal-like properties and correlation characteristics of non-stationary time series, such as HRV data. It helps in detecting long-range correlations in data that exhibit trends or non-stationarities. To perform the DFA analysis, the NN time series is integrated to create a cumulative sum, which effectively smooths out local fluctuation as per the equation below:

$$y(k) = \sum_{i=1}^{k}\left[NN(i) - \overline{NN}\right] \quad (2.3)$$

This integrated series $y(k)$ is then divided into non-overlapping windows of equal length n. Following this, within each window, a local linear trend is fitted and subtracted from the data,

obtaining the detrended fluctuation function, denoted as $F(n)$ as the root-mean-square of these integrated and detrended series. This procedure is calculated for each window size n.

$$F(n) = \sqrt{\frac{1}{N}\sum_{k=1}^{N}[y(k) - y_n(k)]^2} \quad (2.4)$$

Finally, the relationship between the $F(n)$ and the window size n is analyzed on a log-log scale. This relationship is typically linear for a wide range of window sizes, indicating the presence of scaling behavior. The slope of the line in the log-log plot, denoted as α, is calculated using linear regression and represents the overall scaling exponent. The equation for this linear relationship is:

$$\log F(n) = \alpha \log n + \beta \quad (2.5)$$

where α is the scaling exponent and β is the y-intercept of the log-log plot.

The GUI also provide calculation of two distinct scaling regions separated by a breakpoint (*bkp*), suggesting different scaling behaviors over short and long-time scales.

For Short-term Scaling Exponent (α_1) is calculated as:

$$\log F(n) = \alpha_1 \log n + \beta_1 \qquad \text{for } n \leq bkp \quad (2.6)$$

For Long-term Scaling Exponent (α_2) is calculated as

$$\log F(n) = \alpha_2 \log n + \beta_2 \qquad \text{for } n \leq bkp \quad (2.7)$$

Here, α_1 and β_1 are the slope and intercept for the short-term scaling region, respectively, and α_2 and β_2 are the slope and intercept for the long-term scaling region. These dual exponents provide a more nuanced understanding of the underlying dynamics of the time series, with α_1 and β_1 reflecting short-term correlations and fluctuations, and α_2 and β_2 capturing the long-term persistence and trends. By examining both sets of parameters, researchers can gain deeper

insights into the complex regulatory mechanisms and temporal structures inherent in physiological signals such as HRV. The back-end sets the default range for short-term fractal exponent α_1 from 4 to 11 heartbeats and, for long-term fractal exponent α_2, from 11 to the length of the data [72].

Complexity HRV Analysis: Other approaches to study the complexity in a time series, which have been implemented in the back-end, are the Lempel-Ziv complexity (LZc) [73] and the Kolmogorov complexity (Kc) [74].

Lempel-Ziv complexity (LZc) quantifies the intrinsic uncertainty of a time series and is notable for its independence from the length of the data. To measure LZc, the data is transformed into a binary or ternary sequence. For binary conversion, a value of 1 is assigned if the next value in the series is higher (x(i+1) > x(i)), and a value of 0 if it is lower. For ternary conversion, the same rules apply for values 1 and 0, but if the signal remains constant (x(i) = x(i+1)), a value of 2 is assigned [73].

Binary Sequence

$$S(n) = \begin{cases} if\ x_{(n+1)} \leq x_{(n)}, & 0 \\ if\ x_{(n+1)} > x_{(n)}, & 1 \end{cases} \tag{2.8}$$

Ternary Sequence

$$S(n) = \begin{cases} if\ x_{(n+1)} < x(n), & 0 \\ if\ x_{(n+1)} > x(n), & 1 \\ if\ x_{(n+1)} = x(n), & 2 \end{cases} \tag{2.9}$$

Kolmogorov complexity (Kc), often referred to as algorithmic complexity, quantifies the randomness within a symbol sequence. It evaluates the complexity of a string by determining the length of the shortest computer program capable of producing that string, which is

composed of zeros and ones. For our calculations of Kc, we used the same binary conversion criteria adopted by the LZc [74].

Poincaré Plot HRV Analysis: The Poincaré plot analysis works as both visual and quantitative method for detecting patterns in time series data. In the context of HRV analysis, this approach entails plotting each NN interval against the following one to generate a 'lag-1' plot. To quantify the Poincaré plot, the technique involves fitting an ellipse to the data distribution and assessing the dispersion along its major and minor axes [75]. By these quantitative geometric metrics (i.e., SD1 and SD2) an estimation of the short-term and long-term variability, respectively, is pursued.

Lastly, the features mentioned in Table 3. 3 have customizable parameters to allow user to select the optimum parameters with respect to their research objective.

Table 3. 3: HRV metrics with customizable parameters

Metrics	Unit	Customizable parameter	Default Settings
ApEn:	a.u.	m and r	m = 2 and r = 0.2 *SDNN
SampEn:	a.u.	m and r	m = 2 and r = 0.2 *SDNN
DFA:	a.u.	for α1, n1 and bkp for α2, b2 bkp and n2	for α1, n1 = 4 and bkp = 11 for α2, bkp = 11 and n2 = 20

3.3. Assessment of the developed Sleep Heart Rate Variability Analysis software

Since the feature of automatic HRV analysis across different sleep phases was not available in similar tools, to provide an assessment of UNICA-HRV we compared the HRV metrics obtained on a 15-minute ECG segment from PSG data by our tool against other well-established HRV analysis tools, i.e., Kubios, PhysioZoo, HRVAS, and gHRV. The non-parametric Kruskal-Wallis test was adopted to compare the HRV metrics calculated using the different tools and, if necessary, a pairwise comparison using a Wilcoxon signed-rank test was

performed. After Bonferroni's correction, to control type I error, we set $p<0.05$ for statistical significance.

i. Polysomnography Database

As benchmark data, we used the publicly available Haaglanden Medisch Centrum sleep staging database, which includes 151 full-night PSG recordings (85 males and 66 females, with an average age of 53.9 ± 15.4) [76]. The recordings, sampled at 256 Hz, represent a diverse group of patients who were randomly chosen and had been referred for PSG testing due to various sleep disorders. The dataset contains EEG, EOG, chin EMG, and ECG data, along with event annotations related to sleep-pattern scoring in the related hypnogram [76–78].

ii. Comparative analysis with currently established toolboxes

Figure 3. 5 presents the results of the comparative analysis. In the time domain, a good consistency across the compared software tools can be appreciated. Indeed, HR, NNmean, RMSSD, pR50, SD1, and SD2 show almost equal values across all software tools, but the same does not hold for all the HRV metrics analyzed. In the time domain, STDNN presents some minor differences for the Kubios tool, but there is no statistically significant difference to highlight. Conversely, for frequency domain indexes, the variability among the different tools is higher. Statistically significant differences were observed for aVLF, considering UNICA-HRV vs. Kubios ($p < 0.01$) and UNICA-HRV vs. gHRV ($p < 0.01$), and for nLF, among all the tools ($p < 0.01$). This finding could be attributed to the different methodologies employed in calculating nLF (whose value is influenced by aVLF, that also revealed significant differences) or to the various pre-processing techniques used. Conversely, the other frequency-domain metrics, although not identical for the different tools, did not lead to statistically significant differences, which supports the reliability of the tool also in frequency domain.

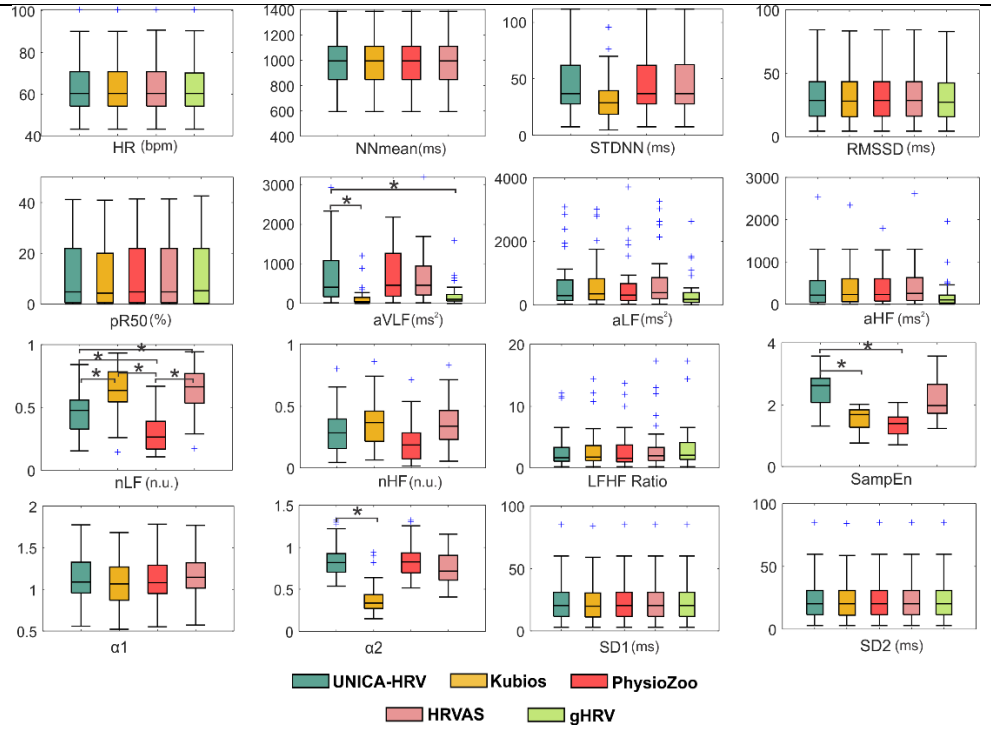


Figure 3. 5: Comparative analysis of HRV metrics across different HRV analysis tools, namely UNICA-HRV, Kubios, PhysioZoo, HRVAS, and gHRV.

In nonlinear HRV analysis, except for α1, which presents a very high consistency among the different tools, both SampEn and α2 parameter revealed statistically significant differences on a subset of the tools (respectively, UNICA-HRV vs. Kubios ($p < 0.01$) and UNICA vs. PhysioZoo ($p < 0.01$) for SampEn, and UNICA-HRV vs. Kubios ($p < 0.01$) for α2). This can be due to the different parameterizations. In particular, the handling of α2 requires careful consideration, as it reflects the long-term correlations in HRV data. Any change in the range settings can alter the interpretation of underlying physiological conditions, particularly those related to autonomic function and intrinsic HR modulation dynamics. Lastly, the Poincaré plot metrics (SD1 and SD2) reveal consistent distributions across the examined tools.

Compared to the other tools used for this assessment, UNICA-HRV also overcomes some of their limitations. The absence of hypnogram integration is the most significant one for sleep studies, as the autonomic regulation varies considerably between rapid eye movement (REM)

and non-rapid eye movement (NREM) sleep stages [24]. The possibility of adapting the code is impossible for tools that are not released under an open-source license, such as Kubios, which however is a popular tool for HRV analysis. The other tools used in this assessment are all open-source, but their use by users without programming skills is not straightforward, thus hampering their use by people with a clinical background. Moreover, while traditional HRV metrics are well-covered, the absence of nonlinear metrics in some tools limits the analysis that can be performed. Table 3. 4 synthetically presents the feature comparison among the tools considered in this section.

3.4. Exemplary analysis performed by UNICA-HRV

This section offers an overview of the tool functionalities in computing HRV indexes across NREM and REM sleep stages by the different segment setting methods, providing the user with cues on the possible discrepancies that can be encountered according to the methods selected for the assessment of HRV during sleep.

Table 3. 4: Feature comparison for the HRV analysis tools used for the UNICA-HRV comparative assessment

Software	**UNICA-HRV**	**Kubios Free Version**	**PhysioZoo**	**HRVAS**	**gHRV**
Open Source	Yes	No	Yes	Yes	Yes
Programming skills Required	No	No	Yes	Yes	Yes
Hypnogram Integration	Yes	No	No	No	No
Batch Analysis	Yes	No	No	Yes	No
User Defined Setting	Yes	No	Limited	Yes	Limited
QRS detection and annotation	Yes	No	Yes	No	No
Time Domain Indexes	Yes	Yes	Yes	Yes	Limited
Frequency Domain Indexes	Yes	Yes	Yes	Yes	Limited
Nonlinear Indexes	Yes	Limited	Limited	Limited	No
Poincaré Plot Indexes	Yes	Yes	Yes	Yes	Yes

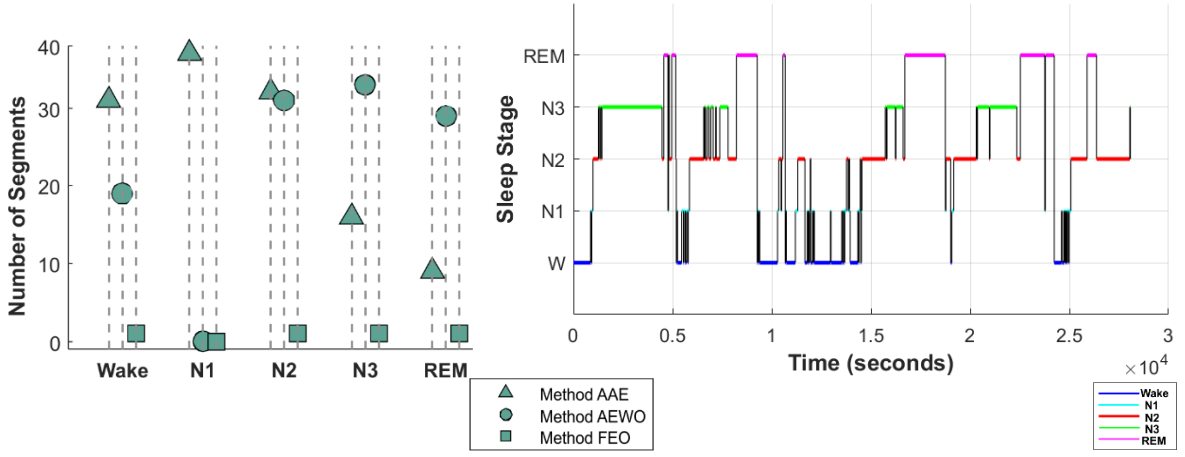
Figure 3. 6(a) presents the number of ECG segments considered for the HRV analysis in three distinct cases, hereafter referred to as methods AAE, AEWO, and FEO:

- Method AAE provides 30, 37, 32, 16 and 8 segments for wake, N1, N2, N3 and REM sleep phases, respectively, regardless of their length. This selection can be done through the HRV analysis settings window, as shown in Figure 3. 4. Simply select all phases under the "Select Phase(s)" option, choose "Methods AAE" option under "Segment Settings," and click "Analyze".
- Method AEWO provides 19, 0, 31, 33 and 29 ECG segments of five-minute length with 50% overlap for wake, N1, N2, N3 and REM sleep phases, respectively, ensuring to analyze more stable periods of HR data. This analysis can be done through the HRV analysis settings window, as shown in Figure 3. 4. Simply select all phases under the "Select Phase(s)" option, choose "Method AEWO" option under "Segment Settings," and click "Analyze".
- Method FEO targets the first available ECG segment of five minutes in each sleep phase. This can be done through the HRV analysis settings window, as shown in Figure 3. 4. Simply select all phases under the "Select Phase(s)" option, choose "Method FEO" option under "Segment Settings," and click "Analyze".

The hypnogram in Figure 3. 6(b) reveals the absence of five-minute or longer epoch for the N1 phase, and this is why Figure 3. 6(a) both methods AEWO, and FEO are not able to process the ECG signal during N1 phase.

Table 3. 5 represents the results of time-domain HRV indexes across different sleep phases (Wake, N1, N2, N3, and REM) using the three segmentation methods. During the wake phase, HR was slightly higher when evaluated by method AEWO, and lower by method AAE, with values slightly decreasing across sleep stages, as physiologically expected. NNmean exhibited an overall increasing trend for all methods from wakefulness through the different sleep phases.

STDNN, SDSD, and RMSSD were higher during wake and REM, while decreased in the N2 and N3 phases for all methods. For R50 and R20, method FEO generally reported higher values during wake and lower values in N2 and REM phases, when compared to methods AAE, and AEWO. Similarly, method FEO showed higher pR50 and pR20 during wake but had more variable results across the sleep stages. Methods AEWO, and FEO did not provide results for the N1 phase due to the absence of segments lasting at least five minutes for analysis. The high values of the standard deviation reveal the large variability of these parameters across the night. Remarkably, the different methods lead to different results, so that the aim of the study must be carefully identified before starting the analysis.



(a) (b)

Figure 3. 6 (a) ECG segmentation of SN012 subject based on three methods i.e., Method AAE, Method AEWO and Method FEO, where (- - -) is for visual clarity. (b) Hypnogram of a complete sleep cycle representing time taking by each phase wake, N1, N2, N2 and REM sleep phase of SN012 subject.

Similarly, the other HRV metrics can be computed and analyzed, revealing consistencies and discrepancies across the segmentation methods. Overall, each method adapts flexibly to different research aims. The AAE method is especially useful in studies where capturing every possible data across the sleep phases is needed, as it provides HRV analysis irrespective of segment length (AAE method provided the HRV information also during N1 phase, whereas both AEWO and FEO methods could not, as no segment longer than five minutes was found for this phase). By considering a 5-minute sliding-window analysis of longer ECG epochs, the

AEWO method captures and reveals the variability over time that is masked by the AAE method and not considered by the FEO one. Lastly, the FEO method is preferred in situations where quick HRV evaluations are necessary, possibly on large datasets.

Table 3. 5: Results (mean ± standard deviation) of HRV time-domain analysis during all phases by three different segment selection methods (AAE, AEWO, and FEO) using UNICA-HRV. (N.A.: not available).

Phases	Method	HR	NNmean	STDNN	SDSD	RMSSD	R50	R20	pR50	pR20
Wake	AAE	58 ±6	1033±87	87±76	56±55	56±55	21±38	74±115	9±9	0.4±0.1
	AEWO	61±3	982±49	143±71	93±53	93±53	39±28	128±33	13±8	0.4±0.1
	FEO	60	998	208	132	131	55	145	19	0.5
N1	AAE	57±6	1061±98	55±62	30±24	30±24	2±3	14±10	6±7	0.3±0.1
	AEWO	N.A.	N.A.	N.A.	N.A.	N.A.	N.A.	N.A.	N.A.	N.A.
	FEO	N.A.	N.A.	N.A.	N.A.	N.A.	N.A.	N.A.	N.A.	N.A.
N2	AAE	56±3	1082±50	43±31	31±34	31±34	17±38	95±166	5±5	0.4±0.1
	AEWO	54±2	1116±48	41±7	28±6	28±6	21±15	112±30	8±6	0.4±0.1
	FEO	52	1146	35	20	20	4	74	2	0.3
N3	AAE	55±2	1094±41	39±13	29±20	29±20	11±18	127±238	4±4	0.3±0.1
	AEWO	55±2	1099±36	32±5	25±10	25±10	6±4	88±12	2±1	0.32 ±0.04
	FEO	56	1079	38	43	43	13	113	5	0.4
REM	AAE	56±2	1070±46	64±21	33±9	33±9	40±47	212±234	8±7	0.4±0.1
	AEWO	56±3	1080±50	65±14	33±11	33±11	19±9	97±25	7±4	0.4±0.1
	FEO	55	1088	63	56	55	19	84	7	0.3

3.5. Conclusion

UNICA-HRV represents MATLAB open-source or HRV analyses in sleep studies. Compared to other well-established tools for HRV analysis, UNICA-HRV supports the computation of the different HRV metrics according to the sleep phases, by considering the patient's hypnogram. Although it was primarily conceived for sleep studies, as the other tools already available, it can be also used in conventional HRV analyses. Moreover, as any open-source tool, it can be

modified to introduce new features, for instance to generalize the implemented methods to protocol-based studies, where the segmentation is not based on the sleep phase but rather on specific events (changes in cognitive load, changes in physical activity, drug administration, etc.). By offering a relatively simple GUI, UNICA-HRV promotes the adoption of the tool for higher-education and research, without any prerequisite in terms of programming skills by the users.

In the future, support for hypnogram files based on the Rechtschaffen and Kales (R&K) method, in addition to the current AASM criteria, will be integrated to offer a more versatile and comprehensive tool. The authors will support the clinicians in the introduction of further improvements and functionalities unavailable on the other platforms.

Chapter 4: Autonomic Regulation in REM sleep behavior disorder and Parkinson's Disease During Sleep

This chapter explores heart rate variability (HRV) as a marker of autonomic dysfunction in idiopathic REM Sleep Behavior Disorder (iRBD) and Parkinson's Disease (PD) with and without RBD. HRV analysis was conducted during N2, N3, and REM sleep phases, focusing on time-domain, frequency-domain, and nonlinear HRV indices to evaluate the progression from iRBD to PD. The study analyzed ECG recordings from 26 controls (CG), 48 iRBD, 36 PD-RBD, and 16 PD patients. Distinct HRV patterns were observed in iRBD compared to CG and PD groups. Time-domain HRV indices, such as SDNN and RMSD, were significantly lower in iRBD during N2 and REM phases, reflecting diminished parasympathetic modulation. Frequency-domain analysis revealed reduced aVLF, aLF, and aTotal during N2, N3, and REM in iRBD, indicating a disruption of autonomic control. Nonlinear measures, including Poincaré plots and complexity indices, showed reduced variability and complexity in iRBD, particularly during REM sleep, suggesting autonomic disruptions. These findings highlight the progressive nature of autonomic dysfunction in alpha-synucleinopathies, with iRBD showing more pronounced alterations than PD. The unique HRV patterns observed in iRBD suggest early neurodegenerative changes, providing a basis for the use of HRV as a biomarker for disease progression. The study's comprehensive analysis of four distinct groups across multiple sleep stages offers a comprehensive understanding of autonomic modulation in alpha-synucleinopathies.

4.1. Introduction

While the previous chapter covered the prevalence and characteristics of RBD, this chapter focuses on the impact of RBD on the ANS, exploring how severely ANS function is affected in both idiopathic and symptomatic RBD, as well as in PD patients. Several studies employed

HRV to explore autonomic dysfunction in neurodegenerative disorders, including PD and iRBD, and in sleep related disorders such as sleep apnea [21–24]. Some studies have investigated alterations in HRV only wakefulness [25–29], while others have also considered sleep stages in both PD [30–34] and iRBD cohorts [33–39]. A reduction in the low-frequency/high-frequency ratio (LF/HF), low (LF) and very low frequency (VLF) components, as well as an increase in high frequency components (HF) have been found in iRBD patients when compared to controls during wakefulness [26, 28, 40–44]. Moreover, other studies reported absence of HRV modifications during the transition from non-REM to REM sleep in iRBD patients, which is physiologically expected in healthy subjects, as the HRV varies across different stages of sleep as well as between sleep and awake states [35].

On the other hand, some studies found that SNS-regulated parameters, i.e., SDNN, VLF, and LF, were lower in PD patients than in the iRBD group ones, when compared to control groups [40]. Interestingly, the scientific literature also revealed that PD patients affected by RBD have reduced LF and VLF components of HRV during wakefulness compared to unaffected controls and exhibit an inverse relation between autonomic dysfunction and disease related factors such as the motor severity of the disease [29, 42, 45, 46]. Moreover, some studies have also examined autonomic dysfunction in PD patients without RBD using spectral analysis, showing lower high frequency components in PD patients without RBD as compared to controls [42, 47–61].

Overall, these findings suggest a consistent autonomic dysfunction in the alpha-synucleinopathy continuum since prodromal stages, with overt patients (i.e. PD) showing more severe dysfunction as compared with prodromal ones (i.e. iRBD). However, there remains a lack of knowledge about the sleep-stage-specific changes in HRV across the alpha-synucleinopathy spectrum. While some studies have focused on the transition from non-REM (N2, N3) to REM sleep, most have not fully characterized the entire spectrum of HRV changes

across all sleep phases in iRBD, PD-RBD, and iRBD cohorts. The interplay between parasympathetic and sympathetic control across these stages, as well as its predictive value for identifying individuals at risk of converting from iRBD to PD, remains underexplored. Furthermore, existing studies often utilize only classical HRV indices such as LF, HF, and LF/HF and do not incorporate advanced HRV features to identify more subtle, disease-relevant patterns. Addressing these gaps is essential to clarify the role of sleep-stage-dependent HRV changes as potential biomarkers for early disease progression.

From the aforementioned studies, it is evident that there are some open issues about the cause of HRV regulation. Indeed, some studies ascribe HRV variations to PD [31, 45, 50, 54, 62]. However, other research suggests that these variations are a result of RBD rather than PD [26, 33]. Meanwhile, some studies argue that both RBD and PD impact HRV [34, 44, 63]. This clearly shows the need for research that can identify the trend of autonomic dysfunction, especially by exploring different groups of patients along the prodromal to overt alpha-synucleinopathy continuum, including iRBD, PD-RBD and PD patients without RBD. Moreover, most studies investigated HRV standard metrics, while using advanced computational techniques may increase our ability in detecting significant differences across the study groups. Finally, while most studies investigated HRV variations during wakefulness, few data are available during sleep, which is a more stable and controlled condition for studying autonomic function. Thus, this study utilizes sophisticated computational techniques that provide a more detailed and accurate analysis of autonomic dysfunction compared to traditional methods. These advanced methods allow us to detect subtle variations in HRV and other autonomic parameters that may be overlooked by conventional analysis.

By explicitly stating these novel aspects and addressing the gaps in existing literature, we aimed to investigate conventional as well as advanced HRV parameters during various sleep phases to evaluate the trajectory of the autonomic dysfunction as iRBD converted to PD, looking at

the sleep-related HRV trends in people suffering from iRBD, PD-RBD, iRBD, and comparing them with a CG. Unlike previous studies, this approach enables a more comprehensive understanding of sleep-stage-specific autonomic modulation across the full alpha-synucleinopathy spectrum. By incorporating both classical and advanced HRV parameters, and analyzing full sleep cycles, this chapter aims to provide novel insights into potential early digital biomarkers of disease progression.

4.2. Methodology

4.2.1. Study population

The participants cohort included 26 participants in the control group (CG, mean age ± standard deviation: 59 ± 10 y.o.; 46% male), 16 PD participants (67 ± 10 y.o.; 50% male), 48 iRBD participants (67 ± 8 y.o.; 73% male), and 36 PD-RBD participants (71 ± 8 y.o.; 66% male).

Inclusion criteria: All participants with a complete PSG exam were enrolled, but only those participants that exhibited at least five minutes of artifact-free ECG signals in N2, N3 and REM phases were considered in this study. Based on the inclusion and exclusion criteria, this study was carried out on 135 out of 224 participants.

4.2.2. Signal processing

A hypnogram was created, according to the available sleep scoring from experienced neurologists, and used to segment the ECG signal according to the different sleep phases. On this basis, the first 5-min artifact-free ECG segment was extracted for N2, N3 and REM sleep phase to maintain data homogeneity. For this purpose, ECG recordings were visually examined using a the UNICA Sleep HRV analysis (UNICA-HRV) tool [79] and available on Github. The N1 phase was excluded because it normally constitutes about 5-10 % of the total sleep time and typically lasts between one to five minutes [7–9] with artifact-free continuous ECG of five

minutes being seldom observed. The R-peak detection and correction was performed as described in Chapter 3.

4.2.3. Heart Rate Variability Analysis

Various time-domain, frequency-domain, and non-linear parameters were analyzed to elucidate insights into cardiac autonomic function by HRV. The following time-domain parameters were calculated: NNmean, SDNN, SDSD, RMSSD, R50, R20, pRR50, and pR20. All parameters were measured in ms. The following frequency-domain parameters were calculated: aVLF, aLF, aHF, nLF, nHF, LF/HF ratio, and aTotal. For nonlinear analysis, we considered LZc, Kc, DFA and Poincaré plots-based parameters.

4.3. Results

4.3.1. Demographic and Polysomnographic Parameters

Table 4.1 presents the demographic and PSG parameters for the iRBD, PD-RBD, PD, and CG groups. The Kruskal-Wallis test showed significant differences in demographic characteristics, specifically for the age ($p < 0.001$). Regarding PSG parameters, significant differences were found in total bedtime (TBT) ($p < 0.05$), % Sleep Efficiency (SE) ($p < 0.05$), %N2 ($p < 0.01$), %N3 ($p < 0.05$), and Apnea-Hypopnea Index (AHI) ($p < 0.05$). Subsequent pair-wise comparisons revealed that the age of the control group (CG) was significantly lower than all the diseased groups (iRBD, PD-RBD, and PD) ($p < 0.01$). No significant age differences were highlighted among the diseased groups themselves. In the pairwise comparisons, significant differences were noted in TBT and SE between the CG and iRBD groups ($p < 0.05$). In the comparison between the CG and the PD-RBD group, notable differences were identified in TBT, %N2, %N3, and AHI ($p < 0.05$). Similarly, when comparing the CG with the PD group, significant differences were found in SE, %N3, and AHI ($p<0.05$). Finally, in comparing the

iRBD group with the PD-RBD group, statistical differences were found only in SE and %N2 ($p < 0.05$).

4.3.2. HRV parameter comparisons across the groups

In Figure 4. 1, time-domain analysis showed statistically significant differences across the examined groups. In comparing the CG vs iRBD group, significant differences were observed during various sleep stages (N2, N3, REM). Specifically, during N2, all time-domain parameters were lower in the iRBD group *($p < 0.05$)* compared to the CG group. Additionally, the STDNN and R20 parameters were also significantly reduced during REM sleep *($p< 0.05$)*. Other parameters showed no significant difference during N3 and REM sleep. The comparison between the CG vs PD and PD-RBD vs PD groups during N2, N3, and REM sleep showed no significant differences in time-domain HRV parameters, except for the R20 and pR20 parameters during REM sleep, where a decrease is observed for the PD group when compared to CG and PD-RBD groups (*$p < 0.05$)*. Comparing iRBD with PD-RBD, significant reduction was observed in iRBD group for STDNN, SDSD and RMSD parameters during N2 (*$p < 0.01$)*. No significant differences were noted in N3 and REM sleep. Additionally, looking at the comparison between iRBD and PD groups, significant reductions in iRBD group were observed for STDNN, SDSD, RMSD and pR50 parameters during N2 , and for STDNN, SDSD, RMSD during N3 *($p < 0.05$)*. Lastly, CG vs PD-RBD comparison did not reveal significant differences in any sleep stage.

Table 4.1: Comparisons across the iRBD, PD-RBD, PD and control groups for demographic and polysomnographic parameters. The * marks those parameters exhibiting statistically different differences.

Variables	CG	iRBD	PD-RBD	PD	*p-value*
% Sex (Male)	46	73	66	50	*0.126*
Age *	59±10	67±8	71±8	67±10	*< 0.001*
TBT (minutes) *	493.29 ±43.19	530.00 ±74.55	532.31 ±70.84	489.75 ±75.06	*0.047*
TST (minutes)	390.00 ±82.41	374.23 ±73.13	412.04 ±87.05	400.56 ±63.83	*0.199*
% Sleep Efficiency (SE) *	77.28 ±13.78	70.95 ±12.05	76.72 ±12.17	81.56 ±6.78	*0.010*
Sleep Latency (SL) (minutes)	20.72 ±19.47	28.53 ±28.44	20.88 ±15.57	16.02 ±16.73	*0.160*
Awakenings No	21.88 ±13.33	32.68 ±19.03	27.12 ±17.99	29.63 ±13.43	*0.117*
WASO (minutes)	78.26 ±55.83	110.15 ±67.88	93.54 ±57.43	71.00 ±35.91	*0.062*
% N1	10.33 ±3.72	12.68 ±5.36	11.28 ±4.65	10.55 ±4.18	*0.399*
% N2 *	43.21 ±7.04	47.81 ±10.08	55.07 ±10.69	49.15 ±13.92	*0.002*
% N3 *	28.85 ±6.15	24.97 ±9.41	20.34 ±7.97	23.36 ±9.69	*0.011*
% REM	16.98 ±6.40	15.22 ±7.25	13.32 ±6.11	16.98 ±6.50	*0.165*
PLMI	11.54 ±16.60	19.88 ±34.54	22.07 ±26.27	6.34 ±10.30	*0.067*
AHI *	2.73 ±3.00	6.45 ±7.87	10.65 ±11.67	12.51 ±18.32	*0.014*
ODI	3.11 ±3.52	7.97 ±9.15	9.04 ±10.56	13.66 ±17.67	*0.082*

TBT = total bedtime, TST = total sleep time, WASO = wake after sleep onset, PLMI = periodic limb movement index, AHI = apnea-hypopnea index, ODI=Oxygen desaturation Index.

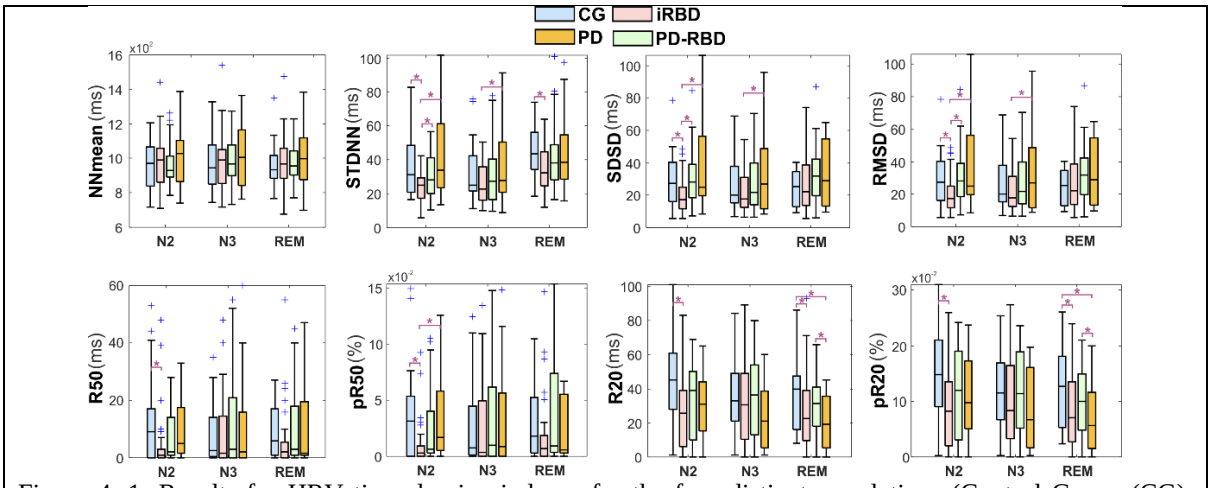


Figure 4. 1: Results for HRV time-domian indexes for the four distinct populations (Control Group (CG), idiopathic REM Sleep Behavior Disorder (iRBD), Parkinson's Disease (PD), and PD with RBD (PD-RBD)) during three sleep phases (N2, N3 and REM).

Indexes include: NNmean = mean of NN intervals, SDNN = standard deviation of NN intervals, SDSD = standard deviation of successive NN interval differences, RMSD = root mean square of successive differences interval, R50 = number of adjacent NN interval pairs exceeding 50 ms, pR50 = ratio of R50 to total NN intervals, R20 = number of adjacent NN interval pairs exceeding 20 ms and pR50 = ratio of R20 to total NN intervals). The statistically significant results are marked by * ($p<0.05$). For improved visual representation, some outliers have been omitted from the SDSD and RMSSD (above 150 ms), R50 and R20 (above 40 counts), and pR20 and pR50 (above 0.15%).

Figure 4. 2 shows frequency-domain HRV values for all the examined populations. When comparing the CG and iRBD groups, there were significantly lower values in iRBD for aVLF (in N2 and REM sleep, $p<0.02$), aLF (in N2 and REM sleep, $p<0.005$), and aHF (in N2, $p <$

0.04). Additionally, aTotal was significantly reduced in the iRBD group compared to CG across all analyzed sleep stages *(p< 0.05)*. In the comparison between CG and PD-RBD group, the only significant difference was related to a lower aLF in the PD-RBD group during N2 *(p < 0.05).* However, in the iRBD vs PD-RBD comparison, significant reductions for the iRBD group were observed in aHF, aLF, and aTotal during N2 (*p<0.03*) and in aVLF and aTotal during REM (*p<0.03*). Furthermore, when comparing the iRBD and PD groups, several parameters showed significant differences. Specifically, aVLF, aLF, aHF, and aTotal were lower in the iRBD group during N2 *(p < 0.03).* Additionally, aHF and aTotal were also lower in the iRBD group during N3 and REM sleep compared to the PD group (*p<0.03*). No significant differences were observed in the comparisons between CG vs PD and PD-RBD vs PD.

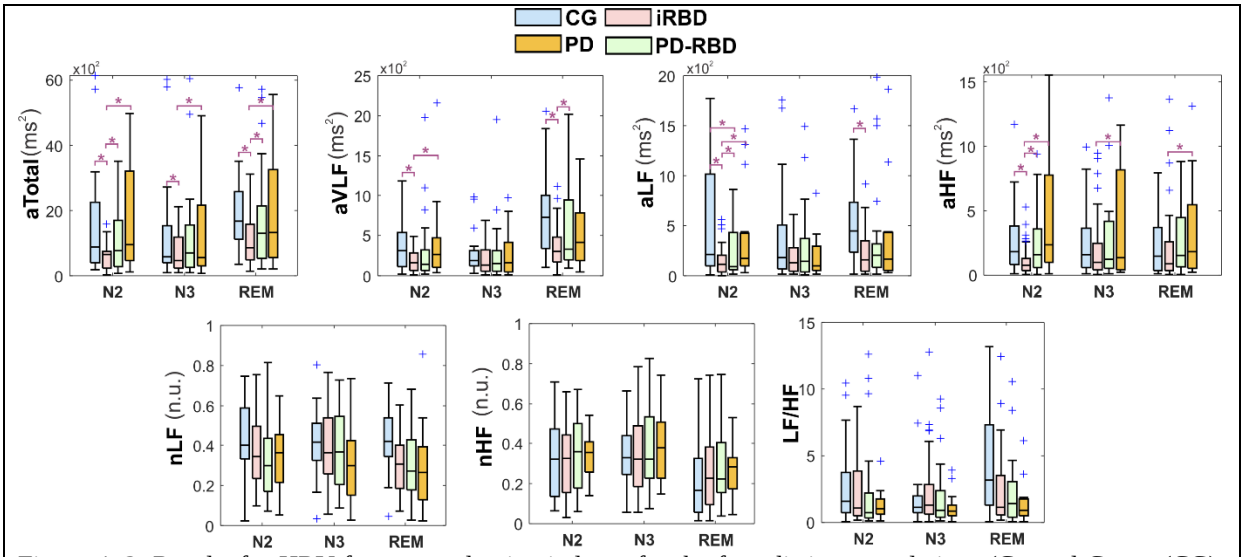


Figure 4. 2: Results for HRV frequency-domian indexes for the four distinct populations (Control Group (CG), idiopathic REM Sleep Behavior Disorder (iRBD), Parkinson's Disease (PD), and PD with RBD (PD-RBD)) during three sleep phases (N2, N3 and REM).

Indexes include: aTotal = total power, aVLF = power in very low frequency (VLF) band, aLF = power in low frequency (LF) band, aHF = power in high frequency band (aHF), nLF = normalized power in LF band, nHF = normalized power in HF band and LF/HF= ratio of LF to HF band. The statistically significant results are marked by * (p<0.05). For improved visual representation, some outliers have been omitted from the aTotal (above 800 ms^2), aVLF (above 2000 ms^2), aLF (above 2500 ms^2), aHF (above 1500 ms^2) and LF/HF ration (above 15).

Finally, in Figure 4. 3 the nonlinear analysis showed that, upon comparison of CG vs iRBD, all parameters were significantly lower in iRBD group during N2 and REM sleep*(p < 0.03),* except for pf=1% for both LZc and Kc and α1 for DFA in N2 phase, and for SD1 and α1 in

REM phase. No significant differences were observed during phase N3. In the comparison between the iRBD and PD-RBD group, only SD1 and SD2 showed significantly lower values in the iRBD group during N2 . However, during REM sleep, all complexity parameters and SD2 were lower in the iRBD group compared to the PD-RBD group. In the comparisons of iRBD versus PD, and PD versus PD-RBD, both showed significant reductions in all complexity parameters, with 1% pf in the RBD groups (i.e., iRBD and PD-RBD) compared to the PD group. Specifically, for iRBD, these differences were observed in N2 , and for PD-RBD, the differences were noted in REM sleep. No significant differences were found in N3 and REM sleep for iRBD, and for PD-RBD no differences were observed in N2 and N3 when compared to the PD group. Additionally, when comparing iRBD versus PD, there was a significant reduction in SD1 during N2 and N3 and in SD2 only during N2. Specifically, for iRBD, these differences were observed in N2 , and for PD-RBD, the differences were noted in REM sleep. No significant differences were found in N3 and REM sleep for iRBD, and for PD-RBD no differences were observed in N2 and N3 when compared to the PD group. Additionally, in the comparison of iRBD versus PD, there was a significant reduction in SD1 during N2 and N3 and in SD2 only during N2 in iRBD patients. No significant differences were observed across CG vs RBD-PD, and CG vs PD.

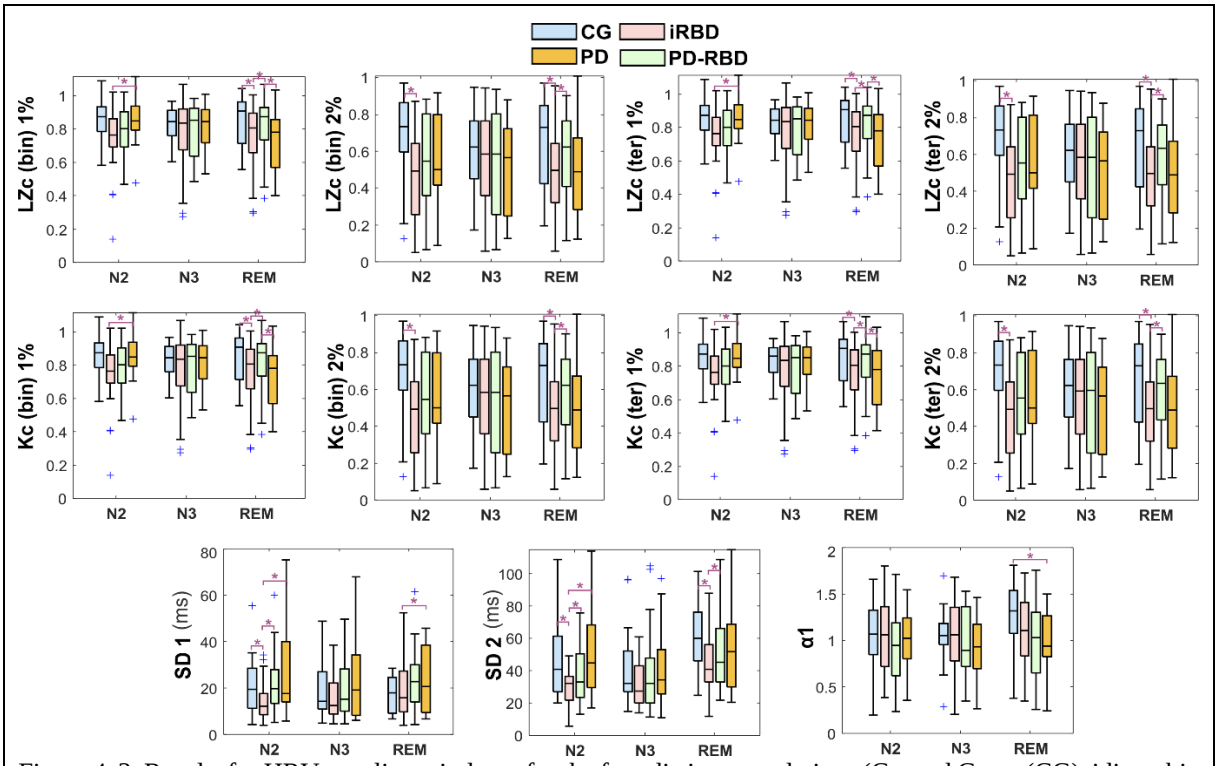


Figure 4. 3: Results for HRV non-linear indexes for the four distinct populations (Control Group(CG), idiopathic REM Sleep Behavior Disorder (iRBD), Parkinson's Disease (PD), and PD with RBD (PD-RBD)) during three sleep phases (N2, N3 and REM).

Indexes include: LZc (bin) 1% = Binary Lampel-Ziv complexity (LZc) with 1% tolerence, LZc (bin) 2% = Binary LZc with 2% tolerence, LZc (ter) 1% = Ternary LZc with 1% tolerence, LZc (ter) 2% = Ternary LZc with 2% tolerence, Kc (bin) 1% = Binary Kolmogrov complexity (Kc) with 1% tolerence, Kc (bin) 2% = Binary Kc with 2% tolerence, Kc (ter) 1% = Ternary Kc with 1% tolerence, Kc (ter) 2% = Ternary Kc with 2% tolerence, SD 1 = Poincaré plots standard deviation (SD) 1, SD 2 = Poincaré plots SD 2 and Alpha1 (α1) = short term fractal exponent of detrended fluction analysis. The Statistically significant results are marked by * ($p<0.05$). For improved visual representation, an outlier have been omitted from the SD 1 (above 115 ms).

4.4. Discussion

Autonomic nervous system dysfunction can occur early in PD even in prodromal stage [80]. Similarly, patients with idiopathic RBD experience a higher prevalence of autonomic symptoms, particularly affecting the digestive, genitourinary, and cardiovascular systems [81]. Although previous studies have shown that RBD can be associated with dysfunction of the autonomic nervous system, there are conflicting results regarding the analysis of heart rate variability as biomarker for autonomic nervous system health [82–85].

In this study, we have assessed autonomic nervous system in RBD patients either idiopathic and converted to PD compared with PD patients without RBD and healthy controls, by means of conventional as well as advanced HRV analysis during various sleep phases. The results of

our study show that individuals with iRBD exhibit distinct HRV patterns during particular sleep stages when compared to the CG and PD groups, with and without RBD. This distinction is particularly evident in the analysis of time-domain HRV parameters during N2, N3 and REM sleep stages, suggesting the presence of lower parasympathetic activity, autonomic dysfunction and a more rigid cardiac function in iRBD compared to PD patients with or without RBD and CG. Based on these findings, the dysregulation of sympathetic autonomic function seems more pronounced in iRBD than CG or PD participants, with or without RBD.

Interestingly, it was recently shown that the HF component was significantly higher in iRBD patients compared to healthy controls [86]. A potential explanation may be that an early degenerative process involving parasympathetic control centers in iRBD subjects such as Dorsal Motor Nucleus of the Vagus (DMNV) could trigger an adaptive compensatory mechanism, leading to an initial hyperactivation of the parasympathetic system. However, in the present study, iRBD patients showed a reduction in various frequency-domain parameters during N2, N3, and REM sleep compared to CG and PD patients with or without RBD, suggesting a more generalized reduction in autonomic modulation, vagal tone, and long-term autonomic regulation. These findings may reflect differences in autonomic behavior across disease stages or measurement conditions (e.g., wakefulness vs. sleep)..

Concerning the nonlinear analysis, iRBD patients showed a reduction in various complex parameters in N2, N3 and REM compared to CG and PD patients with or without RBD, suggesting a lower variability, less adaptability, lower complexity potential and rigidity of autonomic function. Interestingly no differences were found in time-domain and frequency domain HRV parameters when comparing PD-RBD and iRBD. Only nonlinear analysis allowed to show a reduction in all complexity parameters in REM sleep in PD-RBD when compared to iRBD.

The neurodegenerative process that characterizes iRBD is a possible explanation for these findings. The pathogenesis of RDB is believed to involve dysfunction in the sublaterodorsal nucleus, magnocellular reticular formation, and peri-locus coeruleus structures in Braak stage 2 [87]. The degeneration of these structures leads to overt REM sleep behaviour disorder. In Braak stage 1, the DMNV, the olfactory bulb, and the anterior olfactory nucleus complex are affected [87] . The clinical manifestations of autonomic dysfunction and smell dysfunction are likely to appear and may be detectable after a threshold of degeneration is reached [87, 88].

Our results suggest a hyperactivation of the sympathetic autonomic nervous system in iRBD patients. We hypothesized that the increased activity of the sympathetic autonomic nervous system seen in iRBD participants, compared to PD ones, could be linked to an early neurodegenerative process affecting the DMNV in iRBD. This could lead to a predominance of sympathetic tone over parasympathetic tone, which may lead to alterations in HRV.

In PD patients, however, neurodegeneration also affects the centers that regulate the sympathetic autonomic nervous system. Additionally, it has been shown that PD patients exhibit a loss of post-ganglionic sympathetic innervation in the heart, along with functional and molecular changes [89]. It is important to point out that patients with iRBD reported a mild reduction in cardiac uptake in 123I-labeled meta-iodobenzylguanidine scintigraphy suggesting a decrease in cardiac sympathetic activity [90]. It can be assumed that in PD, neurodegeneration progresses and ultimately affects sympathetic heart innervation, leading to balance between sympathetic and parasympathetic nervous systems and PD subjects no longer show sympathetic hyperactivation.

In contrast, the degeneration targeting the parasympathetic system (DMNV) in iRBD patients initially leads to a relative dominance of sympathetic activity because the parasympathetic system deteriorates earlier.

The present study has strength and limitations.

The present study utilizes sophisticated computational techniques that provide a more detailed and accurate analysis of autonomic dysfunction compared to traditional methods. These advanced methods allow us to detect subtle variations in HRV and other autonomic parameters that may be overlooked by conventional analysis and remain relatively underexplored in literature.

One of the unique strengths of our study is the direct comparison across four distinct groups including CG, iRBD, PD patients with RBD (PD-RBD) and PD patients without RBD (iRBD). This comprehensive comparative approach is rare in scientific literature and allows us to explore the specific autonomic profiles associated with each condition. By including these groups, we can better understand the progression from iRBD to PD and the additional impact of RBD on PD patients. Additionally, our study features a larger sample size than many previous studies in this field, which increases the confidence of our analyses, allowing us to detect smaller effects and draw more robust and generalizable conclusions.

In addition, this study emphasized on sleep rather than wakefulness, which is particularly significant as sleep studies provide a more stable and controlled environment to assess autonomic function, reducing the influence of external factors such as physical activity and stress that can affect measurements during wakefulness. Sleep is also a critical period for autonomic regulation, and abnormalities may be more pronounced, offering deeper insights into the underlying pathophysiology of these conditions. In the context of PD, sleep disturbances are common and often precede motor symptoms. Studying autonomic dysfunction during sleep can thus provide early markers of PD pathology and progression. Moreover, REM sleep behavior disorder itself is considered a potential precursor to PD, and analyzing autonomic function during sleep in RBD patients could enhance our understanding of the disease's early stages and mechanisms.

One of the limitations is respiratory events during sleep and their influence on HRV, which might be confounding. Another limitation is the retrospective and transversal nature of the study, as further longitudinal studies are needed to assess whether dysautonomic dysfunction in iRBD can predict phenoconversion, as well as HRV changes over time could be considered as a dynamic biomarker of neurodegeneration in the continuum of alpha-synucleinopathies.

4.5. Conclusions

In conclusion, the autonomic nervous system impairment observed in iRBD participants is indicative of early neurodegenerative changes that predominantly affect sympathetic regulation. The unique HRV profile of these individuals highlights the critical need for early identification and monitoring of autonomic dysfunction in iRBD, which could have implications for understanding the progression of neurodegenerative diseases and their associated autonomic disturbances.

Chapter 5: Impact of Respiration on Autonomic Regulation in REM sleep behavior disorder[4]

Autonomic dysfunction has been suggested to be often associated with the iRBD, and HRV is a commonly used tool to assess it. However, the accuracy of HRV is heavily influenced by respiratory rate (RespR), potentially causing misinterpretation of frequency domain HRV indices. This study compares sleep-related ANS function in iRBD patients and in a CG group, using respiratory-adjusted HRV spectral analysis. It involves 20 iRBD and 20 CG participants in each group, from which five-minute ECG signal epochs during N2, N3, and REM sleep phases are analyzed. RespR was estimated from ECG-derived respiratory signals (EDR). Both low and high frequency bands definition for HRV analysis were redefined using the RespR. The results indicate significant differences in HRV parameters between iRBD and CG subjects during REM sleep, highlighting disrupted autonomic regulation in iRBD. This finding is also evident in non-REM phases, thus emphasizing the need to incorporate RespR in HRV analysis, especially in sleep-related studies, for a comprehensive understanding of autonomic dysfunction.

5.1. Introduction

The interaction between respiration and autonomic regulation has emerged as a critical area of investigation specifically in the context of RBD [85] which has been extensively described in previous chapters, along with the calculation of HRV and the identification of general confounding factors that influence HRV [35]. Deepening this understanding, this chapter provides insights into the specific impact of respiration on HRV in the RBD population.

[4] Note: This chapter/part of the chapter is the reprint of article submitted in IEEE Engineering in Medicine and Biology Society conference 2024

HRV serves as a critical biomarker for assessing ANS activity, providing insights into the balance between sympathetic and parasympathetic regulation of cardiac activity. One of the key physiological factors influencing HRV is respiration, which modulates heart rate through RSA — a process where heart rate accelerates during inspiration and decelerates during expiration [91, 92]. This phenomenon is primarily mediated by the vagus nerve, a major component of the parasympathetic nervous system. Consequently, fluctuations in HRV driven by respiration offer valuable information about vagal tone and overall autonomic regulation [91, 92].

The influence of respiration on HRV has gained significant attention, particularly in the context of cardiac autonomic regulation where respiratory patterns substantially affect HRV, and this impact becomes significant in sleep studies and pathological conditions such as RBD [85]. During sleep, careful consideration must be given to the definition of frequency bands for spectral analysis of HRV, as respiratory-induced changes can influence the interpretation of autonomic activity, since respiration patterns and frequency change with respect to wakefulness [93]. Moreover, the RR intervals themselves should be analyzed in combination with respiratory rate to achieve a comprehensive assessment of autonomic control. Despite the well-established impact of respiratory patterns on HRV, many HRV-based studies of RBD have not taken into account the impact of respiration in their analyses. This motivated the study about respiration-guided HRV, to provide more insights on autonomic dysfunction in iRBD and other sleep-related disorders.

In people with RBD, autonomic dysfunction can be considered a prodromal indicator of phenoconversion to neurodegenerative diseases such as Parkinson's disease, multiple system atrophy, and dementia with Lewy bodies. The unique sleep-related characteristics of RBD, such as the loss of muscle atonia and increased motor activity during REM sleep, may further worsen autonomic dysregulation [15, 16]. Understanding how respiration influences HRV in this

specific population can provide critical insights into the pathophysiological mechanisms linking RBD to neurodegeneration.

Various physiological processes influence the relationship between respiration and HRV in RBD [94]. Alteration in the respiratory cycle due to abnormal sleep architecture and altered control during REM sleep may lead to changes in RSA patterns [83, 95] . Additionally, the increased sympathetic activity and reduced parasympathetic control observed in individuals with RBD may attenuate the respiratory-driven modulation of HRV [96].

This chapter aims to provide a detailed exploration of the impact of respiration on HRV within the RBD population. To address these challenges, we focused on limiting the impact of spectral analysis confounding factors on HRV. As such, we proposed to personalize HF and LF bands definition according to the respiratory rate. Our hypothesis is that, by applying this respiration-guided spectral HRV analysis during N2, N3, and REM sleep phases in people with iRBD, and control subjects, we can obtain a more accurate physiological interpretation of the observed HRV patterns. This approach has the potential to assist in identifying the specific type of autonomic dysfunction and its underlying causes.

5.2. Methodology

5.2.1. Study Population

A total of 40 people were enrolled in this preliminary research study, recruited from Italian Sleep Medicine Centers located in Cagliari and Genova. These participants were divided into two distinct groups as follows:

- 20 iRBD participants (70 ± 5 y.o., 70% male)
- 20 control (CG) participants (59 ± 10 y.o., 50% male)

The inclusion criteria were consistent with those outlined in the dataset chapter. In addition, people with at least 5 minutes of artifact-free ECG signals during N2, N3, and REM phases were included in the subsequent analyses.

5.2.2. Respiration-Guided HRV Analysis

The first five minutes of artifact-free ECG signals (visually validated) from overnight PSG were extracted from various sleep phases i.e., N2, N3 and REM for HRV analysis. R peaks were detected using a wavelet-based delineation algorithm [40]. These R-peak locations $t(k)$ were then used to estimate an instantaneous HR signal using the integral pulse frequency modulation (IPFM) model which also accounts for the presence of ectopic beats [97]. To understand and quantify the influence of the ANS on the beat occurrence time series $t(k)$, the IPFM framework is employed. This model hypothesizes that the ANS's effect on the sinoatrial (SA) node is represented through a modulating signal $m(t)$; a heartbeat is triggered whenever the cumulative integral of 1+ $m(t)$, exceeds a fixed threshold T, corresponding to the average heart cycle duration. This process resets the integrator after each heartbeat [see Fig. 1(a)]. The modulating signal $m(t)$ is assumed to be causal, band-limited, and satisfies $m(t) < 1$.

Given the IPFM framework and assuming the initial beat occurs at time $t_o = 0$, the sequence of beat occurrence times can be derived from the following equation:

$$k \approx \int_0^{t_k} \frac{1+m(t)}{T(t)} \tag{5.1}$$

where k represents the beat index, $t(k)$ is the time of the k-th beat, and $T(t)$ is the constant between the two beats. So, for instantaneous heart rate $d_{HR}(t)$, in Hertz, is expressed as:

$$d_{HR}(t) = \frac{1+m(t)}{T(t)} \tag{5.2}$$

Assuming that the changes in $1/T(t)$ are gradual compared to those in $m(t)/T(t)$ and that their respective spectral components remain distinct without overlapping, the time-varying mean heart rate $d_{HRM}(t)$ can be expressed as:

$$d_{HRM}(t) = \frac{1}{T(t)} \tag{5.3}$$

Using this, the HRV signal can be calculated as:

$$d_{HRV}(t) = d_{HR}(t) - d_{HRM}(t) = \frac{m(t)}{T(t)} \tag{5.4}$$

Finally, from the last equation, it can be observed that, to obtain the ANS modulating signal $m(t)$, we need to correct the HRV signal by $d_{HRM}(t)$ [97].

$$m(t) = d_{HRV}(t)T(t) = d_{HRV}(t)/d_{HRM}(t) \tag{5.5}$$

In scenarios where the mean heart period T varies over time, such as during stress testing, the estimated signal $m(t)$ may also include the effects of T(t), typically of much lower frequency. To address this, it is high-passed to remove low-frequency variations unrelated to the modulating signal at 0.03 Hz. Followed by interpolating the unevenly sampled HR signal is at 4 Hz using by cubic spline method.

Then, to perform respiratory-adjusted HRV analysis, the respiratory rate was estimated from the ECG-derived respiratory (EDR) signal, calculated by using the slope range approach [98].

This method provides respiratory information by measuring the difference between values of the maximum up-slope and minimum down-slope within the QRS complex $y_i(t)$, regardless of their occurrence order:

$$d_{sr}(\mathrm{i}) = \max_t\{y'_i(t)\} - \min_t\{y'_i(t)\} \tag{5.6}$$

where $y'_i(t)$ is the first derivative of the QRS complex.

Then, we analysed all EDR signals to determine the necessity of respiratory adjustment. This involves calculating the power spectral density (PSD) of each EDR signal to assess whether the power of the EDR signal falls outside the conventional high-frequency (HF) band range.

Following this assessment, we adjusted both low frequency (LF) and HF bands, based on the respiratory frequency content defined as:

$$P_{LF} = power\ in\ [0.04 \quad \Delta_L] \tag{5.7}$$

$$P_{HF} = power\ in\ [\Delta_L \quad \Delta_U] \tag{5.8}$$

where Δ_L and Δ_U represent the lower and upper limits of the frequency band that contains 70% of the total power of the EDR signal. In addition to the redefined LF and HF bands, we also calculated normalized power of LF ($P^{n_{LF}}$) and HF ($P^{n_{HF}}$) as:

$$P^{n_{LF}} = \frac{P_{LF}}{P_{LF}+P_{HF}} \tag{5.9}$$

$$P^{n_{HF}} = \frac{P_{HF}}{P_{LF}+P_{HF}} \tag{5.10}$$

$$LF/HF = \frac{LF}{HF} \tag{5.11}$$

$$P_{HRV} = power\ in\ [0.0033 \quad \Delta_U] \tag{5.12}$$

Finally, the PSD of $m(t)$ is computed using Welch's method and the power in the previously defined band is computed from it. In this computation, the window length is set to half the

length of the m(t) signal, the number of FFT points is defined as 2^{10} (i.e., 1024), and the overlap between segments is set to 50% of the window length.

5.2.3. Statistical Analysis

To assess any potential statistical difference in respiratory rate and HRV parameters, we conducted a statistical analysis by using the pairwise, non-parametric Mann-Whitney U test across CG and iRBD populations. Results were considered significant for $p < 0.05$ with Bonferroni correction to control type-I error, and adjusted p-values are reported. Moreover, we applied a non-parametric Kruskal-Wallis test across the sleep phases, followed by pairwise comparisons using the Mann-Whitney U test within each group separately, to determine which phases exhibited significant different trends.

5.3. Results & Discussion

Table 5. 1 presents the demographic and polysomnographic features for both iRBD and CG groups. Figure 5. 1 (a) illustrates that, for 60% of CG participants and for 75% of the iRBD ones, the power of the EDR signals falls outside the traditional HF band range, suggesting the opportunity to carry out respiratory-adjusted HRV analysis. Moreover, in Figure 5. 1 (b) we also observed a significant difference in respiratory rate across the groups during all sleep phases. The results show that the respiratory rate is significantly higher in iRBD group compared to CG group during all sleep phases ($p < 0.015$).

Table 5. 1: Comparisons across idiopathic REM sleep behaviour disorder (iRBD) and control group (CG) for demographics and polysomnographic (PSG) parameters

Parameter	CG (n = 20)	iRBD (n = 20)
Gender (Male)	10 (50 %)	14 (70 %)
Age [years]*	59 ± 10	70 ± 5
TST [mins]	380 ± 85	380 ± 63
RBD duration [months]	N/A	46 ± 40
UPDRS III tot [-]	N/A	0.94 ± 1.7
PLMI [events/h]	13 ± 63	19 ± 41
AHI [events/h]	2 ± 63	7 ± 8
ODI [events/h]	3 ± 63	7 ± 10

Figure 5. 2 shows the pairwise comparison across the two groups (i.e., CG vs. iRBD) during N2, N3 and REM phases for all respiratory-adjusted spectral domain parameters. The study reveals distinct variations in HRV parameters between the CG and the iRBD groups during various sleep phases. The observed decrease in P_{HF} and P_{HRV} in the iRBD group across all sleep stages ($p < 0.004$) suggests a reduced autonomic modulation, particularly marked in the parasympathetic activity, as these parameters are often associated with the vagal tone.

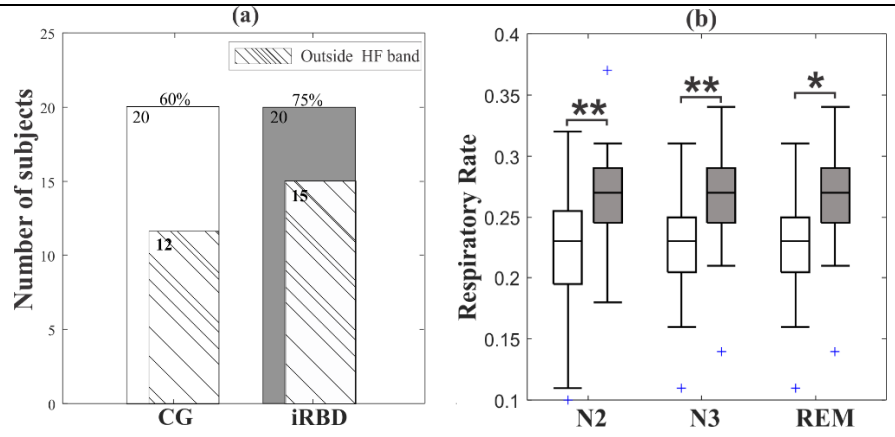


Figure 5. 1: Respiratory frequency content (a) and respiratory rate (b) for CG (in white) and iRBD (in grey) in different sleep phases. Statistical significances for CG vs. iRBD analysis is represented as * ($p < 0.05$) or ** ($p < 0.01$).

The specific reduction of P_{LF} for the iRBD group ($p < 0.004$) could indicate a distinct autonomic dysfunction, as P_{LF} is linked to sympathetic activity only, as the respiratory influence has been removed. Similarly, the reduction in $P^{n_{LF}}$, and the increment in $P^{n_{HF}}$ in the iRBD group during REM ($p < 0.003$), might suggest a compensatory response or an altered

autonomic balance in this sleep phase. These results, overall, point towards a disrupted autonomic regulation in iRBD patients, especially during REM sleep.

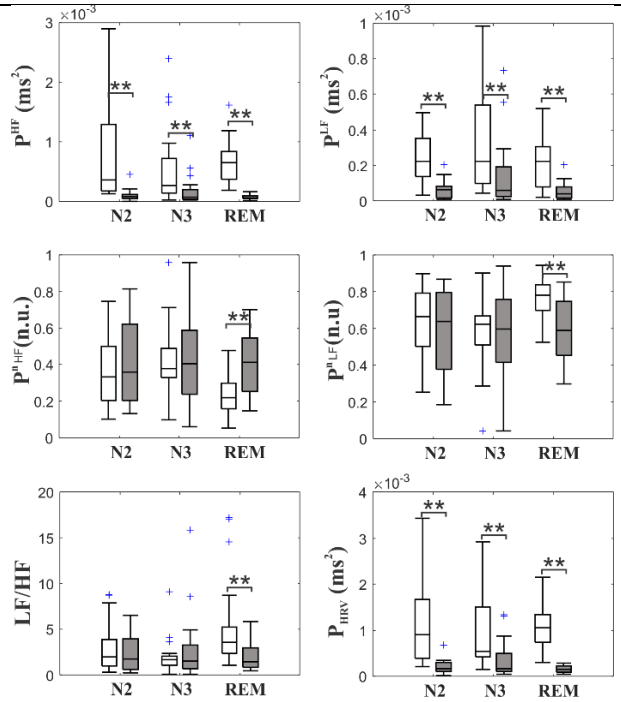


Figure 5. 2: Respiration-guided HRV indexes for CG (in white) and iRBD (in grey) in different sleep phases. The statistically significant results across (CG vs. iRBD) are represented as * ($p < 0.05$) or ** ($p < 0.01$).

Figure 5. 3 highlights the significant differences in HRV indexes across the three sleep phases (N2, N3 and REM phase) within each group separately. The comparison across multiple sleep phases revealed significant differences in $P^{n_{LF}}$, $P^{n_{HF}}$, and the LF/HF ratio in the CG group ($p < 0.05$). However, these differences were not observed in the iRBD group. This suggests a variation in cardiac autonomic regulation in different sleep phases in the unaffected individuals, i.e., CG group. The lack of similar behavior in the iRBD group points to potential disruptions or modulation in cardiac autonomic regulation in such pathology during sleep. This indicates stronger sympathetic activity and reduced parasympathetic influence in REM sleep in the CG group, when compared to N2 and N3. This contrasts with the iRBD group, where such variations are absent, implying a possible dysregulation or blunting of the normal autonomic responses during sleep.

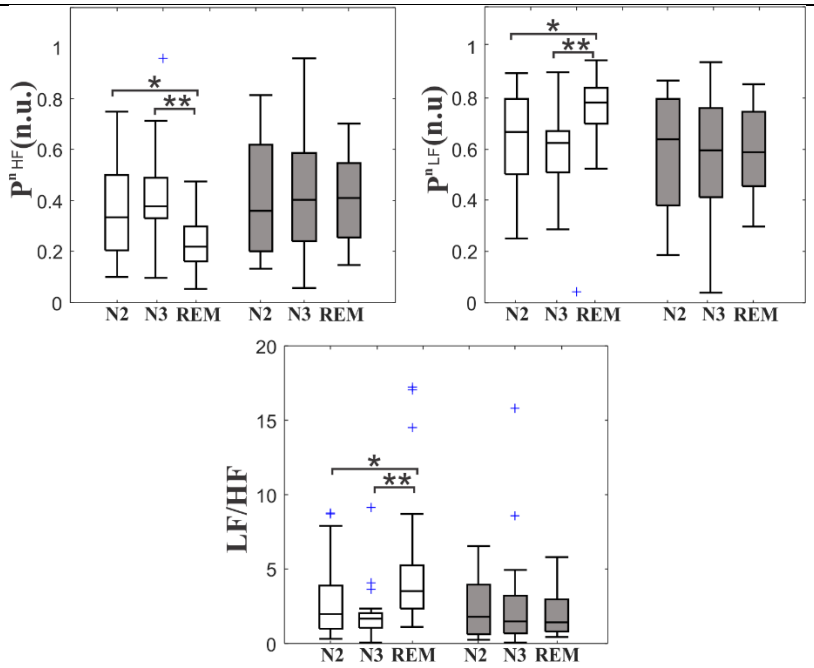


Figure 5. 3: Respiration-guided HRV indexes for CG (in white) and iRBD (in grey) in different sleep phases. The stastically significant results across (CG vs. iRBD) are represented as * ($p < 0.05$) or ** ($p < 0.01$).

5.4. Conclusion

The study reveals significant differences in HRV parameters between the CG and iRBD participants, indicating disrupted autonomic regulation in iRBD during sleep, which is typically not observed in tradition spectral analysis. The adjusted LF and HF spectrum, redefined according to the respiratory rate, provided novel insights into autonomic modulation, suggesting variations in cardiac autonomic regulation during different sleep phases. These findings suggest the importance of incorporating respiratory rate analysis in HRV studies to accurately assess autonomic function in sleep disorders, particularly iRBD. Indeed, by respiratory-adjusted HRV analysis, the contributions of sympathetic and parasympathetic nervous systems may be more accurately identified, thus potentially highlighting important issues that have not been unravelled yet for early detection and intervention in managing these conditions.

5.5. Limitation and future work

As a preliminary study, a key limitation is the small data size, which may affect the generalizability of the findings. Future studies should aim to include larger, more diverse participant cohorts to ensure robust and generalizable results.

Another significant aspect of this study is the consideration of respiratory information in the analysis. While this approach offers valuable insights, it also introduces complexity. To address this, future work should aim to isolate the impact of respiratory activity on HRV measures. Techniques such as orthogonal space projection (OSP) and spectral removal of respiratory components from HRV signals could be employed to achieve this isolation. This approach would provide a clearer understanding of how sympathetic and parasympathetic nervous system contributions to HRV are modulated by respiratory factors. Lastly, given the significant difference in age across the two groups, future studies should also consider investigating the impact of age in addition to the respiratory information.

Chapter 6: Ventricular repolarization variability in REM sleep behavior disorder[5]

Autonomic dysfunction in iRBD and PD-RBD increases the risk of cardiovascular mortality, yet its association with cardiac risk markers remains underexplored. This study investigates QT-variability (QTV), a digital biomarker of ventricular repolarization variability linked to sympathetic outflow and cardiovascular risk, and RR variability (RRV)[6] in iRBD and PD-RBD compared to CG. For the first part of the study, we included 18 healthy participants, 20 people with iRBD, and 20 with PD-RBD. QTV and RRV were derived from 5-minute ECG epochs recorded during polysomnography in two wake states: before sleep (WBS) and after sleep (WAS). Analyses encompassed time and frequency domain indexes, followed by non-parametric statistical methods to evaluate intra- and inter-group patterns. For the second part of the study, 10 drug-naïve PD participants, 10 PD-RBD participants, and 10 control participants were included. Five-minute ECG epochs from polysomnographic recordings during REM sleep were analyzed. QTV was assessed using both time and frequency domain indexes. The first part of the study revealed significant differences in frequency domain RRV and QTV unrelated to RRV (QTVuRRV) indexes between WAS and WBS for both iRBD and PD-RBD groups. Additionally, both iRBD and PD-RBD demonstrated a significant reduction in low- and high-frequency RRV indexes and QTVuRRV compared to the CG group. These findings suggest altered autonomic regulation in iRBD and PD-RBD. However, the absence of significant differences in overall QTV indexes indicates no heightened risk of cardiovascular mortality in these groups. The second part of the study further highlighted that PD patients

[5] This chapter is taken from two articles presented at the 2024 Computing in Cardiology Conference and at the 2024 International Conference of the European Study Group on Cardiovascular Oscillations.
[6] In this chapter, HRV is referred to as RRV to align with the comparison to QTV, as the naming approach is based on specific components of the ECG signal.

exhibited higher QTV compared to both CG and PD-RBD groups during REM phase, suggesting significant cardiac autonomic dysregulation in PD patients.

6.1. Introduction

The details of iRBD, its potential phenoconversion to alpha-synucleinopathies, and the prevalence of autonomic dysfunction in RBD have been extensively discussed in previous chapters. This chapter focuses on further exploring the specific types of autonomic dysfunction observed in iRBD and PD. It is well-established that iRBD and PD patients frequently experience autonomic irregularities such as altered HRV, blood pressure dysregulation, and other cardiovascular changes [99]. HRV has been extensively studied as a marker of autonomic regulation in these populations [100–102]. However, some studies report contrary findings [103], which could be due to HRV analysis only providing information about the irregularities of autonomic function via the SA node [104], but these autonomic irregularities may elevate the risk of cardiovascular mortality [46]. In this context, QTV emerged as an indicator of ventricular repolarization duration variability and cardiac electrical instability. QTV reflects the variation of QT interval in ECG, which represents the time needed for the ventricles to repolarize after each contraction [104] . Given that the duration of the QT interval, particularly when corrected for heart rate (QTc), is commonly associated with cardiovascular risk, QTV indices have similarly been linked to cardiovascular risk in certain patient populations, highlighting its potential as a valuable tool in assessing cardiac health [104].

Despite the recognition of autonomic disturbances in iRBD and PD, the direct relationship between these irregularities and cardiovascular mortality risk remains insufficiently explored. To gain a more comprehensive understanding of cardiac autonomic dysfunction in RBD and PD, it is useful to also consider QTV measures. QTV measures ventricular repolarization

variability and it is usually associated with sympathetic ventricular outflow, especially the part that is not related to HRV [104]. This is crucial because irregularities in ventricular repolarization are linked to increased risk of arrhythmias and sudden cardiac death, which PD patients are prone to [105]. Moreover, PD manifests in various phenotypes, each associated with different outcomes and prognoses. For example, the presence of RBD is often linked to a more severe subtype of PD [99].

To the best of our knowledge, in previous literature, there is no study that has explored the QT interval or QTV in iRBD population. However, previous studies have analyzed prolongation of QT interval in PD patients due to PD severity, autonomic dysfunction or due to the pharmacological therapies such as antidepressants, antiemetics, and atypical antipsychotics drugs [106]. While PD patients experience QT interval prolongation, it is important to differentiate this from QTV. Although both QT duration and QTV are related to ventricular repolarization, there has been no research analyzing QTV specifically in PD patients. Therefore, understanding how QTV characterizes PD is crucial for comprehensively assessing and managing the cardiac risks in PD patients.

On this premise, this pilot study was performed to investigate QTV in two different parts: The first part of the pilot study examines QTV and HRV during two wake states: wake before sleep (WBS) and wake after sleep (WAS), in both RBD groups (i.e., iRBD and PD-RBD). By comparing QTV in these two states, the research aims to find potential variations that could indicate higher cardiovascular risk in these populations. The second part of the study is focused on exploring the QTV in drug-naïve PD patients (i.e., PD and PD-RBD) compared to a CG during REM sleep, as the impact of RBD is more prominent during this phase. In this way, we can highlight any possible link between QTV and cardiovascular risk that could lead to sudden cardiac deaths in RBD patients and also we will be able to enhance our understanding of cardiovascular dysregulation in PD and its subtypes. This will provide critical insights into the

underlying mechanisms of autonomic dysfunction, leading to the development of targeted interventions to reduce cardiovascular mortality risk, ultimately improving patient's outcome.

6.2. Methodology

6.2.1. Study population

i. Wake states analysis

This study involved three groups of participants:

- 18 participants in the control group (CG, average age: 59 ± 8 years, 61% female),
- 20 participants in the iRBD group (average age: 68 ± 9 years, 15% female),
- 20 participants in the PD-RBD group (average age: 73 ± 5 years, 35% female).

Inclusion criteria: In addition to the criteria explained in Chapter 2, subjects with at least five minutes of artifact-free ECG signals in the two wake states—wake before sleep and wake after sleep—were included in the study. The exclusion criteria are the same as those described in Chapter 2.

ii. REM phase analysis

Three groups of participants were included in this study:

- 10 CG participants (55±7 y.o., 70% females),
- 10 PD participant (65±10 y.o., 30% females) and
- 10 PD-RBD participants (66±7 y.o., 30% females).

Inclusion criteria: In addition to the criteria explained in Chapter 2, subjects with at least five minutes of artifact-free ECG signals in the REM sleep phase were included in the study. The exclusion criteria are the same as those described in Chapter 2.

6.2.2. Signal processing

To maintain homogeneity, for every participants, a single 5-minute ECG epoch was extracted from PSG data during wake state before sleep, wake state after sleep, and REM phase. The detection of Q-wave onset, R-peak and T-wave end were performed by a wavelet-based ECG delineator [6], followed by automatic R-peak position refinement and ectopic beat correction, followed by outlier rejection in QT series.

6.2.3. QT variability Analysis

To measure QTV in wake states, time and frequency domain indexes were computed. The time-domain indexes included the corrected QT interval (QTc) with the Bazett's formula, the average of normal RR intervals (RRmean), the average of normal QT intervals (QTmean), the standard deviation of QT interval (SDQT), the normalized QT interval variance (QTVN), and the short-term QT interval variability (STVQT). Frequency-domain indexes included the power of QT-based tachograms (in ms^2) and RR based tachograms (in ms^2) in two frequency bands: i.e., the power at low frequencies (LF), i.e., in the range [0.04-0.15] Hz, namely QTVLF and RRVLF, and the power at high frequency (HF), i.e., in the range [0.15-0.4 Hz], called QTVHF and RRVHF hereinafter. Lastly, the time-frequency coherence between QTV and RRV was calculated to evaluate the local linear coupling of spectral components in both time and frequency domains between the QTV and RRV signals. The time-frequency spectrum of QTV was divided into two parts: QTV related to RRV (QTVrRRV) and QTV unrelated to RRV (QTVuRRV). This division was accomplished by modulating the time-frequency spectrum of QTV with the time-frequency coherence between QTV and RRV [5, 8].

To measure QTV in the REM sleep phase, in addition to the above time domain parameters we have also calculated the QTV index (QTVi), and the QTV ratio (VR). For the frequency-domain analysis, indexes included the power of QT-based tachograms (in ms^2) in three

frequency bands, i.e., the total power (QTVTOT) in [0.04-0.4 Hz], the power at low frequencies (QTVLF), in [0.04-0.15 Hz], and the power at high frequency (QTVHF), in [0.15-0.4 Hz] [2].

6.2.4. Statistical Analysis

A statistical analysis was performed using the pairwise Wilcoxon signed-rank test to assess potential differences in QTV parameters between the two wake states i.e. WBS vs. WAS, for each of the three groups (CG, iRBD, and PD-RBD) individually. Additionally, comparisons were made between the groups (CG vs. RBD, CG vs. PD-RBD, and PD-RBD vs. RBD) during WBS and WAS separately. For this purpose, the non-parametric Wilcoxon rank-sum test was employed, and results with $p<0.05$ were deemed statistically significant. Similarly, to assess any potential statistical difference in QTV parameters during REM phase, statistical analysis was carried out by using the pairwise, non-parametric Wilcoxon rank-sum test across populations, i.e. CG vs. PD, CG vs. PD-RBD, and PD-RBD vs. PD. Results were considered significant for $p < 0.05$.

6.3. Results and Discussion

i. QTV during two wake states

Figure 6. 1 illustrates the time domain indexes (i.e., RR mean, QT mean, QTc mean, SDQT, QTVN, and STVQT) across three groups during the two wake states. For RR mean, all groups showed similar medians (around 1000 ms), as well as for QT and QTc mean (approximately 400-450 ms) revealing no significant differences among all groups and across the different wake states. Similarly, also the other QTV time domain parameters (i.e., SDQT, QTVN and STVQT) did not demonstrate any significant difference across the groups and wake states, thus potentially suggesting a similar cardiovascular risk in iRBD and PD-RBD population compared with CG [104]. However, these parameters require further investigation to capture

the full picture of physiological changes which can be done by comprehensive analysis of all relevant parameters.

Figure 6. 1 represents the frequency domain indexes (i.e., QTVLF, RRVLF, QTVHF and RRVHF) for three groups in the two wake states. Focusing on the comparison between WBS and WAS, iRBD and PD-RBD showed higher RRVLF during WAS than WBS, whereas the CG group did not present the same trend. This suggests that people with iRBD and PD-RBD might suffer from unique disruption in sympathetic and parasympathetic nervous systems. The LF band reflects both of these autonomic influences [46]. Thus, an increase in RRVLF after sleep could suggest a more adaptive autonomic response to stress. Since people with iRBD [107] and PD-RBD [108] often have poor sleep quality, the increased LF variability might be a compensatory mechanism that manifests upon awakening. This shows that their autonomic nervous system is trying to manage the stress caused by disrupted sleep.

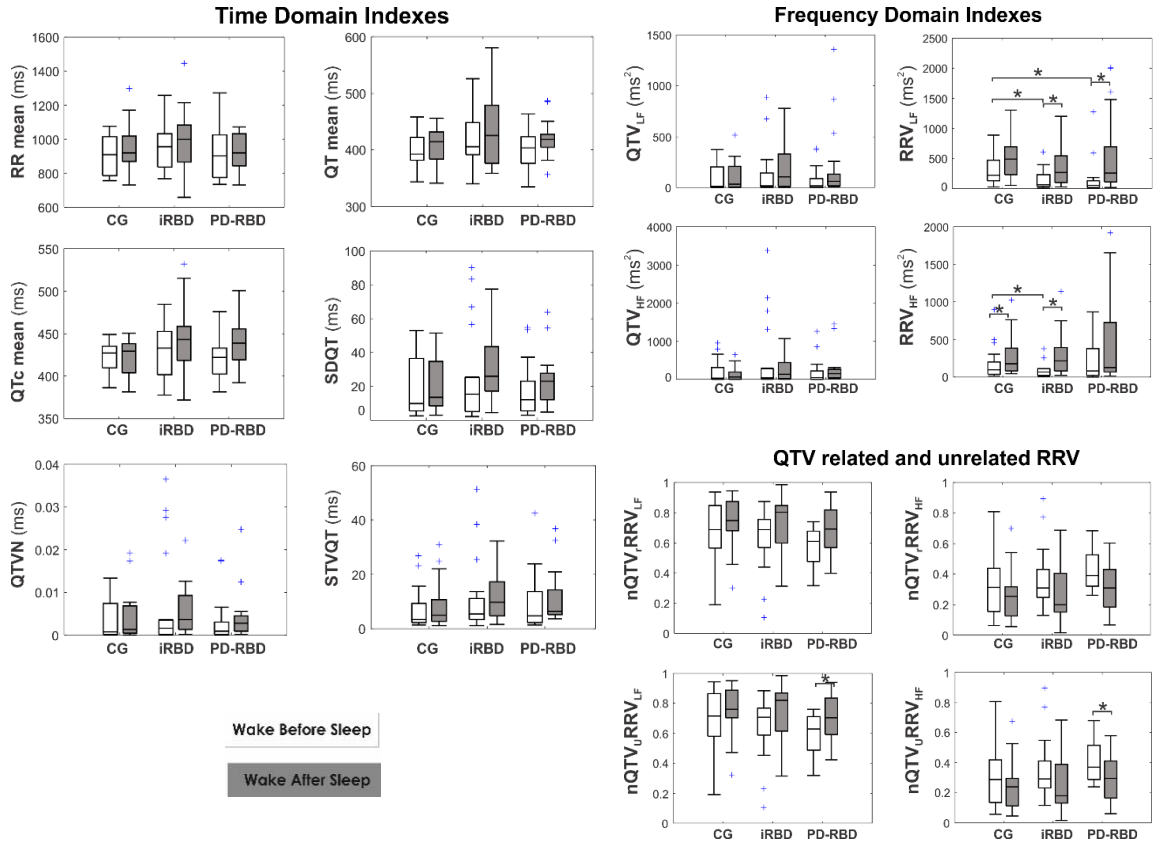


Figure 6. 1: Time domain indexes, Frequency domain indexes and QTV related and unrelated to RRV indexes during wakefulness before (WBS, white) and after (WAS, grey) sleep. Significant differences are marked by *.

The analysis of wake states revealed that both the iRBD and PD-RBD groups had significantly lower RRV_{LF} during WBS compared to WAS, unlike the CG. This suggests that individuals with iRBD and PD-RBD experience autonomic imbalance. These results align with the findings from the analysis conducted across all groups.

Moreover, iRBD group showed significant decrease in RRV_{HF} compared to CG in WBS, thus indicating a decrease in parasympathetic activity. Additionally, iRBD group exhibited significantly higher RRV_{HF} during WAS compared to WBS. A similar trend was observed in the CG group but not in the PD-RBD group. This suggests that the autonomic regulation in the iRBD group is attempting to manage the physiological stress resulting from disrupted sleep. Furthermore, the sleep period is known to boost parasympathetic activity, which likely contributes to the observed increase in RRV_{HF} in the CG group. In contrast, the PD-RBD group appears to lack this compensatory response suggesting a disruption in parasympathetic activity.

Lastly, QTV_{LF} and QTV_{HF} show no significant difference across the groups and wake states. By considering that no statistical differences were found in QTV_{LF}, QTV_{HF}, but significant differences were highlighted in RRV_{LF}, RRV_{HF}, which might suggest that the population studied did not exhibit a higher risk for cardiac events, such as sudden cardiac death, based on these specific indices. Figure 3 shows the results for normalized QTVrRRV and QTVuRRV. By comparing WBS and WAS in PD-RBD group, a significantly higher $nQTVuRRV_{LF}$ and lower $nQTVuRRV_{HF}$ were observed after sleep. This finding indicates higher intrinsic variability and autonomic dysregulation after sleep. Despite this, there were no significant differences in $QTVrRRV_{LF}$ and $QTVrRRV_{HF}$ between WBS and WAS, suggesting stable coupling between HRV and QTV wake states. This highlights that autonomic dysregulation in PD-RBD is more pronounced in intrinsic repolarization processes rather than in HR-modulated processes. In contrast, iRBD groups exhibited no significant differences in QTVuRRV or QTVrRRV in both

LF and HF band, between WBS and WAS, nor across the groups during either wake states, suggesting the autonomic disruption is unique for the PD-RBD group.

ii. QTV during REM sleep phase

Figure 6. 2 shows the time and frequency domain QTV analysis across the three groups during REM sleep phase. There were no significant differences in RRmean, QTmean and QTc values across the three groups. In comparison with CG, PD patients exhibited higher STVQT, QTVLF and QTVHF. This indicates increased variability in ventricular repolarization and suggests more pronounced autonomic dysfunction. Additionally, PD patients had higher SDQT, QTVN, STVQT, QTVi, QTVLF, QTVHF, and QTVTOT compared to PD-RBD, further indicating greater autonomic instability. In contrast, the PD-RBD group showed no significant differences from CG except for significantly lower SDQT and QTVN, suggesting a distinct pattern of autonomic regulation possibly due to the impact of RBD on autonomic control during REM sleep.

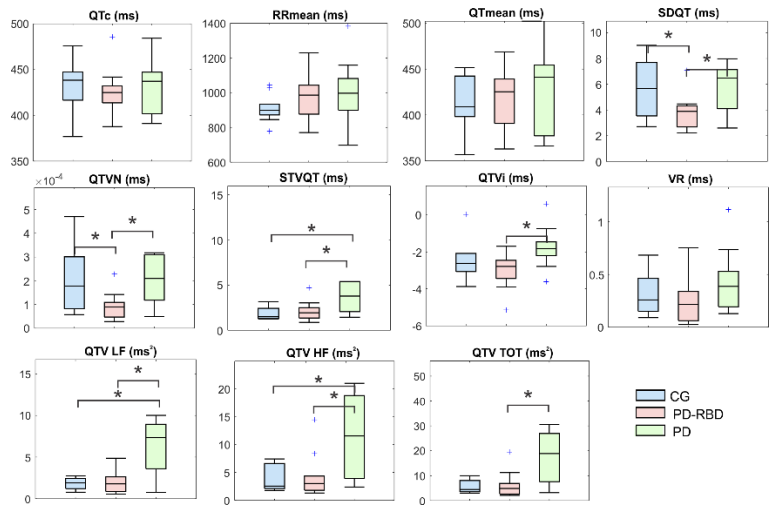


Figure 6. 2: Time and frequency domain QTV indexes during REM. The statistically significant results are marked by *.

6.4. Conclusion

The findings of this pilot study indicated no significant differences in basic cardiovascular parameters across CG, iRBD, and PD-RBD groups during different wakefulness states (both before and after sleep). Despite most of the time and frequency domain parameters show no significant differences (thus suggesting no elevated cardiovascular risk specific to the iRBD and PD-RBD populations), some frequency-domain metrics revealed subtle variations in autonomic responses, particularly an adaptive increase in RRV_{LF} after sleep in iRBD and PD-RBD groups, potentially compensating for poor sleep quality. Moreover, PD-RBD group exhibited specific autonomic alterations in intrinsic repolarization processes, highlighting the need for comprehensive analysis to understand these physiological changes. Moreover, analysis during REM sleep phase indicates that QTV measures provide valuable insights into autonomic dysfunction in PD and its subtypes, offering a preliminary understanding that requires further investigation.

This study has some limitations that should be considered. Firstly, the sample size was relatively small, which may limit the generalization of the findings. Secondly, this study does not account for potential confounding factors that could influence the RRV and QTV indexes, such as respiratory effects and age. Lastly, the research considered wake states and REM state separately: it would be beneficial to extend the analysis to different sleep phases and during wakefulness altogether.

Chapter 7: Adaptive Sigmoid NLMS Filter for Cardiac and Ocular Noise Removal in Polysomnographic EEG

7.1. Introduction

EEG has become a core technology for exploring brain activity, with applications in cognitive neuroscience, clinical diagnostics, and brain-computer interfaces (BCIs). However, the utility of EEG signals is often compromised by artifacts and noise arising from physiological sources, such as ECG/ EOG signals and muscle activity, as well as environmental interferences. These contaminants necessitate robust artifact removal techniques to ensure reliable and accurate EEG analysis, especially in real-time applications [109].

Over the years, significant advancements have been made in EEG noise removal [109, 110] , with various state-of-the-art techniques tackling the challenges of artifact suppression in PSG data in real-time EEG systems [111–119]. Traditional methods, including adaptive [119] and notch filters, have been widely used to mitigate powerline interference and baseline wander. Despite their simplicity, these approaches often compromise signal fidelity. Advanced methods, such as Complete Ensemble Empirical Mode Decomposition with Adaptive Noise [118], offer high accuracy in artifact isolation but at the cost of computational complexity, which makes them unsuitable in real-time applications. Similarly, Blind Source Separation techniques, such as Independent Component Analysis, excel in separating mixed signals, including ocular and muscular artifacts, but require significant computational resources and manual intervention [109, 110], and are more suitable for batch processing. While promising, hybrid models and deep learning approaches frequently involve complex pipelines and dependency on large datasets, limiting their applicability in wearable EEG systems [109, 110].

One of the most computationally efficient techniques for real-time EEG denoising is the Least Mean Squares (LMS) algorithm and its variants [120]. The Normalized LMS (NLMS) algorithm has gained popularity for its adaptability and stability under various signal conditions [120–124]. However, standard NLMS-based approaches face notable limitations when dealing with dynamic and non-stationary signal conditions. These include challenges such as limited capacity to model non-linear relationships in the data, lack of effective mechanisms to manage large and abrupt variations in the error signal, and susceptibility to instability during rapid changes in noise characteristics [120–124]. Furthermore, standard NLMS filters often struggle to achieve optimal performance in scenarios requiring precise artifact suppression without compromising the integrity of the EEG signal [120–124]. These limitations highlight the need for enhancements that can address such challenges while retaining the computational efficiency of the NLMS framework.

This work draws inspiration from the NLMS filtering approach and explores potential enhancements to its framework by incorporating Polynomial Non-Linearity, Sigmoid-Based Activation, and Variable Step Size. These modifications aim to address challenges associated with artifact suppression while maintaining computational efficiency. The Sigmoid-Based Activation introduces a scaling mechanism for the error signal, potentially improving the filter's response to noise variability. Additionally, the Variable Step Size dynamically adjusts the learning rate based on the normalized error, providing flexibility in adapting to different noise characteristics. Together, these concepts aim to build on the foundational strengths of NLMS filtering for more robust signal processing.

7.2. Methodology:

7.2.1. Dataset

The study utilized the publicly available "MIT-BIH Polysomnographic (PSG)" database, comprising 18 recordings from the Beth Israel Hospital Sleep Laboratory in Boston. Participants had a mean age of 44 years (±12), and the dataset includes over 80 hours of PSG data with four-, six-, and seven-channel configurations. Signals recorded at 250 Hz include EEG, ECG, blood pressure, respiratory signals, and, in some cases, oxygen saturation, EOG, and EMG. For this study, only EEG and ECG signals segments of 10 minutes were analyzed to meet the research objectives.

7.2.2. Adaptive Sigmoid NLMS

The Adaptive Sigmoid-Polynomial NLMS (AS-NLMS) algorithm incorporates two key features—Sigmoid-Based Activation, and Variable Step Size—to improve adaptability, stability, and robustness, particularly for non-linear and dynamic artifact removal scenarios in EEG signals.

AS-NLMS Framework

The AS-NLMS algorithm operates by minimizing the error signal $e(n)$, which is defined as the difference between the corrupted EEG signal $d(n)$ and the filter output $y(n)$:

$$e(n) = d(n) - y(n) \tag{7.1}$$

where $y(n)$ is computed as:

$$y(n) = w^T(n)x(n) \tag{7.2}$$

where $w(n)$ represents the filter weight vector at iteration n, and $x(n)$ the input signal vector containing artifact information i.e., ECG noise.

Sigmoid-Based Activation

To manage the impact of abrupt changes in noise or large error values, the algorithm employs a sigmoid activation function. This function dynamically scales the error signal, ensuring smoother weight adjustments:

$$activation = \frac{\alpha}{1-\exp(-\beta.e(n))} \tag{7.3}$$

where:

- α: Scaling parameter for controlling the activation magnitude,
- β: Parameter governing the steepness of the sigmoid curve.

Variable Step Size

The algorithm introduces a dynamic step size, k, that changes over time based on the error and the sigmoid activation:

$$k = \frac{\mu \cdot activation}{a+\|x(n)\|^2} \tag{7.4}$$

where:

- μ: Initial step size
- a: Bias parameter to stabilize learning in low-power conditions to avoid division by zero.
- $\|x(n)\|^2$: Power of the input signal

Weight Update Rule:

The weight update equation for the ASP-NLMS algorithm combines these features:

$$w(n+1) = w(n) + k \cdot e(n) \cdot x(n)) \quad (7.5)$$

7.2.3. Performance Evaluation Metrics

The performance of the proposed AS-NLMS algorithm is compared against three widely used adaptive filter algorithms: LMS, NLMS, and Recursive Least Squares (RLS). The evaluation was conducted using three key metrics: Mean Square Error (MSE), peak Signal-to-Noise Ratio (pSNR), and Computational Time Efficiency (CTE), considering different filter orders (32, 64, and 128 taps). These metrics offer a comprehensive assessment of the algorithms' effectiveness and efficiency in real-world noise removal scenarios.

7.2.4. Statistical Analysis

The data were evaluated for normality using the Shapiro-Wilk test. Since the results indicated that the data followed a non-normal distribution a non-parametric Friedman test was used to assess the significant differences across the four algorithms. The Friedman test, a non-parametric test equivalent to the parametric repeated measures ANOVA, is suitable for analyzing data collected under multiple conditions from the same subjects. After the Friedman test, pairwise comparisons were conducted using Wilcoxon signed-rank test to directly compare AS-NLMS with the other algorithms. Lastly, to account for multiple comparisons, Bonferroni correction was applied, with adjusted significance levels set at $p<0.05$ for the first level of significance, $p<0.01$ for the second level, and $p<0.002$ for the third level.

7.3. Results and Discussion

The AS-NLMS filter performance was evaluated against LMS, NLMS, and RLS filters across three key metrics: Mean Square Error (MSE), Peak Signal-to-Noise Ratio (PSNR), and execution time, for filter with 32, 64, and 128 taps. The results demonstrate that the AS-NLMS filter achieves a good balance between signal morphology preservation and computational efficiency, making it a robust choice for real-time signal processing applications.

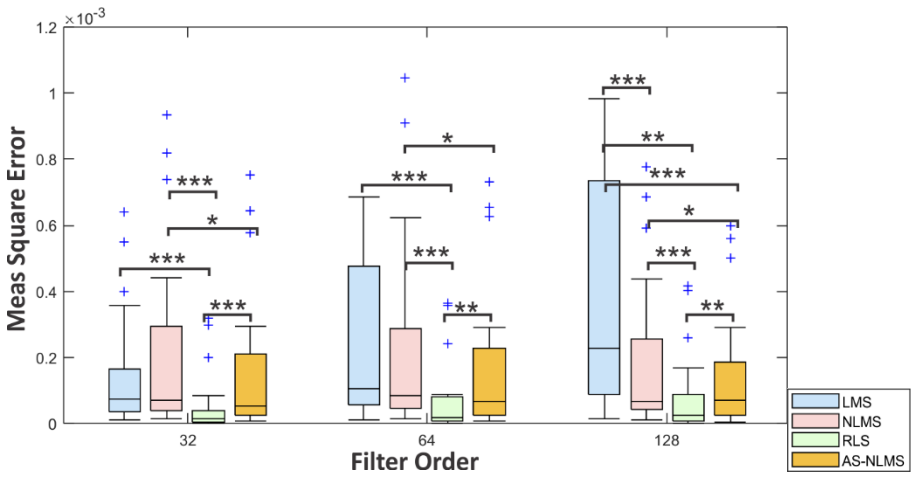


Figure 7. 1: Mean Square Error (MSE) comparison of the Adaptive LMS filter, Adaptive NLMS filter, Adaptive RLS filter, and Adaptive AS-NLMS filter across filter orders (32, 64, and 128 taps).

Some outliers have been removed for visualization specifically from LMS filter. Outlier 1 with a value of 9.78×10^{15} was removed at a filter order of 64, Additionally, two outliers were removed at a filter order of 128: one with a value of 1.37×10^{89} and another with a value of 7.87×10^{53}

The MSE metric quantifies the average squared error between the original signal and the denoised signal, where lower values represent better noise suppression and signal reconstruction accuracy, in case of spiky noise (as the QRS of the ECG can be considered in this case). The AS-NLMS filter achieved significantly lower MSE values compared to the LMS filter ($p < 0.002$) at 128 taps and the NLMS filter across all filter lengths (32, 64, and 128); $p < 0.05$) demonstrating its superior ability in preserving the underlying EEG signal. For instance, at higher filter orders, the LMS filter exhibited increasing instability, with higher MSE values due to overfitting or improper adaptation. Both LMS and NLMS filters struggled

to maintain low MSE values as filter orders increased, as shown in Figure 7. 1 with NLMS filter performing slightly better than LMS. Moreover, for some records, LMS filter degrades the EEG signal completely as shown in Figure 7. 2. In contrast, the AS-NLMS filter demonstrated remarkable robustness, maintaining consistent MSE values even at higher filter orders, i.e. with 128 taps. Moreover, it also maintains the comparable MSE as of RLS filter at higher filter orders, showing second level ($p < 0.01$) of significant difference between RLS and AS-NLMS. Conversely, LMS ($p < 0.002$) and NLMS ($p < 0.005$) still showed third level of significantly higher MSE value compared to AS-NLMS. This stability highlights its adaptability in handling complex signal patterns while effectively suppressing noise. Although the RLS filter achieved the lowest MSE across all orders, this improvement came at a significantly higher computational cost, as discussed below. Thus, the AS-NLMS filter provides an optimal trade-off by balancing accuracy and efficiency, particularly in scenarios where low error is desirable but computational resources are limited.

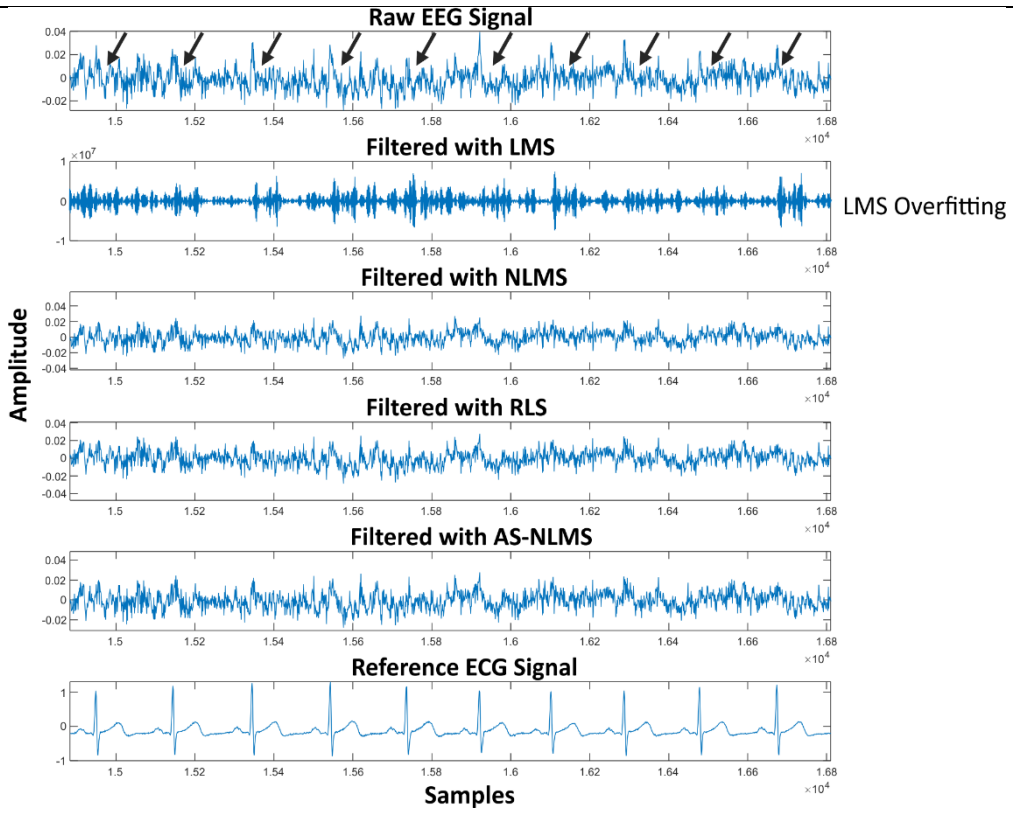


Figure 7. 2: Comparison of Adaptive Filtering Algorithms for EEG Signal Noise Suppression, Highlighting Overfitting Behavior in the LMS Filter.

The pSNR metric evaluates the ratio between the signal's power and the power of the noise, with higher values indicating better signal reconstruction quality. In Figure 7. 3 the AS-NLMS filter showed significantly higher pSNR values compared to both the LMS filter *($p < 0.002$)* with 128 taps and the NLMS filter across all lengths (32, 64, and 128; *$p < 0.05$).* This highlights its ability in effectively suppressing noise while preserving the integrity of the EEG signal. The AS-NLMS filter showed improved performance, with the difference between RLS and AS-NLMS decreasing from the third level *($p < 0.002$ at 32 taps)* to the second level ($p < 0.01$ at 128 taps) as its pSNR improved with higher filter orders. In contrast, LMS and NLMS experienced a decline in pSNR as the filter order increased, while their significant differences with RLS remained at the third level *($p < 0.002$)*. This demonstrates AS-NLMS filter capacity to avoid overfitting and adapt efficiently to different noise conditions. While the RLS filter exhibited marginally higher pSNR values than the AS-NLMS filter, the difference is relatively

minor compared to the substantial computational cost. Therefore, the AS-NLMS filter is particularly advantageous for applications requiring a high-quality denoised signals without excessive computational demands.

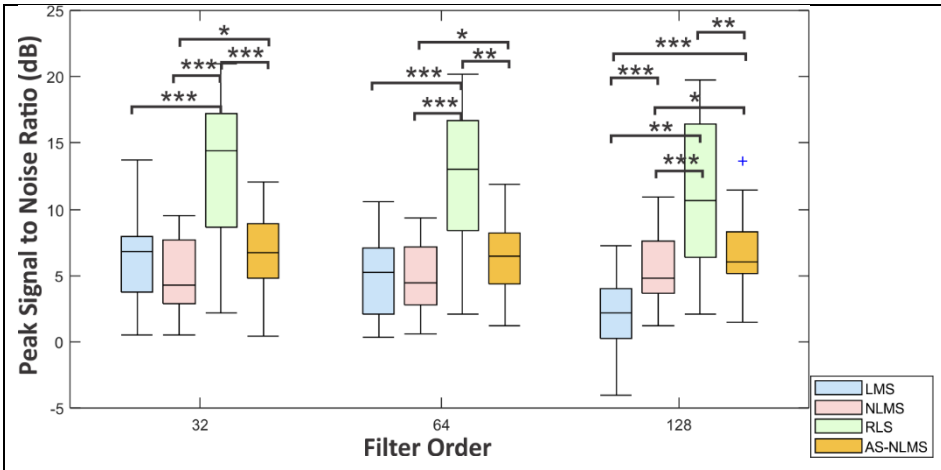


Figure 7. 3: Peak signal to noise ratio (pSNR) comparison of the Adaptive LMS filter, Adaptive NLMS filter, Adaptive RLS filter, and Adaptive AS-NLMS filter across filter orders 32, 64, and 128.

Some outliers have been removed for visualization specifically from LMS filter. Outlier one with a value of -194.96 was removed at a filter order of 64, Additionally, two outliers were removed at a filter order of 128: one with a value of -926.42, second with a value of and another with a value of -575.80.

The Figure 7. 4 represents the execution time metric highlighting the computational efficiency of each filter, particularly critical for real-time applications. The RLS filter, while achieving the best performance in terms of MSE and PSNR, incurred the highest execution time, which increased significantly with higher filter orders. For instance, at a filter order of 128, the RLS filter's execution time was several orders of magnitude greater than that of the AS-NLMS filter, making it impractical for applications with strict time constraints. In contrast, the AS-NLMS filter demonstrated excellent computational efficiency, with execution times comparable to or only slightly higher than those of LMS and NLMS filters. This efficiency ensures that the AS-NLMS filter is well-suited for real-time signal processing tasks, particularly in embedded systems, wearable devices, or low-power environments. The filter's ability to deliver

competitive performance with minimal computational overhead make it a practical solution for scenarios where both accuracy and speed are required.

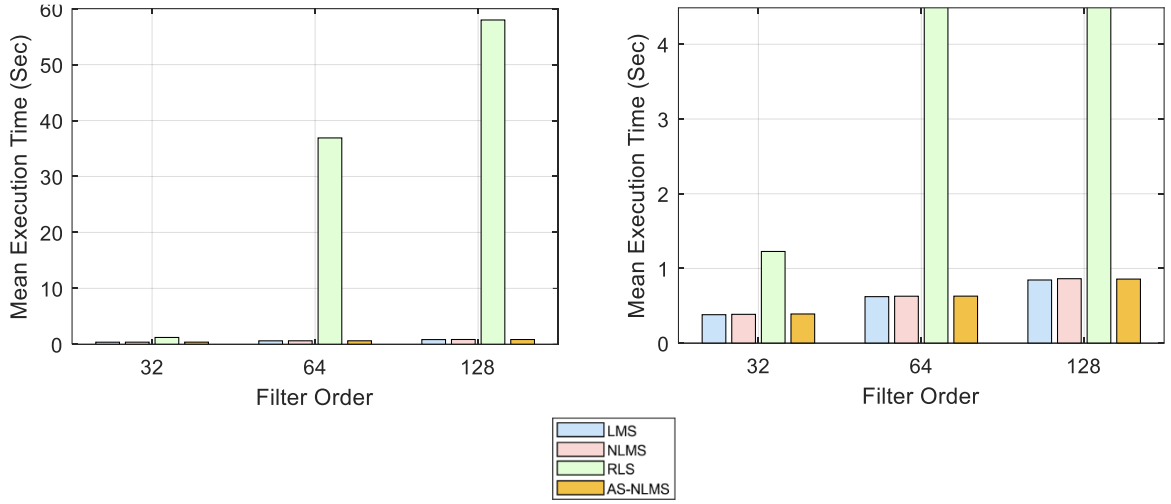


Figure 7. 4: Comparison of mean execution times for different adaptive filters (LMS, NLMS, RLS, and AS-NLMS) across filter orders of 32, 64, and 128 (a). A zoomed-in view of the execution times for LMS, NLMS, and AS-NLMS filters (b)

The AS-NLMS filter's overall performance positions it as a middle ground between the computationally intensive RLS filter and the simpler LMS and NLMS filters. While the RLS filter achieved the best MSE and pSNR values, its excessive execution time makes it less suited for real-time resource-constrained applications. Conversely, the LMS and NLMS filters, though computationally efficient, exhibited instability and degraded performance at higher filter orders, making them less reliable for accurate signal recovery. The AS-NLMS filter, on the other hand, provided consistent and reliable performance across all filter orders. Its low MSE and high PSNR values, combined with its efficient execution time, highlight its ability to balance accuracy and computational efficiency. This makes it a robust and scalable choice for applications requiring stable performance across varying conditions, particularly in real-time scenarios. An example of the filter out in time domain and frequency domain is represented in Figure 7. 5.

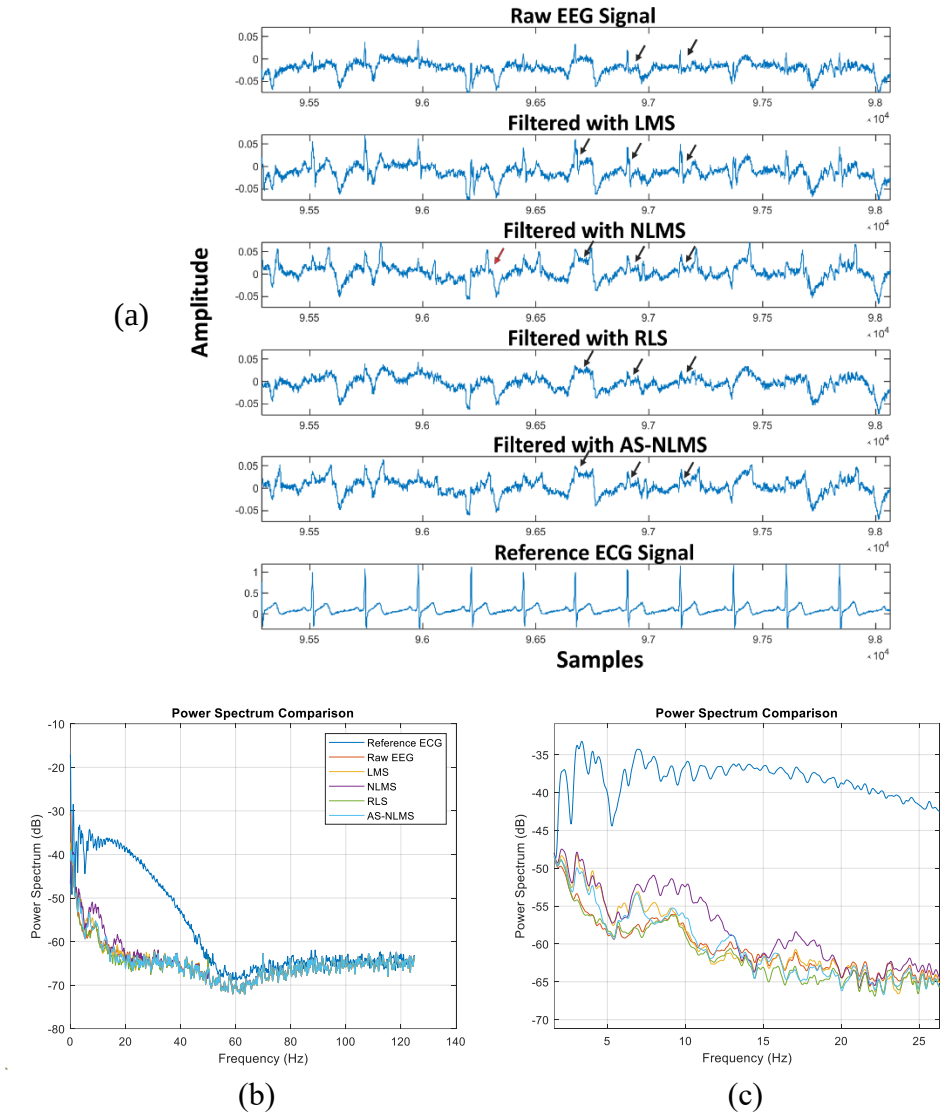


Figure 7. 5: Raw EEG signal, filtered EEG signals using Adaptive LMS, NLMS, RLS, and AS-NLMS filters, and the reference ECG signal (a). The power spectrum comparison of these signals is shown in (b),. A zoomed-in view of the power spectrum comparison in the 0–15 Hz range is presented in (c) for detailed analysis.

7.4. Conclusion

The AS-NLMS filter stands out as a practical and effective solution for real-time EEG denoising tasks in PSG recording systems. It combines superior noise suppression capabilities with computational efficiency, making it suitable when real-time performance and accuracy are critical. Its ability to maintain stability and consistent performance even at high filter orders further enhances its applicability in resource-constrained environments, such as wearable

medical devices or embedded systems. While the RLS filter remains the best solution in terms of signal quality, the AS-NLMS filter provides a compelling alternative for scenarios where speed and efficiency are equally important.

Chapter 8: Conclusion and Future Directions

This thesis sheds light on autonomic dysfunction in neurodegenerative conditions, particularly focusing on iRBD, by studying ECG-derived indexes that could be refined to give raise to digital biomarkers of neurodegeneration. By integrating novel methodologies and tools, this work highlights the significant potentialities of HRV and QTV for early detection and disease progression monitoring.

The findings demonstrate that iRBD patients exhibit distinct autonomic patterns during sleep, characterized by sympathetic dominance and reduced parasympathetic control, particularly during the REM and N2 phases. This early disruption in autonomic regulation, often preceding the clinical onset of neurodegenerative diseases, underscores the critical role of HRV analysis in phenotyping and risk stratification. Moreover, the exploration of respiration guided HRV-analysis also revealed distinct patterns of autonomic dysregulation for iRBD patients in N3 sleep phase, which was not observed in this thesis with simple HRV analysis without respiration correction. Additionally, the thesis investigated QTV to explore ventricular repolarization variability in the study population, offering complementary perspectives on autonomic and cardiac dysfunction.

In this context, the development of the UNICA-HRV tool represents a relevant contribution to HRV analysis in sleep research, especially for clinicians and people with limited programming skills. This customizable and user-friendly platform bridges critical gaps in existing HRV software tools, primarily thanks to the integration of hypnogram with ECG signal, thus streamlining the process of stage-specific analyses.

As a part of my industrial experience, still in the path of the PSG signals, this thesis introduced the Adaptive Sigmoid Normalized Least Mean Square (AS-NLMS) algorithm for artifact removal in EEG signals, by addressing the challenges of dynamic and nonlinear environments.

This algorithm, conceived for resource-constrained real-time EEG processing scenarios, is able to enhance the quality of EEG signals, facilitating accurate neural activity interpretation. The algorithm is currently being ported by the company to be integrated in their systems.

Overall, this work demonstrates the transformative potential of combining engineering and neuroscience to develop advanced tools and methodologies. These contributions pave the way for early diagnosis, improved patient outcomes, and personalized management of neurodegenerative diseases. Future research can build upon these findings by integrating additional digital and non-digital biomarkers, along with metadata, and exploring longitudinal datasets, to define predictive models of phenoconversion hitherto unavailable.

8.1. Future Directions

One of the most promising opportunities is the exploration of additional biomarkers. Integrating various physiological data, demographic factors, and digital biomarkers—such as the Mini-Mental State Examination, lifestyle habits (e.g., smoking, alcohol consumption), gait analysis, and neurophysiological data like EEG or neuroimaging—could offer a more holistic understanding of the mechanisms underlying RBD. This comprehensive approach has the potential to enhance predictive capabilities for phenoconversion to neurodegenerative diseases, including PD and DLB.

Another promising direction is the integration of machine learning in the loop. By leveraging advanced algorithms to analyze complex, multidimensional datasets, researchers can uncover hidden patterns and interactions among biomarkers that may not be evident through traditional statistical methods. Machine learning could enable the development of automated systems for early diagnosis, risk stratification, and prediction of disease progression. Such approaches could also enhance the scalability and accuracy of diagnostic tools, potentially transforming clinical practice.

Expanding the UNICA-HRV tool to include features that account for factors influencing HRV analysis, such as gender, age and respiration, would significantly enhance its utility. Additionally, incorporating options for statistical analysis within the software would provide a comprehensive package for sleep HRV analysis, benefiting the research and clinical community alike.

Longitudinal studies are also crucial to understand the temporal dynamics of autonomic and cardiac biomarkers. Tracking patients over time would help establishing the trajectory of changes in HRV, QTV, and other biomarkers, clarifying their relationship with the onset and progression of neurodegenerative diseases. Such studies could also aid in identifying critical time windows for therapeutic interventions.

Together, these research directions represent a roadmap for advancing the field, building upon the contributions of this thesis, and working toward the ultimate goal of early diagnosis, effective intervention, and improved outcomes for patients with RBD and related.

Reference:

[1] Watson NF, Safwan Badr ; M, Belenky ; Gregory, et al. Recommended Amount Of Sleep For A Healthy Adult Non-Participating Observers. *Sleep* 2015; 38: 1161–1183.

[2] Almeneessier AS, Gupta R, Pandi-Perumal SR, et al. Overview of sleep disorders. *The Behavioral, Molecular, Pharmacological, and Clinical Basis of the Sleep-Wake Cycle* 2019; 103–122.

[3] Luyster FS, Strollo PJ, Zee PC, et al. Sleep: A health imperative. *Sleep* 2012; 35: 727–734.

[4] Reiter RJ, Sharma R, Cucielo MS, et al. Brain washing and neural health: role of age, sleep, and the cerebrospinal fluid melatonin rhythm. *Cellular and Molecular Life Sciences* 2023; 80: 1–22.

[5] Carley DW, Farabi SS. Physiology of sleep. *Diabetes Spectrum* 2016; 29: 5–9.

[6] Van Hout S. The American Academy of sleep Medicine Inter-scorer Reliability Program: Sleep stage scoring Richard S. Rosenberg1. *Journal of Clinical Sleep Medicine* 2013; 9: 81–87.

[7] Suzuki Y, Abe T, Kawana F. Instability of scoring stage n1 is a factor that reduces repeatability of human sleep staging. *Sleep Med* 2019; s369: 64.

[8] Basner M, Griefahn B, Penzel T. Inter-rater agreement in sleep stage classification between centers with different backgrounds. *Somnologie* 2008; 12: 75–84.

[9] Zhang D, Sun J, She Y, et al. A two-branch trade-off neural network for balanced scoring sleep stages on multiple cohorts. *Front Neurosci*; 17. Epub ahead of print 2023. DOI: 10.3389/fnins.2023.1176551.

[10] Swihart BJ, Caffo B, Bandeen-Roche K, et al. *Characterizing Sleep Structure Using the Hypnogram*. 2008.

[11] Fekedulegn D, Andrew ME, Shi M, et al. Actigraphy-based assessment of sleep parameters. *Ann Work Expo Health* 2020; 64: 350–367.

[12] Chokroverty S, Bhat S. Physiological changes in sleep. *Case Studies in Clinical Psychological Science: Bridging the Gap from Science to Practice* 2017; 1–7.

[13] Bramich S, King A, Kuruvilla M, et al. Isolated REM sleep behaviour disorder: current diagnostic procedures and emerging new technologies. *Journal of Neurology* 2022; 269: 4684–4695.

[14] St Louis EK, Boeve BF. REM Sleep Behavior Disorder: Diagnosis, Clinical Implications, and Future Directions. *Mayo Clinic Proceedings* 2017; 92: 1723–1736.

[15] Inoue Y, Sasai-Sakuma T. RBD and the Autonomic Nervous System. *Rapid-eye-movement sleep behavior disorder* 2019; 465–474.

[16] Pérez-Carbonell L, Iranzo A. Clinical Aspects of Idiopathic RBD. *Rapid-eye-movement sleep behavior disorder* 2019; 33–52.

[17] Fantini ML, Ferini-Strambi L. Idiopathic rapid eye movement sleep behaviour disorder. *Neurological Sciences*; 28. Epub ahead of print January 2007. DOI: 10.1007/s10072-007-0734-z.

[18] Haba-Rubio J, Frauscher B, Marques-Vidal P, et al. Prevalence and determinants of rapid eye movement sleep behavior disorder in the general population. *Sleep*; 41. Epub ahead of print 1 February 2018. DOI: 10.1093/sleep/zsx197.

[19] Wang H, Zhang T, Fan W. Prevalence and impact of rapid eye movement sleep behavior disorder in multiple system atrophy: a systematic review and meta-analysis. *Frontiers in Neurology*; 15. Epub ahead of print 2024. DOI: 10.3389/fneur.2024.1453944.

[20] Zhang X, Sun X, Wang J, et al. Prevalence of rapid eye movement sleep behavior disorder (RBD) in Parkinson's disease: a meta and meta-regression analysis. *Neurological Sciences* 2017; 38: 163–170.

[21] Selvam S, Ayyavoo V. Biomarkers in neurodegenerative diseases: a broad overview. *Exploration of Neuroprotective Therapy* 2024; 119–147.

[22] Koníčková D, Menšíková K, Tučková L, et al. Biomarkers of Neurodegenerative Diseases: Biology, Taxonomy, Clinical Relevance, and Current Research Status. *Biomedicines*; 10. Epub ahead of print 1 July 2022. DOI: 10.3390/biomedicines10071760.

[23] Chen-Plotkin AS. Unbiased approaches to biomarker discovery in neurodegenerative diseases. *Neuron* 2014; 84: 594–607.

[24] Chudzik A, Śledzianowski A, Przybyszewski AW. Machine Learning and Digital Biomarkers Can Detect Early Stages of Neurodegenerative Diseases. *Sensors*; 24. Epub ahead of print 1 March 2024. DOI: 10.3390/s24051572.

[25] Dorsey ER, Papapetropoulos S, Xiong M, et al. The first frontier: Digital biomarkers for neurodegenerative disorders. *Digital Biomarkers* 2017; 1: 6–13.

[26] Sun YM, Wang ZY, Liang YY, et al. Digital biomarkers for precision diagnosis and monitoring in Parkinson's disease. *npj Digital Medicine*; 7. Epub ahead of print 1 December 2024. DOI: 10.1038/s41746-024-01217-2.

[27] Gibbons CH. Basics of autonomic nervous system function. In: *Handbook of Clinical Neurology*. Elsevier B.V., 2019, pp. 407–418.

[28] Gordan R, Gwathmey JK, Xie L-H. Autonomic and endocrine control of cardiovascular function. *World J Cardiol* 2015; 7: 204.

[29] Shaffer F, McCraty R, Zerr CL. A healthy heart is not a metronome: an integrative review of the heart's anatomy and heart rate variability. *Front Psychol*; 5. Epub ahead of print 30 September 2014. DOI: 10.3389/fpsyg.2014.01040.

[30] Kusuki H, Tsuchiya Y, Mizutani Y, et al. QT Variability Index is Correlated with Autonomic Nerve Activity in Healthy Children. *Pediatr Cardiol* 2020; 41: 1432–1437.

[31] Coumel P, Maison-Blanche P. *7. Heart rate variability and QT interval: their relationships with the cardiac frequency*.

[32] Zhong L, Tan RS, Ghista DN. *Anatomy and Physiology of the Heart*, www.worldscientific.com.

[33] Bayés De Luna A, Batchvarov VN, Malik M. *The Morphology of the Electrocardiogram*.

[34] Sammito S, Thielmann B, Böckelmann I. Update: factors influencing heart rate variability–a narrative review. *Frontiers in Physiology*; 15. Epub ahead of print 2024. DOI: 10.3389/fphys.2024.1430458.

[35] Damoun N, Amekran Y, Taiek N, et al. Heart rate variability measurement and influencing factors: Towards the standardization of methodology. *Glob Cardiol Sci Pract*; 2024. Epub ahead of print 1 August 2024. DOI: 10.21542/gcsp.2024.35.

[36] Rundo JV, Downey R. Polysomnography. In: *Handbook of Clinical Neurology*. Elsevier B.V., 2019, pp. 381–392.

[37] AASM | International Classification of Sleep Disorders, https://aasm.org/clinical-resources/international-classification-sleep-disorders/ (accessed 7 December 2024).

[38] Gauld C, Lopez R, Geoffroy PA, et al. A systematic analysis of ICSD-3 diagnostic criteria and proposal for further structured iteration. *Sleep Medicine Reviews*; 58. Epub ahead of print 1 August 2021. DOI: 10.1016/j.smrv.2021.101439.

[39] Postuma RB, Berg D, Stern M, et al. MDS clinical diagnostic criteria for Parkinson's disease. *Movement Disorders* 2015; 30: 1591–1601.

[40] Martínez JP, Almeida R, Olmos S, et al. A Wavelet-Based ECG Delineator Evaluation on Standard Databases. *IEEE Trans Biomed Eng* 2004; 51: 570–581.

[41] Article J. The electronic evaluation of the fetal heart rate: Preliminary report. *Obstetrical & Gynecological* 1958; 13: 654–656.

[42] Akselrod S, Gordon D, Ubel FA, et al. Power Spectrum Analysis of Heart Rate Fluctuation: A Qantitative Probe of Beat-to-Beat Cardiovascular Control. 1981; 213: 220–222.

[43] Acharya UR, Joseph KP, Kannathal N, et al. Heart rate variability: A review. *Med Biol Eng Comput* 2006; 44: 1031–1051.

[44] Shaffer F, Ginsberg JP. An Overview of Heart Rate Variability Metrics and Norms. *Front Public Health* 2017; 5: 1–17.

[45] Lehrer P, Eddie D. Dynamic processes in regulation and some implications for biofeedback and biobehavioral interventions. *Applied Psychophysiology Biofeedback* 2013; 38: 143–155.

[46] Stauss HM, Physiol AJ, Integrative R, et al. Heart rate variability, Standards of Measurement, Physiological Interpretation, and Clinical Use Task. 2005; 93: 927–931.

[47] Plews DJ, Laursen PB, Stanley J, et al. Training adaptation and heart rate variability in elite endurance athletes: Opening the door to effective monitoring. *Sports Medicine* 2013; 43: 773–781.

[48] Kemp AH, Quintana DS, Felmingham KL, et al. Depression, comorbid anxiety disorders, and heart rate variability in physically healthy, unmedicated patients: Implications for cardiovascular risk. *PLoS One* 2012; 7: 30777.

[49] Malik M, Camm AJ. Heart rate variability and clinical cardiology. *Br Heart J* 1994; 71: 3.

[50] Ahmad S, Ramsay T, Huebsch L, et al. Continuous multi-parameter heart rate variability analysis heralds onset of sepsis in adults. *PLoS One* 2009; 4: 642.

[51] Jahrami H, Drury RL, Yin G, et al. Using sleep heart rate variability to investigate the sleep quality in children with obstructive sleep apnea. *Front Public Health* 2023; 11: 1103085.

[52] Lee S, Hwang H Bin, Park S, et al. Mental Stress Assessment Using Ultra Short Term HRV Analysis Based on Non-Linear Method. *Biosensors (Basel)* 2022; 12: 465.

[53] Kim KK, Baek HJ, Lim YG, et al. Effect of missing RR-interval data on nonlinear heart rate variability analysis. *Comput Methods Programs Biomed* 2012; 106: 210–218.

[54] Kim KK, Kim JS, Lim YG, et al. The effect of missing RR-interval data on heart rate variability analysis in the frequency domain. *Physiol Meas* 2009; 30: 1039–1050.

[55] Molina-Picó A, Cuesta-Frau D, Miró-Martínez P, et al. Influence of QRS complex detection errors on entropy algorithms. Application to heart rate variability discrimination. *Comput Methods Programs Biomed* 2013; 110: 2–11.

[56] Nabil D, Bereksi Reguig F. Ectopic beats detection and correction methods: A review. *Biomed Signal Process Control* 2015; 18: 228–244.

[57] Sim CS, Sung JH, Cheon SH, et al. The effects of different noise types on heart rate variability in men. *Yonsei Med J* 2015; 56: 235–243.

[58] Hu A, Ghiasi S, Windsor-Plainsboro W. The Role of Morphology and Heart Rate Variability Features in Detecting Arrhythmias from Short ECGs. *Journal of Student Research*; 12.

[59] Tarvainen MP, Niskanen JP, Lipponen JA, et al. Kubios HRV - Heart rate variability analysis software. *Comput Methods Programs Biomed* 2014; 113: 210–220.

[60] Behar JA, Rosenberg AA, Weiser-Bitoun I, et al. PhysioZoo: A novel open access platform for heart rate variability analysis of mammalian electrocardiographic data. *Front Physiol* 2018; 9: 1390.

[61] Ramshur JT. *Design, evaluation, and application of Heart Rate Variability Analysis Software (HRVAS)*. 2010.

[62] Rodríguez-Liñares L, Lado MJ, Vila XA, et al. GHRV: Heart rate variability analysis made easy. *Comput Methods Programs Biomed* 2014; 116: 26–38.

[63] Niu C, Guo D, Eng M, et al. HRnV-Calc: A Software for Heart Rate n-Variability and Heart Rate Variability Analysis. *J Open Source Softw* 2023; 8: 5391.

[64] Woerd C van der, van Gorp H, Dujardin S, et al. Studying sleep: towards the identification of hypnogram features that drive expert interpretation. *Sleep* 2024; 47: zsad306.

[65] Kligfield P, Gettes LS, Bailey JJ, et al. Recommendations for the standardization and interpretation of the electrocardiogram: Part I: The electrocardiogram and its technology: A scientific statement from the American Heart Association Electrocardiography and Arrhythmias Committee, Council on Clinical Cardiology; the American College of Cardiology Foundation; and the Heart Rhythm Society. *Circulation* 2007; 115: 1306–1324.

[66] Luo S, Johnston P. A review of electrocardiogram filtering. *J Electrocardiol* 2010; 43: 486–496.

[67] ECG morphological analysis — pecg documentation, https://pecg.readthedocs.io/en/latest/tutorials/pecg_analysis.html (accessed 27 September 2024).

[68] filtfilt - Zero-phase digital filtering - MATLAB - MathWorks Italia, https://it.mathworks.com/help/signal/ref/filtfilt.html (accessed 25 September 2024).

[69] Mitra SK. *Digital Signal Processing*. Second. McGraw-Hill Higher Education, 2001.

[70] Shaffer F, Ginsberg JP. An Overview of Heart Rate Variability Metrics and Norms. *Frontiers in Public Health*; 5. Epub ahead of print 28 September 2017. DOI: 10.3389/fpubh.2017.00258.

[71] Delgado-Bonal A, Marshak A. Approximate entropy and sample entropy: A comprehensive tutorial. *Entropy*; 21. Epub ahead of print 1 June 2019. DOI: 10.3390/e21060541.

[72] Peng C-K, Israel B, Havlin S, et al. *Quantification of scaling exponents and crossover phenomena in nonstationary heartbeat time series*, http://ojps.aip.org/chaos/chocr.jsp.

[73] Ladysz R. Nonlinear dynamical and entropic complexity measures as indicators of nonstationarities in short-term ECG signals. In: *2009 IEEE International Conference on Bioinformatics and Biomedicine, BIBM 2009*. 2009, pp. 269–278.

[74] Acharya UR, Fujita H, Sudarshan VK, et al. Automated Prediction of Sudden Cardiac Death Risk Using Kolmogorov Complexity and Recurrence Quantification Analysis Features Extracted from HRV Signals. In: *Proceedings - 2015 IEEE International Conference on Systems, Man, and Cybernetics, SMC 2015*. Institute of Electrical and Electronics Engineers Inc., 2016, pp. 1110–1115.

[75] Hsu CH, Tsai MY, Huang GS, et al. Poincaré plot indexes of heart rate variability detect dynamic autonomic modulation during general anesthesia induction. *Acta Anaesthesiologica Taiwanica* 2012; 50: 12–18.

[76] PhysioNet. Haaglanden Medisch Centrum sleep staging database (version 1.0. 1).

[77] Goldberger AL, Amaral LA, Glass L, et al. PhysioBank, PhysioToolkit, and PhysioNet: components of a new research resource for complex physiologic signals. *Circulation*; 101. Epub ahead of print 2000. DOI: 10.1161/01.CIR.101.23.E215.

[78] Alvarez-Estevez D, Rijsman RM. Inter-database validation of a deep learning approach for automatic sleep scoring. *PLoS One* 2021; 16: e0256111.

[79] Sattar P, Baldazzi G, Puligheddu M, et al. The UNICA Sleep HRV Analysis Tool: an Integrated Open-Source Tool for Heart Rate Variability Analysis during Sleep. *Physiol Behav*.

[80] Mendoza-Velásquez JJ, Flores-Vázquez JF, Barrón-Velázquez E, et al. Autonomic dysfunction in α-synucleinopathies. *Front Neurol*; 10. Epub ahead of print 2019. DOI: 10.3389/fneur.2019.00363.

[81] Ferini-Strambi L, Oertel W, Dauvilliers Y, et al. Autonomic symptoms in idiopathic REM behavior disorder: A multicentre case-control study. *J Neurol* 2014; 261: 1112–1118.

[82] Zitser J, During EH, Chairo G, et al. Autonomic impairment as a potential biomarker in idiopathic REM-sleep-behavior disorder. *Auton Neurosci* 2019; 220: 102553.

[83] Yang JH, Choi SH, Lee MH, et al. Association of heart rate variability with REM sleep without atonia in idiopathic REM sleep behavior disorder. *Journal of Clinical Sleep Medicine* 2021; 17: 461–469.

[84] Ferini-Strambi L, Smirne S, Ferini-St~ambi L, et al. *Cardiac autonomic function during sleep in several neuropsychiatric disorders*. 1997.

[85] Lanfranchi PA, Fradette L, Gagnon JF, et al. Cardiac autonomic regulation during sleep in idiopathic REM sleep behavior disorder. *Sleep* 2007; 30: 1019–1025.

[86] Rocchi C, Placidi F, Liguori C, et al. Daytime autonomic activity in idiopathic rapid eye movement sleep behavior disorder: a preliminary study. *Sleep Med* 2018; 52: 163–167.

[87] Braak H, Ghebremedhin E, Rüb U, et al. Stages in the development of Parkinson's disease-related pathology. *Cell and Tissue Research* 2004; 318: 121–134.

[88] Chen YN, Kostka JK. Beyond anosmia: olfactory dysfunction as a common denominator in neurodegenerative and neurodevelopmental disorders. *Frontiers in Neuroscience*; 18. Epub ahead of print 2024. DOI: 10.3389/fnins.2024.1502779.

[89] Tipre DN, Goldstein DS. *Cardiac and Extracardiac Sympathetic Denervation in Parkinson's Disease with Orthostatic Hypotension and in Pure Autonomic Failure*. 2005.

[90] Barateau L, Jaussent I, Lopez R, et al. Cardiac sympathetic activity differentiates idiopathic and symptomatic rapid eye movement sleep behaviour disorder. *Sci Rep*; 8. Epub ahead of print 1 December 2018. DOI: 10.1038/s41598-018-25547-w.

[91] Owens AP. The Role of Heart Rate Variability in the Future of Remote Digital Biomarkers. *Frontiers in Neuroscience*; 14. Epub ahead of print 13 November 2020. DOI: 10.3389/fnins.2020.582145.

[92] Neff RA, Wang J, Baxi S, et al. Respiratory sinus arrhythmia: Endogenous activation of nicotinic receptors mediates respiratory modulation of brainstem cardioinhibitory parasympathetic neurons. *Circ Res* 2003; 93: 565–572.

[93] Sornmo L, Bailon R, Laguna P. Spectral Analysis of Heart Rate Variability in Time-Varying Conditions and in the Presence of Confounding Factors. *IEEE Rev Biomed Eng*. Epub ahead of print 2022. DOI: 10.1109/RBME.2022.3220636.

[94] Gasior JS, Sacha J, Jelen PJ, et al. Heart rate and respiratory rate influence on heart rate variability repeatability: Effects of the correction for the prevailing heart rate. *Front Physiol*; 7. Epub ahead of print 18 August 2016. DOI: 10.3389/fphys.2016.00356.

[95] Niizeki K, Saitoh T. Association between phase coupling of respiratory sinus arrhythmia and slow wave brain activity during sleep. *Front Physiol*; 9. Epub ahead of print 25 September 2018. DOI: 10.3389/fphys.2018.01338.

[96] Ministeri CM, Modica AA, Coco D Lo, et al. 50. Decreased heart rate variability in REM sleep behavior disorder. *Clinical Neurophysiology* 2016; 127: e144.

[97] Bailón R, Laouini G, Grao C, et al. The integral pulse frequency modulation model with time-varying threshold: Application to heart rate variability analysis during exercise stress testing. *IEEE Trans Biomed Eng* 2011; 58: 642–652.

[98] Kontaxis S, Lázaro J, Corino VDA, et al. *ECG-derived Respiratory Rate in Atrial Fibrillation*.

[99] Postuma RB, Iranzo A, Hu M, et al. Risk and predictors of dementia and parkinsonism in idiopathic REM sleep behaviour disorder: A multicentre study. *Brain* 2019; 142: 744–759.

[100] Sattar P, Facchini E, Baldazzi G, et al. Heart Rate Variability during Sleep-Related Wake Phases in REM Sleep Behavior Disorder. *Comput Cardiol (2010)* 2023; 50: 1–4.

[101] Sattar P, Baldazzi G, Mandas N, et al. Parkinson and REM Sleep Behaviour Disorder: HRV Difference During Polysomnography. INSTICC, 2023, pp. 366–370.

[102] Mandas N, Mollura M, Baldazzi G, et al. Characterization of Sleep Structure and Autonomic Dysfunction in REM Sleep Behavior Disorder. *IEEE Open J Eng Med Biol*. Epub ahead of print 2024. DOI: 10.22489/CinC.2022.389.

[103] Heimrich KG, Lehmann T, Schlattmann P, et al. Heart rate variability analyses in parkinson's disease: A systematic review and meta-analysis. *Brain Sci*; 11. Epub ahead of print 2021. DOI: 10.3390/brainsci11080959.

[104] Baumert M, Porta A, Vos MA, et al. QT interval variability in body surface ECG: Measurement, physiological basis, and clinical value: Position statement and consensus guidance endorsed by the European Heart Rhythm Association jointly with the ESC Working Group on Cardiac Cellular Electroph. *Europace* 2016; 18: 925–944.

[105] Scorza FA, Guimarães-Marques M, Nejm M, et al. Sudden unexpected death in Parkinson's disease: Insights from clinical practice. *Clinics* 2022; 77: 1–6.

[106] Cunnington AL, Hood K, White L. Outcomes of screening Parkinson's patients for QTc prolongation. *Parkinsonism Relat Disord* 2013; 19: 1000–1003.

[107] Jo H, Kim D, Song J, et al. Sleep disturbances and phenoconversion in patients with rem sleep behavior disorder. *J Clin Med*; 10. Epub ahead of print 1 October 2021. DOI: 10.3390/jcm10204709.

[108] Najafi MR, Chitsaz A, Askarian Z, et al. *Quality of Sleep in Patients with Parkinson's Disease*, www.ijpm.ir.

[109] Sharma R, Meena HK. Emerging Trends in EEG Signal Processing: A Systematic Review. *SN Comput Sci*; 5. Epub ahead of print 2024. DOI: 10.1007/s42979-024-02773-w.

[110] Johari S, Meedinti GN, Delhibabu R, et al. Noise removal methods on ambulatory EEG: A Survey. 1–16.

[111] Almarshad MA, Islam S, Bahammam S, et al. Polysomnography Raw Data Extraction, Exploration, and Preprocessing. *Springer Optimization and Its Applications* 2024; 216: 45–65.

[112] Klekowicz H, Malinowska U, Piotrowska AJ, et al. On the robust parametric detection of EEG artifacts in polysomnographic recordings. *Neuroinformatics* 2009; 7: 147–160.

[113] Fairley J, Johnson AN, Georgoulas G, et al. Automated polysomnogram artifact compensation using the generalized singular value decomposition algorithm. *2010 Annual International Conference of the IEEE Engineering in Medicine and Biology Society, EMBC'10* 2010; 5097–5100.

[114] Nguyen QTN, Le T, Vu QTT, et al. An Algorithm for Removing Artifacts in Polysomnography Signals. *IFMBE Proc* 2022; 85: 1017–1031.

[115] Laouhingamaye D. Insomnia EEG Signal Preprocessing Using ICA Algorithms. DOI: 10.1145/3454127.3457630.

[116] Dora C. Automated Detection of Nonphysiological Artifacts in Polysomnographic EEG using Conventional Signal Processing Techniques. 2017; 1568–1572.

[117] Berryman MJ, Messer S, Allison A, et al. Techniques for noise removal from EEG , EOG and air flow signals in sleep patients.

[118] Gurrala V, Yarlagadda P, Koppireddi P. Artifact Removal from Sleep Hipnograms using Complete Ensemble Empirical Decomposition with Adaptive Noise. 10. Epub ahead of print 2017. DOI: 10.17485/ijst/2017/v10i47/108645.

[119] Garces Correa MA, Laciar E. Noise Removal from EEG Signals in Polisomnographic Records Applying Adaptive Filters in Cascade. *Adaptive Filtering Applications*. Epub ahead of print 2011. DOI: 10.5772/17219.

[120] Sharma P. Removal of Artifacts in EEG Signals Using Sign Based LMS Adaptive Filtering Techniques. *1st IEEE International Conference on Innovations in High Speed Communication and Signal Processing, IHCSP 2023* 2023; 199–203.

[121] Landau ID, Bismor D, Airimitoaie T, et al. Speeding up VSLMS adaptation algorithms using dynamic adaptation gain: Analysis and Applications. *Analysis and Applications*.

[122] Pandey a, Malviya L, Sharma V. Comparative Study of LMS and NLMS Algorithms in Adaptive Equalizer. *International Journal of Engineering …* 2012; 2: 1584–1587.

[123] Paleologu C, Ciochină S, Benesty J, et al. An overview on optimized NLMS algorithms for acoustic echo cancellation. *EURASIP J Adv Signal Process* 2015; 2015: 1–19.

[124] La Rosa AB, Pereira PTL, Ücker P, et al. Exploring NLMS-Based Adaptive Filter Hardware Architectures for Eliminating Power Line Interference in EEG Signals. *Circuits Syst Signal Process* 2021; 40: 3305–3337.

UNIONE EUROPEA
Fondo Sociale Europeo

PON RICERCA E INNOVAZIONE

REACT EU

UNIVERSITÀ DEGLI STUDI DI CAGLIARI

La borsa di dottorato è stata cofinanziata con risorse del
Programma Operativo Nazionale Ricerca e Innovazione 2014-2020, risorse FSE REACT-EU
Azione IV.4 “Dottorati e contratti di ricerca su tematiche dell’innovazione”
e Azione IV.5 “Dottorati su tematiche Green”